12-2010

Molecular engineering design of the SAPO-34 and ZIF-8 membranes for CO2 separation from CH4 and N2.

Surendar Reddy Venna
University of Louisville

Follow this and additional works at: http://ir.library.louisville.edu/etd

Recommended Citation

Venna, Surendar Reddy, "Molecular engineering design of the SAPO-34 and ZIF-8 membranes for CO2 separation from CH4 and N2." (2010). *Electronic Theses and Dissertations.* Paper 1489.
https://doi.org/10.18297/etd/1489

MOLECULAR ENGINEERING DESIGN OF THE SAPO-34 AND ZIF-8 MEMBRANES FOR CO$_2$ SEPARATION FROM CH$_4$ and N$_2$

Surendar Reddy Venna

A dissertation Submitted to the Chemical Engineering Department of the

University of Louisville in Partial Fulfillment of the Requirements for the Degree of

Doctor of Philosophy

Department of Chemical Engineering

University of Louisville

Louisville, Kentucky

December 2010

MOLECULAR ENGINEERING DESIGN OF THE SAPO-34 AND ZIF-8 MEMBRANES FOR CO_2 SEPARATION FROM CH_4 and N_2

By
Surendar Reddy Venna

A Dissertation Approved on
October 25, 2010

By the Following Dissertation Committee

_____

Dr. Moises A Carreon (Dissertation Director)

_____

Dr. James C Watters

_____

Dr. Mahendra K. Sunkara

_____

Dr. Gerold Willing

_____

Dr. Yongsheng Lian

Dedicated to my parents

Venkat Reddy Venna and Kamalamma Venna

and

Frineds

ACKNOWLEDMENTS

ABSTRACT

MOLECULAR ENGINEERING DESIGN OF THE SAPO-34 AND ZIF-8 MEMBRANES FOR CO_2 SEPARATION FROM CH_4 and N_2

Surendar Reddy Venna

October 25th, 2010

The separation of CO_2 from light gases is a very important environmental and energy issue. The state-of-the-art process for the purification of CO_2 uses amine adsorption, which is a complex, and costly. Membrane technology is far less expensive and requires less energy consumption. Although polymeric membranes can separate CO_2, high pressures plasticize them and decrease their separation ability considerably. Zeolite membranes have significant advantages over traditional polymeric membranes, such as high thermal, mechanical, and chemical stability. Furthermore, the development of superior performance membranes for gas mixture separations requires novel materials with fundamentally different structural, adsorption and transport properties than those of polymers and zeolites. In this respect, zeolitic imidazolate frameworks (ZIFs) a subclass of metal organic frameworks, have emerged as a novel crystalline porous materials which combine highly desirable properties, such as uniform pores and exceptional thermal and chemical stability, making them ideal candidates for molecular separations. *This work demonstrates the development of continuous zeolite (SAPO-34) and metal organic framework (ZIF-8) membranes able to separate CO_2 from CH_4 and N_2.*

The membranes were prepared on tubular porous supports by *secondary seeded growth*. Therefore, first we focused on the synthesis of small homogeneous crystals (both SAPO-34 and ZIF-8) with high surface area and used as *"seeds"* for membrane nucleation and growth. Crystal growth inhibitors, and microwave heating were used to prepare SAPO-34 seeds ($\sim$ 0.5 μm). Solvothermal synthesis was employed to prepare ZIF-8 seeds displaying ($\sim$ 50 nm). The entire process from gel formation, nucleation, crystallization and growth of ZIF-8 at room temperature was followed.

The resultant SAPO-34 membranes were functionalized with organic amino cations to promote CO_2 preferential adsorption and evaluated for the separation of CO_2/CH_4 and CO_2/N_2 gas mixtures. CO_2/CH_4 selectivities as high as 245 with CO_2 permeances of $\sim$5 $\times 10^{-7}$ mol/m^2 s Pa at 295 K and 138 KPa were observed. To our best knowledge, our SAPO-34 membranes display one of the best (if not the best) overall separation performance for the separation of CO_2/CH_4 gas mixtures. Moreover, we demonstrate the successful synthesis of novel ZIF-8 membranes for CO_2/CH_4 gas separation. This work represents one of the first examples (and the only example on CO_2/CH_4 separation) of the successful preparation of continuous, thin, and reproducible zeolitic imidazolate framework membranes for a functional *gas mixture* separation. Our ZIF-8 membranes displayed unprecedented high CO_2 permeances up to $\sim$ 2.4 x 10^{-5} mol/ m$^2 \cdot$s$\cdot$Pa and CO_2/CH_4 selectivities from $\sim$4 to 7.

The central intellectual thrust of this work is the rational design of SAPO-34 and ZIF-8 membranes, which offer the possibility of demonstrating high separation performance for CO_2 purification from light gases, and other functional gas separations.

The specific research objectives are:

1. Rational design of small SAPO-34 and ZIF-8 crystals, displaying narrow size distribution and enhanced CO_2 sorption properties.

2. Development of continuous SAPO-34 and ZIF-8 membranes for CO_2/CH_4 and CO_2/N_2 gas separations.

3. Elucidate and understand the basic information mechanisms governing the transformation of precursor solutions into ZIF phases.

4. Establish the fundamental structure/separation relationships of SAPO-34 and ZIF-8 membranes in relevant functional gas separations such as CO_2/CH_4 and CO_2/N_2.

This work represents an important advance in the rational design of zeolite and metal organic framework membranes and in basic fundamental understanding of its structure/separation relationships.

In particular, the proposed research has practical implications in *energy* and *environmental* issues, which are areas of great societal importance. For the targeted applications of carbon dioxide purification from methane and nitrogen, the proposed work may have an important economic impact in reducing considerably the separation costs associated to natural gas pretreatment, and reduction of greenhouse gases emissions respectively. It is anticipated that this work could serve as a model for the rational design of zeolitic imidazolate framework membranes for other important relevant molecular gas separations, such as hydrogen purification from synthesis gas.

TABLE OF CONTENTS

LIST OF TABLES

LIST OF FIGURES

CHAPTER 1

INTRODUCTION

1.1.   Importance of Carbon dioxide separation

The concentration of greenhouse gases like CO_2, CH_4, NO_x in the environment are increasing at fast rate since the beginning of industrial revolution. In particular, CO_2 emissions have increased dramatically, largely due to the burning of fossil fuels, such as coal or natural gas for the production of electricity and petroleum for transportation. World energy-related carbon dioxide emissions are projected to rise from 29.7 billion metric tons in 2007 to 33.8 billion metric tons in 2020 and 42.4 billion metric tons in 2035, an increase of 43 percent over the projection period as shown in Figure 1.1.[1] The CO_2 emissions from different energy sources is summarized in Figure 1.2.[1] With strong economic growth and continued heavy reliance on fossil fuels expected for most of the non-OECD (Organization for Economic Cooperation and Development) economies under current policies, much of the projected increase in CO_2 emissions occurs among the developing non-OECD nations. In 2007, non-OECD emissions exceeded OECD emissions by 17 percent; in 2035, they are projected to be double the OECD emissions.[2] High temperature process produces significant amount of CO_2. Especially, coal-burning power plant is producing large amount of CO_2 in the atmosphere. Typical flue gas from

1

the coal-burning power plant is composed of about 13% carbon dioxide, 73% nitrogen, 3% oxygen and less than 1%pollutants.[3] It has been estimated that the total CO_2 emissions in the U.S. grew to 6,022 million metric tons (MMT) in 2007 which represents more than 80% of the total greenhouse emissions.[4]
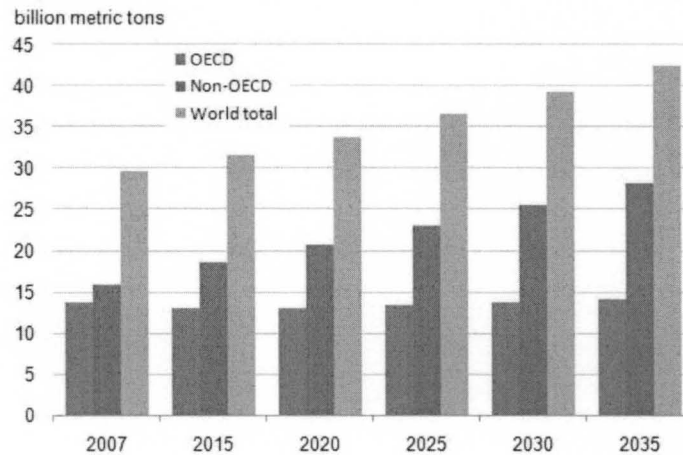
Figure 1.1. World energy-related carbon dioxide emissions[1]
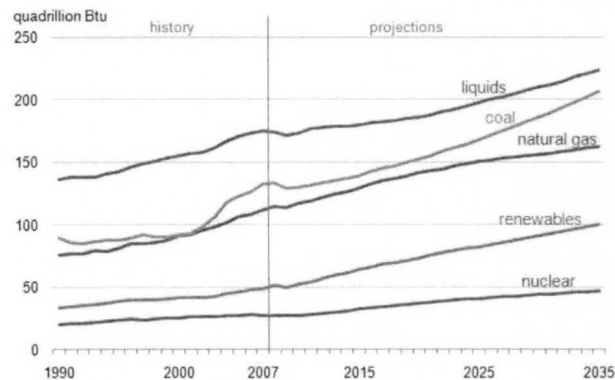
Figure 1.2. World marketed energy use by fuel type[1]

The increase in demand for energy worldwide has led to the search for alternative sources of primary energy with less environmental impact; natural gas is one such source. The US demand for natural gas stood at 23.0 trillion cubic feet for 2002 and is expected to continue to rise to approximately 31.3 trillion cubic feet by 2025 according to the

2

Energy Information Association (EIA).[5] Methane is the major component (75-90%), but natural gas also contains significant amounts of ethane, propane, butane and 1-3% of other higher hydrocarbons as shown in Table 1.1. In some deposits, it may contain contaminants such as CO_2, H_2S, CO which constitute environmental hazards and also hindered natural gas processes. The upgrading of low quality crude natural gas is an attractive field due to the high demand for pipeline-grade gas in recent years.

Table 1.1. Typical Composition of Natural Gas[6]

Component	Formula	Mole fraction
Main component		
Methane	CH_4	$\geqslant 0.70$
Nitrogen	N_2	$\leqslant 0.20$
Carbon dioxide	CO_2	$\leqslant 0.20$
Ethane	C_2H_6	$\leqslant 0.1$
Propane	C_3H_8	$\leqslant 0.035$
Butane	C_4H_{10}	$\leqslant 0.015$
Pentane	C_5H_{12}	$\leqslant 0.005$
Hexane	C_6H_{14}	$\leqslant 0.001$
Heptane	C_7H_{16}	$\leqslant 0.0005$
Octane and above	C_{8+}	$\leqslant 0.0005$
Hydrogen	H_2	$\leqslant 0.1$
Carbon monoxide	CO	$\leqslant 0.03$
Helium	He	$\leqslant 0.005$
Water	H_2O	$\leqslant 0.00015$

Carbon dioxide, which falls into the category of acid gases, is commonly found in natural gas streams at levels as high as 70%. In combination with water, it is highly corrosive and rapidly destroys pipelines and equipment unless it is removed. CO_2 also reduces the heating value of a natural gas stream and wastes pipeline capacity. Therefore, CO_2 found in natural gas must be removed to meet specifications before the gas can be delivered to the pipeline. About 17% of all domestic natural gas in the U.S. is treated to remove CO_2 before it is passed to the pipeline, which requires a CO_2 concentration below 2–3%. A large part of the world's natural gas reserves that have been discovered to date

3

are currently not available for production due to limitations in separation technology. In the process of removal, it is ideal to maintain the natural gas at high pressure to save recompression costs. Therefore, it has become necessary to develop efficient processes for the removal of CO_2 from natural gas. Flue gases have long been an important source of CO_2 and need to be separated before releasing to the atmosphere in order to reduce the concentration of greenhouse gases. *From the environmental and energy perspective, the purification and recovery of CO_2 from flue gas and natural gas are of great interest.*

1.2.   Techniques for CO_2 separation

Several options exist to abate CO_2 emissions from fossil fuel utilization, including increasing the efficiency of fossil fuel combustion systems, or replacing fossil fuels with renewable energy sources. Carbon capture and sequestration refers to the process of capturing and securely storing the CO_2, which is emitted from fossil-fuel-fired power plants. Carbon capture and sequestration could enable large reduction of CO_2 emissions from fossil fuel combustion in power generation, industrial processes and synthetic fuel production.
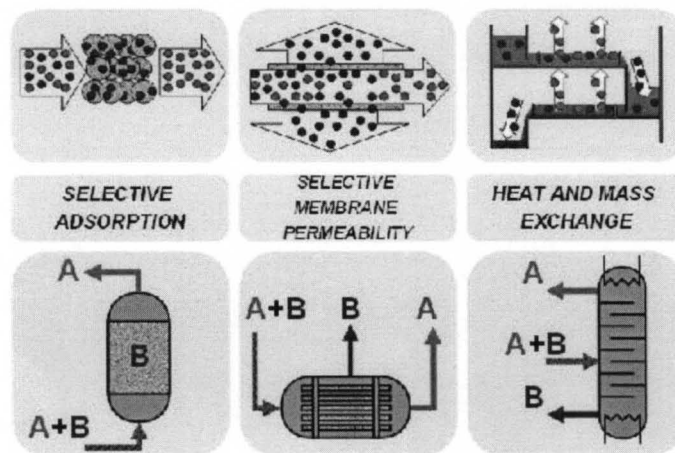
Figure 1.3. Typical carbon dioxide separation methods[7]

Varieties of processes have been developed over the years to treat natural gas with the aim of optimizing capital and operating cost, meet gas specifications and for environmental purposes. Ease of operation, quick start-up, and high on-stream factors are needed. The major processes (Figure 1.3) for CO_2 removal are: a) chemical and physical absorption; b) pressure swing adsorption; c) low temperature distillation; and d) membrane separation.

1.2.1. Chemical and physical absorption

Absorption in solvents is presently one of the main techniques used at industrial scale, in natural gas treatment and in coal plants for CO_2 capture. The basic process, patented in 1930, is one in which CO_2 is absorbed from a fuel gas near ambient temperature into an aqueous solution of amine by contacting them counter-currently in an absorption tower (Figure 1.4).[8] Conventionally, the gas to be scrubbed enters the absorber at the bottom and the solvent enters the top of the absorber. The solvent regeneration can be carried out at low pressures to enhance desorption of CO_2 from the liquid.
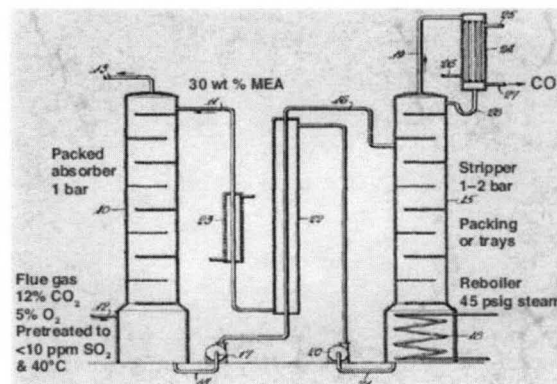
Figure 1.4. The amine scrubbing process invented by Bottoms in 1930[8]

Chemical solvents are mostly amines such as monoethanolamine, methyldiethylamine, and potassium carbonate. With these solvents, a reversible reaction

5

occurs at ambient or higher temperatures and desorption typically takes place at high temperature. Solvents like glycols do not interact with CO_2 as strongly as alkanolamines and require less energy for regeneration. Secondary and tertiary amines have lower heat of reaction with CO_2over primary amines and react more slowly with CO_2 than primary amines thus require higher circulation rate of liquid to remove CO_2 and require less heat for solvent regeneration. Physical solvents, such as dimethylether of polyethylene glycol and cold methanol, are also used for CO_2absorption by absorbing physically. Regeneration of the spent solvent can be achieved by stripping with vapor or inert gas.

Amine systems are used frequently but are complex and have high capital, operating, and installation costs; a relatively high fuel cost and potential environmental issues. Vaporization of part of the solvent is an additional disadvantage. Reducing the energy requirement is an essential condition for a breakthrough in absorption techniques.

1.2.2. Pressure swing adsorption
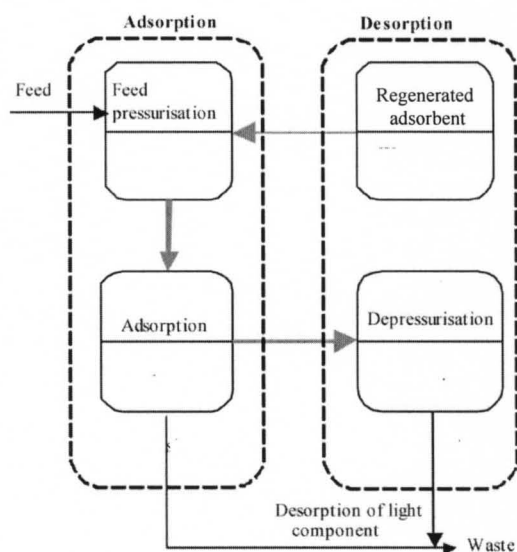
Figure 1.5. Pressure swing adsorption process for the separation of CO_2[9]

Pressure swing adsorption (PSA) is known to be one of the most economic and widespread processes for gas purification. PSA was introduced in 1960s and it is used for the recovery of methane from landfill gas and the production of CO_2. The molecules to be adsorbed interact with the internal surface of microporous solids such as activated carbons and zeolite molecular sieves as shown in Figure 1.5. Polar and condensable species like CO_2 will be strongly retained by different equilibrium capacities, together with sulphur compounds and hydrocarbons, whereas the light components like N_2, O_2 will be less retained. Thermal-swing adsorption or a pressure-swing adsorption method is employed for the regeneration of the adsorbent.

The main advantage of physical adsorption over chemical or physical absorption is its simple and energy efficient operation and regeneration and other advantages are simple process, simultaneous dehydration of the gas and acid removal is possible. The disadvantages of this process are limited gas stream adsorption, unsuitable for continuous circulation due to attrition, complex design of the process and difficult to scale up.

1.2.3. Low temperature distillation
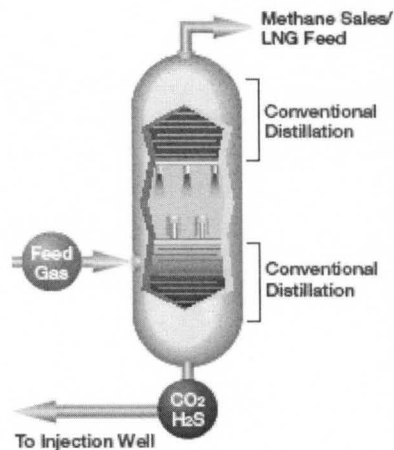
Figure 1.6. Cryogenic process for the removal of CO_2 from natural gas.[10]

7

Low temperature distillation (cryogenic separation) is a commercial process commonly used to liquefy and purify CO_2 from high CO_2 concentrations. Cryogenic separation unit are operated at extremely low temperature and high pressure to separate components by phase change according to their different boiling temperatures as shown in Figure 1.6. Reducing the temperature of the natural gas stream, carbon dioxide will liquefy at temperatures much higher than methane being removed in an intermediate step. This method is advantageous with respect to direct production of liquid CO_2 or pure CO_2 gas stream in high pressure which would be liquefied more easily and ready for transportation by pipeline. The major disadvantages of this process are high energy requirement, high operating cost, high tendency for blockage of process equipment, difficulty in processing toxic and flammable cryogenic fluids. The other disadvantage is that the by-products such as NO_x, SO_x and water must be removed before the stream is introduced to the low temperature section.

1.2.4. Membrane technology

Membranes have been widely used in various industrial separation applications for the last two decades.[11] It is estimated that the annual revenue of the worldwide membrane industry is over a billion dollars, and growing at a fast rate.[11] Currently, the industry is dominated by polymeric membranes that have been used in a wide variety of applications. Recently, research directed at the development and application of inorganic membranes is gaining momentum because of their excellent properties for molecular gas separations. Membrane processes consist in the selective permeation of molecules through a thin layer of polymeric or inorganic material. The performance of a membrane process is largely determined by the membrane's transport properties like permeability

8

and selectivity for a specific gas in a mixture. Industrial membrane processes have been developed for recovery of relatively concentrated CO_2 from natural gas. It is a viable energy-saving alternate for CO_2 separation, since it does not require any phase transformation and the necessary process equipment is very simple with no moving parts, compact, relatively easy to operate and control, and also easy to scale-up. Membranes processes are commercially proven technology for natural gas processing application. Therefore, membrane technology has been gradually replacing amine systems.

Gas separation membranes offer a number of benefits over other gas separation technologies. Conventional technologies such as the cryogenic distillation, amine absorption and adsorption on solids have several disadvantages like high energy requirement, chemical involvement, phase changes and complex equipment. Membrane technology, on the other hand, does not require any chemicals or phase change; furthermore, it consists of simple equipment and it is easy to scale up.

1.3.   Motivation for this work

A continuous zeolite membrane has great advantages over other materials as an effective membrane due to its uniform pore structure atthe molecular level. One of the major problems confronting the use of membrane-based gas separation processes is the lack of membranes with high flux and high selectivity. The development for the crystalline membranes with minimum thickness and desirable adsorption properties for gas separation still remains challenging. Herein, we present the development of two important and relevant membrane compositions for CO_2/CH_4 and CO_2/N_2 gas separation: a) a traditional zeolite composition (SAPO-34) and b) a novel metal-organic framework composition (ZIF-8). In particular, the proposed research has practical implications in

energy and environmental issues, which are areas of great societal importance. For the targeted applications of carbon dioxide purification from methane and nitrogen, the proposed work may have an important economic impact in reducing considerably the separation costs associated with natural gas pretreatment and reduction of greenhouse gases emissions respectively.

1.4. Objectives of this work

The central thrust of this work is the rational design of a zeolite (SAPO-34) and metal organic framework (ZIF-8) membranes which offer the possibility of demonstrating high separation performance for carbon dioxide purification from light gases. The specific deliverables of this work include:

1. Rational design of small SAPO-34 and ZIF-8 crystals, displaying narrow size distribution and enhanced CO_2 sorption properties.

2. Development of continuous SAPO-34 and ZIF-8 membranes for CO_2/CH_4 and CO_2/N_2 gas separations.

3. Elucidate and understand the basic information mechanisms governing the transformation of precursor solutions into ZIF phases.

4. Establish the fundamental structure/separation relationships of SAPO-34 and ZIF-8 membranes in relevant functional gas separations such as CO_2/CH_4 and CO_2/N_2.

1.5. Thesis organization

In the first chapter, a brief introduction about the importance of carbon dioxide separation and different carbon dioxide separation techniques, such as adsorption,

adsorption, distillation and membranes, is given. The motivation of this work and objectives are stated in this chapter too.

In the second chapter, a brief introduction on zeolites is given. Different membrane synthesis technologies and their prospects for gas separation, as well as different membrane compositions for molecular separations are presented. Finally, a review of experimental data of different membranes for the separation of CO_2/CH_4 and CO_2/N_2 is discussed.

In chapter three, experimental details on the preparation of SAPO-34 and ZIF-8 seeds and membranes are presented. The characterization and evaluation of the resulting membranes for CO_2/CH_4 and CO_2/N_2 gas separation is described.

In the fourth chapter, a detailed description on the preparation of small SAPO-34 seed crystals displaying narrow size distribution employing crystal growth inhibitors and microwave hydrothermal treatment is presented. The resultant seeds were used to prepare membranes as explained in Chapter 5.

Chapter five describes the preparation of continuous SAPO-34 membranes via secondary seeded growth. The functionalization of SAPO-34 using different organic amino cations is explained. The resultant SAPO-34 membranes were evaluated for the separation of CO_2/CH_4 and CO_2/N_2 gas mixtures.

In Chapter six, we discuss the synthesis of novel zeolitic imidazolate framework-8 seeds and its formation mechanism. We identified the different stages of ZIF-8 formation: nucleation, crystallization, growth, and stationary periods; and elucidated its kinetics of transformation.

Chapter seven describes the preparation of continuous ZIF-8 membranes. It explains the successful synthesis of ZIF-8 membranes on alumina supports. The synthesized membranes were evaluated for the separation of CO_2/CH_4 and CO_2/N_2 gas mixtures.

Chapter eight includes the meaningful conclusions obtained in the present study and some suggestions and recommendations to further improve the separation performance of the membranes. Finally future research directions are proposed.

CHAPTER 2

BACKGROUND

Zeolites are one of the most important porous materials for wide variety of applications, including gas separations. In this chapter, generalities on zeolites are presented. Structural features and different synthesis methods employed for SAPO-34 are described. The importance and advantages of microwave heating as an alternative approach to prepare zeolite crystals is highlighted. In the second part of this chapter we present the state of the art on the separation performance of different types of membranes employed for CO_2/CH_4 and CO_2/N_2 gas separations. Finally we discuss the structural properties of a subclass of metal organic frameworks: zeolitic imidazolate frameworks and their potential for molecular gas separations.

2.1. Introduction to Zeolites

The demand for novel functional zeolites with controlled desired properties is steadily increasing. Zeolite molecular sieves comprise a class of microporous, crystalline compounds composed of three-dimensional network of atoms such as Si, Al, Ga, Ge, Zn, Be, etc. These tetrahedrally coordinated atoms (T atoms), are coordinated to four oxygen atoms and are linked to other T-atoms by sharing each oxygen with a neighboring T-atom tetrahedron. Zeolites exhibits very uniform pore size distribution, high specific surface area, high porosity, variable chemical composition and controllable acid-base properties.

Natural zeolites are found in volcanic or metamorphic rocks and their growth involves geological conditions (low temperature and pressure, low pH (8-9)) and time scale (thousands of years). The first precise confirmation of zeolite synthesis can be traced in 1948 when Barrer reported the synthesis of mordenite.[12] In the early 1960s Barrer and Denny were the first to replace inorganic bases in the synthesis mixture with organic molecules.[13] Zeolite formation is a kinetically controlled process. Zeolites are reaction intermediates during the formation of dense phases from silica precursors. In zeolite synthesis, the reaction is stopped when the thermodynamically meta-stable zeolite hasformed. Extended reaction time at high temperature and/or high pressure usually results in dense phases. Modern synthetic methodologies for preparing zeolites and zeolite-like materials typically involve the use of organic molecules that direct the assembly pathway and ultimately fill the pore space. Structure direction occurs when inorganic or organic molecules are used to direct the crystallization towards a specific zeolite structure. Structure-directing agents, currently called templates, are generally: (1) charged molecules which are mostly cations, (2) neutral molecules and (3) ionic pairs.

The formation mechanism of zeolite under hydrothermal condition is complex and not fully understood. The crystallization of molecular sieves is a very complicated process influenced by reactants, mixing procedure, temperature, pH, etc. It involves several reaction steps, molecular level self-organization, nucleation, aggregation, crystallization and growth as shown in Figure 2.1.[14] Two mechanisms regarding the crystallization process have been proposed.[15,16,17] One of which is the solution-mediated transport mechanism involving the dissolution of reagents followed by transport mechanisms to the nucleation sites where the crystal growth takes place, and the other is

the solid hydrogel transformation mechanism involving the reorganization of the solid phase from amorphous components to crystalline. A combination of both mechanisms may also be possible; however, no general roles have hitherto been developed due to the complexity of crystallization process.
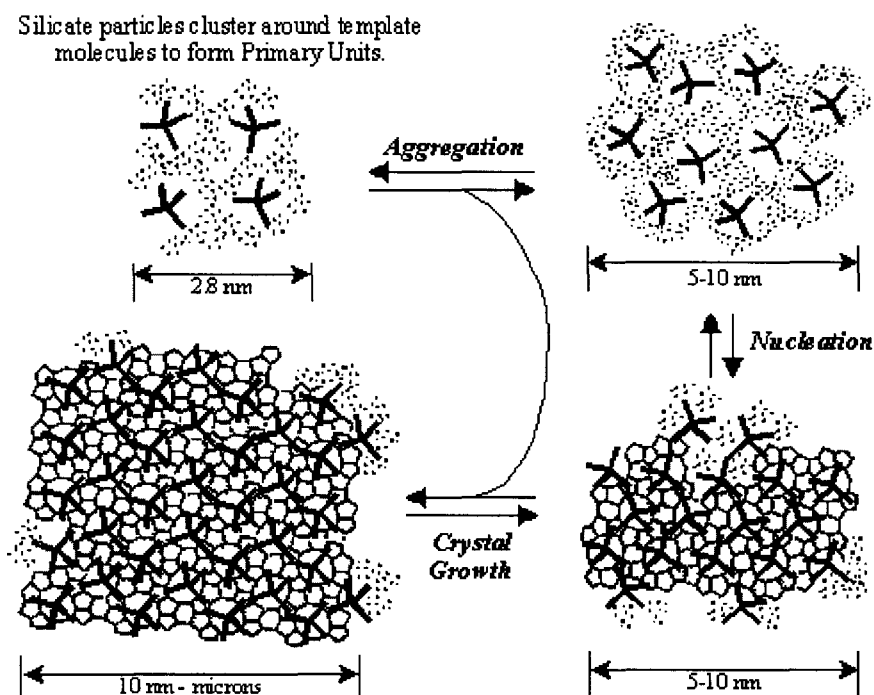
Figure 2.1. Formation mechanism of silicalite zeolite particles[14]

The presence of molecular-sized inter-connected pores and electrical charge or polarity makes them effective for a wide range of applications. Zeolites are mainly used for the adsorption and separation of ions and small gas molecules, and as heterogeneous catalysts. More recently, these materials are receiving attention in other applications, such as medical diagnosis and as components in electronic devices. More recent applications include as solid state devices for encapsulating quantum wires and dots, as medical drug delivery systems and as animal feed supplements. Now these materials are also more

involved in our current life, for example, as additive in detergent for clothes washing and in the environmental protection such as in water purification and nuclear waste disposal.

2.2. SAPO-34 importance and synthesis

SAPO-34, $(Si_xAl_yP_z)O_2$ where x = 0.01–0.98, y = 0.01–0.60, and z = 0.01–0.52, a type of silicoaluminophosphate microporous zeolite, is of particular interest in separation, catalytic and adsorption technologies because of its chemical and thermal stability, unique shape selectivity, molecular sieving properties and atomically ordered ~ 0.38 nm pore structure.[18-23] Silicoaluminophosphates (SAPOs) are crystalline nanoporous materials formed by silicon, aluminum, phosphorus, and oxygen atoms in tetrahedral coordination and arranged in an orderly fashion. SAPO-34 has the framework characteristics of natural zeolite chabazite (CHA) as shown in Figure 2.2. This molecular sieve includes 8-ring apertures with a pore diameter of~0.38 nm that permit access to a 3-D channel and cage system. Such geometry allows molecules with small kinetic diameters to easily diffuse through the crystal structure. SAPOs also have a framework with a net charge that varies depending upon how the silicon substitution into an aluminophosphate group is achieved.[24]

SAPO-34 has been successfully employed to separate CO_2 and H_2 from different gases.[18-23] Properties such as fairly strong Brønsted acidity, adsorption of desired components and excellent shape selectivity make SAPO-34 an ideal active and selective catalyst in methanol-to-olefin reaction[25,26] and hydrocarbons transformation.[27] SAPO-34 has been used for the trapping of hydrocarbons, in particular, for cold start emission control in the automobile industry.[28] It has also been used for the thermo chemical storage of heat because of its unique water adsorption properties.[29]

16
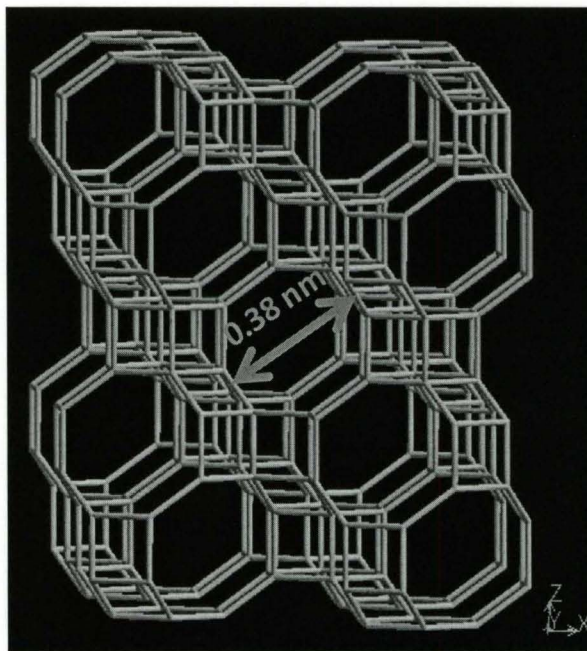
Figure 2.2. SAPO-34 crystal structure and pore opening

SAPO-34 was first discovered at Union Carbide Corporation,[30] the crystal structure of SAPO-34 and its analogy to natural chabazite was first reported by Ito et al.[31] Numerous groups have investigated the SAPO-34 material in respect to further applications. SAPO-34 has been prepared by several synthetic routes, for example, Lok and co-workers first reported the hydrothermal synthesis of SAPO-34 using tetraethylammonium hydroxide (TEAOH) as structure directing agent.[30] Different structure-directing agents such as morpholine,[32] piperidine,[33] diethylamine,[34,35] triethylamine,[36,37] isopropylamine[38] and TEAOH-dipropylamine[23] and TEAOH-cyclohexylamine[23] havebeen employed to prepare SAPO-34. Other synthetic approaches for SAPO-34, involve different heat treatment methods such as two-stage temperature

17

varying hydrothermal synthesis,[32] microwave synthesis,[39] vapor phase transport method,[40,41] ultrasound irradiation synthesis,[42] the use of various sources of silica and alumina as precursors[43] and the incorporation of different metals.[44,45,46] However, the control of the crystal size of SAPO-34 with high surface area, high crystallinity, homogeneity and preferential adsorption capacities over light gases is still challenging. SAPO-34 with small crystal size and narrow particle size distribution potentially leads to larger-accessible surface area, reduced diffusion resistance and increased adsorption capacity phases, which may impact positively its performance in functional applications such as gas separation and heterogeneous catalysis.

2.3. Microwave heating approach

The reduction of zeolite crystal size has been a major research field for the past several years as the decrease of dimension leads to substantial changes in the properties of the materials.[47] This has an impact on the performance of zeolites in applications such as catalysis and separation.[48,49] Additionally, this development has led to developments of new synthesis strategies yielding nanosize materials with narrow particle size distributions. The possibility of stabilizing these nanoparticles in suspensions has facilitated the production of thin-to-thick films, which are interesting for membrane and sensing applications. The most promising route for preparation of microporous and particularly zeolite nanocrystals is the use of clear solutions or colloidal suspensions as precursor media.

Heating and driving chemical reactions by microwave energy has been an increasingly popular theme in the scientific community, and so in the fields of zeolite and zeolite membranes. The pioneer work on microwave synthesis of zeolite can be traced to

1988.Mobil researchers claimed the microwave synthesis of microporous zeolites, such as zeolite NaA and ZSM-5.[50] The first published article on microwave synthesis of zeolite appeared in 1993, in which Jansen and co-workers reported that microwave-assisted crystallization of Y-type and ZSM-5 zeolite could be finished in a much shorter synthesis time and free of undesired phase as compared with conventional heating.[51]
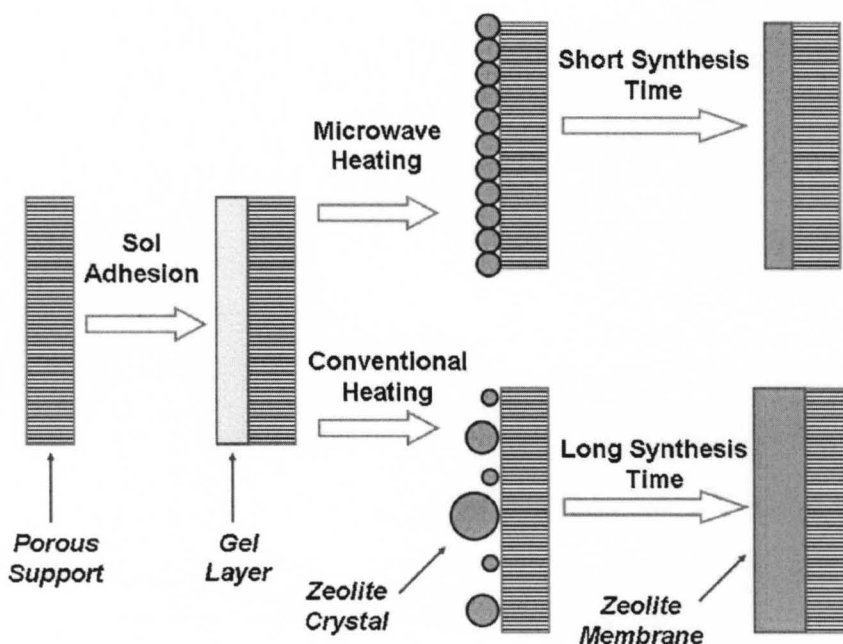
Figure 2.3. Comparion of synthesis of zeolite membranes using microwave and conventional heating[52]

Conventional heating has a heat source on the outside and relies on transferring the heat to the surface of the material and then conducting the heat to the middle of the material. Compared with conventional heating, microwave dielectric heating has the following advantages for chemical synthesis[53] (thermal effects of microwave): (1) the introduction of microwave energy into a chemical reaction can lead to much higher heating rates than those which are achieved conventionally; (2) the microwave energy is

19

introduced into the chemical reactor remotely without direct contact between the energy source and the reacting chemicals;(3) it is volumetric and instantaneous (or rapid) heating with no wall or heat diffusion effects; (4) it can realize selective heating because chemicals and the containment materials for chemical reactions do not interact equally with microwaves; (5) "hot spots" yielded on local boundaries by reflections and refractions may result in a "super-heating" effect, which can be described best as local overheating and is comparable to the delayed boiling of overheated liquids under conventional conditions. The first patent on MW synthesis was reported on the synthesis of zeolite A.[50] Since then, MW heating has been widely used in the synthesis of different zeolite compositions[54,55] including membranes,[23] catalysts,[56] and films.[57] Comprehensive reviews on zeolite synthesis using MW have been reported.[58,59]

Microwave heating can remarkably reduce synthesis time compared with conventional heating. In the synthesis of porous materials, it has been reported that the microwave synthesis method could provide an efficient way to control particle size distribution, phase selectivity, and macroscopic morphology. Besides this morphological difference, microwave synthesis can also lead to a compositional difference of the synthesized zeolite membranes.

2.4.   Types of membranes for molecular separations

Membranes that preferentially permeate CO_2 at high selectivities can significantly reduce the costs of natural gas purification and flue gas treatment. Membrane separation is projected to attain a high efficiency for CO_2 capture owing to their selective extraction of CO_2 from mixed gas streams, low energy requirements and the flexibility in industrial

plant configuration relative to conventional amine absorption. Membranes are thin semipermeable barriers that selectively separate some compounds from others.[11] This definition is necessarily broad because of the large variety of membrane materials separating an equally vast number of compounds in all phases. Membrane gas separation is a pressure-driven process with different industrial applications that represent only a smallfraction of the potential applications in refineries and chemical industries. The two intrinsic criteria determining performance are selectivity and permeability and they depend on their chemical nature and structure. The membrane materials should be thermally and chemically robust, resistant to plasticization and aging affects to ensure continual performance over long time periods, as well as cost effective.

Gas separation membranes were first commercialized in 1977 when Monsanto/Perma released their hydrogen recovery system.[60] Extensive research resulted in innovations that improved the gas separation efficiency and membrane durability, making membrane gasseparation commercially competitive with existing separation technologies. Gas separation membranes are now applied for the sweetening of natural gas by the removal of carbon dioxide.

Generally, any material that can be made into sufficiently thin and stable films can be used as membrane. This includes metal, glass, ceramics and polymers as well as ordered molecular monolayers of liquids. Currently, the most widely used membrane materials for gas separation are polymers because of the relatively low cost of manufacturing, but they cannot operate at high temperatures or in harsh chemical environments.[61] Silica membranes are not stable in humid atmosphere at high temperatures, carbon membranes have low fluxes, and metal membranes are vulnerable

to surface poisoning and suffer from hydrogen embrittlement.[62] Zeolite membranes have the ability to sieve molecules at high temperature, high pressure, and in chemically harsh environments, and thus have significant potential.[63] The types of membranes for molecular separations can be mainly divided as: a) polymeric; b) inorganic; c) mixed matrix; and d) metal-organic framework membranes.

2.4.1. Polymeric membranes

Polymeric membranes are generally non-porous, and therefore gas permeation through them is described by the solution-diffusion mechanism.[64] These membranes separate based on how different compounds dissolve into the membrane and then diffuse through it.[65] Hence, separation is not just diffusion dependent but also reliant on the physical-chemical interaction between the various gas species and the polymer, which determines the amount of gas that can accumulate in the membrane polymeric matrix. The first CO_2 separating membranes were based on cellulose acetate and derivatives and originally designed for reverse osmosis.[66] Membrane plants using CO_2-selective cellulose acetate membranes were installed in 1980s, and currently the largest membrane facility for CO_2 removal is 700 million scfd. However, the CO_2 flux of cellulose acetate based membranes decreases substantially with time, due to plasticization and compaction.[67] Improving the performance of the CO_2-selective polymeric membrane is achieved by two approaches: increasing the solubility of CO_2 in the membrane, and increasing the diffusion of CO_2 by altering the polymer packing within the membrane.[68] Some reported polymeric membranes[67] are based on polyamides, polysemicarbazides, polycarbonates, polyarylates, poly(phenylene oxide), polyaniline and polypyrrolones. These all have reasonable permeability and selectivity, with some achieving performance around

Robeson's upper bound.[68] Stronger interactions between a gas and the functional groups of a polymer result in higher solubility of that gas in the polymer.[69] Therefore, CO_2, which has a quadrupolar moment, is highly soluble in polar polymers.

Gas transport in polymeric membranes is affected by several polymer properties, such as morphology, free volume content, inter-segmental chain spacing (*d*-spacing), orientation, cross-linking, polymer polarity, defects, thermal processing history, glass transition temperature, average molecular weight, molecular weight distribution, composition, degree of crystallization, types of crystallites, etc. Two types of polymeric membranes, such as glassy membranes and rubbery membranes, are widely used commercially for gas separations. Glassy membranes are rigid and glass-like, and operate below their glass transition temperatures.[70] On the other hand, rubbery membranes are flexible and soft and operate above their glass transition temperatures.[71] Mostly, rubbery polymers show a high permeability, but a low selectivity, whereas glassy polymers exhibit a low permeability but a high selectivity. The presence of crystalline domains in a polymer adds a tortuosity factor to gas diffusion and, thus, makes gas transport more complicated.[61]

Permeability (P) and permselectivity ($\alpha_{i/j}$) are used to determine the separation performance of the polymeric membrane. The permeationability of component i in the membrane, P_i is the product of diffusivity coefficient D_i, and solubility coefficient S_i of the gas i in the membrane material. The separation ability of a membrane, $\alpha_{i/j}$ is defined as the ratio of the permeabilities of components i and j. It can be written as:[72]

$$\alpha_{i/j} = \frac{P_i}{P_j} = \left(\frac{S_i}{S_j}\right) \times \left(\frac{D_i}{D_j}\right) \qquad \text{-------- Equation (2.1)}$$

$\alpha_{i/j}= \alpha_S \times \alpha_D=$ solubility selectivity x diffusive selectivity   -------- Equation (2.2)

The actual separation factor is: $\alpha_{i/j}=\dfrac{x_j\, y_i}{x_i\, y_j}$ -------- Equation (2.3)

Where x and y are the fraction of the components in feed and permeate respectively.

Significant improvements in the performance of polymeric gas separation membranes have been witnessed in the last two decades. Despite all these efforts, polymeric membranes are not in a position above the trade-off curves between gas permeability and selectivity, as suggested by Robeson.[73]

Polymeric membranes,[67] such as cellulose acetate, poly(ethylene oxide), polyamide, polyimide, and hollow fibers, can separate CO_2/CH_4 and CO_2/N_2 mixtures. The separation performance of various polymeric membranes for CO_2/CH_4 and CO_2/N_2 mixtures has been summarized recently by Robeson.[73] So far commercially successful gas separation membranes are mainly thin nonporous polymeric membranes, in which gas separation is achieved due to the differences in permeation rates through the thin separating layer. Most of these membranes fall below the upper bound of the Robeson plot. Also, most of the industrial application requires high pressures and temperatures at which plasticization of the polymeric membranes occurs resulting in poor separation performances. Therefore, there is a need to develop other membranes which have the ability to separate gases with higher separation performance. Due to its superior thermal, mechanical, and chemical stability, zeolite membranes are preferred over polymeric membranes for CO_2 separation from CH_4 and N_2. To the best of our knowledge, SAPO-34 has shown the best CO_2/CH_4 separation performance as compared to any other

membrane composition, mainly due to its remarkable molecular sieving and enhanced competitive CO_2 adsorption properties.
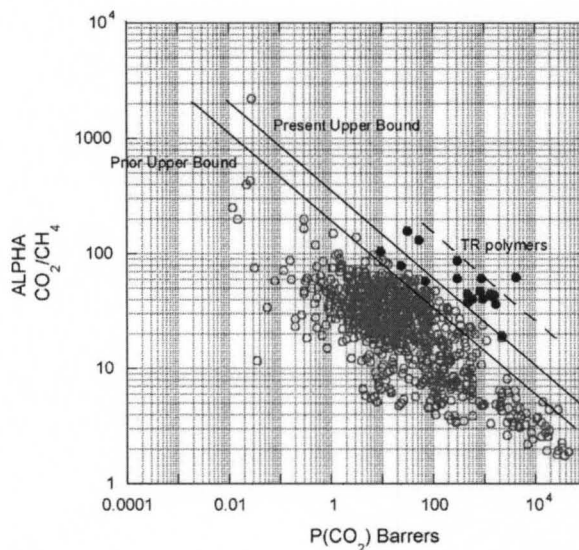
Figure 2.4. Modified Robnson plot for CO_2/CH_4 gas selectivity and permeances of polymeric membranes.[73] (1 Barrer = 3.348 x 10^{-19} mol/m^2 s Pa)

2.4.2. Inorganic membranes

Inorganic zeolite membranes have significant advantages over polymeric membranes. They do not deform under high CO_2 pressures, have high thermal, mechanical, and chemical stability, and good erosion resistance. Inorganic membranes can be classified into two categories based on structure: porous and dense. In porous inorganic membranes, a porous thin top layer is supported on a porous metal or ceramic support, which provides mechanical strength with minimum mass-transfer resistance. Alumina, carbon, glass, silicon carbide, titania, zeolites, and zirconia membranes are mainly used as porous inorganic membranes supported on different substrates, such as α-alumina, γ-alumina, zirconia, titania, zeolite, or porous stainless steel. Dense membranes

provide high selectivity, but poor gas permeances. These membranes are prepared with and without porous supports. The mechanism of gas transport in dense membranes is solution-diffusion mechanism.

There are four main transport mechanisms by which gas separation take place in inorganic porous zeolite membranes as shown in Figure 1.8.[61] The basis of these transport mechanisms are the molecular weight (Knudsen diffusion), surface interactions (surface diffusion and capillary condensation), and the size of molecules (molecular sieving) to be separated. Pores in gas separation membranes can be classified as follows: micropores equivalent to molecular dimensions, meso and macropores of the Knudsen diffusion regime; and pinholes of the Poiseuille flow regime.

Knudsen diffusion occurs in the gas phase through the pores in the membrane layer having diameters smaller than the mean free path dimensions of the molecules in the gas mixtureeither by concentration or by pressure gradients.[74] As a result, the movement of molecules inside the narrow pore channels takes place through collision of the diffusing molecules with the surface rather than with each other. The relative permeation rate of each component is inversely proportional to the square root of its molecular weight. According to Knudsen diffusion, N_2 molecules preferentially permeate in the case of CO_2/N_2 separation. The selectivities of CO_2 with respect to N_2, CH_4, and H_2 by Knudsen diffusion will be 0.8, 0.6, and 4.7, respectively.[61] Hence, the selectivity of CO_2 achievable by the Knudsen mechanism is very low and not attractive in this particular gas mixture.

According to Knudsen diffusion mechanism, the diffusive selectivity can be defined as:

$$\frac{D_i}{D_j} \propto \sqrt{\frac{MW_i}{MW_j}} \qquad \text{-------- Equation (2.4)}$$

Where, D_i, and D_j are the diffusion coefficients of i and j, and MW_i and MW_j are the molecular weight of component i and j

In the surface diffusion mechanism, the diffusing species adsorb on the walls of the pore, and then readily transport across the surface in the direction of decreasing surface concentration. Typically, the molecules with larger molecular weight and with larger polarity and polarizability are selectively adsorbed on the membrane surface.[75] The adsorbed species on the membrane pores can also drastically reduce the transport of other species across the pore by reducing the size of accessible void space through the pore. This hindrance effect introduces non-adsorptive separation selectivity for the adsorbed species when the pore size is between 2 to 3 molecular diameters of the adsorbed species. The concentration of adsorbed species depends upon the temperature, pressure, and the nature of the surface. Interaction between a gas and the pore can also be introduced by modification of adsorbent layers.

Surface diffusion coefficient,[76] $D_s = (P_s K_s^2)/\rho(1 - \epsilon)(C - C_0)$ -------- Equation (2.5)

Where, P_s = surface permeability, K_s = tortuosity factor, ρ = density of the adsorbent, ϵ = porosity and $C - C_0$ = concentration gradient

Multilayer diffusion occurs when species adsorb in several layers. A gas mixture permeates through the pores of membranes; vapor species condense in the pores at a pressure lower than the saturation pressure at a given temperature. The multilayer diffusional flux is much larger than the gas phase flux.[77] The second important aspect is

that by capillary condensation a pore is blocked by condensate, preventing gas transport

of other components of the gas mixture. Both aspects can result in increased selectivities.

The condensation pressure depends on the pore size and shape and also the strength of

the interaction between the fluid and pore walls.[78]

A. Knudsen diffusion

B. Surface diffusion

C. Capillary condensation

D. Molecular sieving
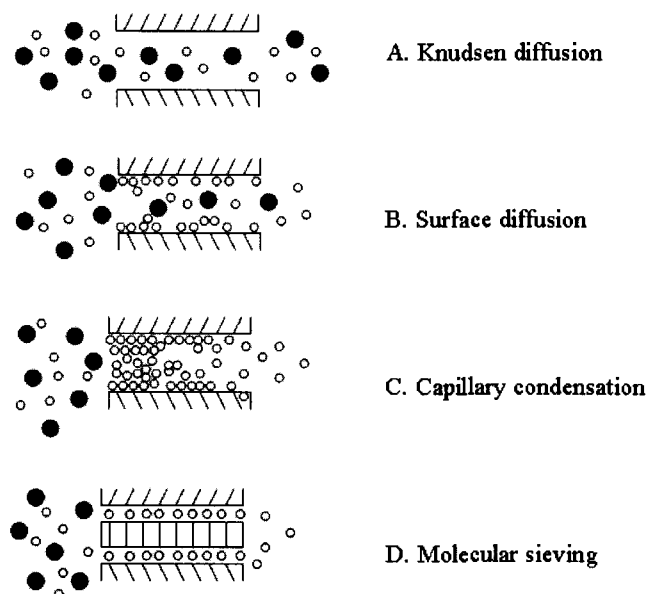
Figure 2.5. Schematic representation of the different possible mechanisms for membrane gas separation.[61]

According to the molecular sieving mechanism, the separation is caused by

passage of smaller molecules of a gas mixture through the pores of porous inorganic

membranes, while the larger molecules cannot enter into this pores.[79] But a very fine-

tuning of the membrane pore sizes is required to achieve the desired separation

efficiency.

All the inorganic membrane materials can be divided into two main groups: a)

zeolite membranes; and b) Metal and metal oxide membranes.

2.4.2.1. Zeolite membranes

Zeolite membranes have been extensively studied because of their higher thermal and chemical resistance as compared to polymeric membranes.[80] The separation ability of a microporous membrane can be described by the interplay of the mixture adsorption equilibrium and the mixture diffusion in a way similar to the solubility-diffusion model established for dense organic polymer membranes.[81] The first commercial application is that of LTA zeolite membranes for solvent dehydration by pervaporation.[82] The reasons for this limited applicationin industry might be due to economic feasibility and poor reproducibility. The rapidly growing progress in the field of zeolite membranes is reflected by some recent reviews.[83-90] New ways of synthesis, improved permeation tests, and proper applications shall improve the zeolite membranes for their technical use.

A zeolite membrane can be prepared as a single crystal[91] or as a self-supported film,[92] but typically, it is prepared as a continuous polycrystalline layer on a porous support to ensure mechanical strength.[93] Various porous materials have been used as supports for depositing zeolite membranes, and among them, porous alumina[93] or stainless steel supports[94] are most common. The flow resistance is an important factor in choosing a support, especially for thin zeolite layers. Asymmetric supports with good strength and low flow resistance are preferred. The geometry of the support is also an important consideration. A disc is easier to usethan a tube for preparation of zeolite membranes, but a tube has a higher surface area to volume ratio.

Secondary growth of a supported seed layer is an effective approach for the formation of consolidated supported membranes with good quality and reproducibility and to better control the membrane thickness and orientation, nucleation and crystal

growth.[95] Seeding consists in the deposition of the crystal seeds on the surface of a support, followed by a crystal growth by means of a hydrothermal treatment.[96] The advantage of the membranes made by secondary growth is the high flux and the possibility to orient the seed crystals.[97] The drawback is the ease of formation of defects or non-zeolitic pores. In an interesting one-step method (pore-plugging synthesis) zeolite crystals are grown within the pores of a macroporous support, yielding very robust, defect-free membranes, whose permeance however is not very high.[98] To obtain higher fluxes, the penetration of the gel into the support should be inhibited. Hedlund et al. used a masking technique to plug the support pores during zeolite membrane synthesis by coating a poly(methyl methacrylate) (PMMA) layer on the support surface.[99]

Pre-seeding the support with zeolite nanocrystals is a convenient way of circumventing the complex processes involved in the early formative stage of zeolite and allows the direct measurement of zeolite crystal growth.[100] Most of the porous supports used in the preparation of zeolite membranes are made of sintered crystalline particles and are inherently heterogeneous. Some supports like the stainless steel, are alloys and contain several structural phases. The heterogeneous nature of the support material contributes to the poor reproducibility of the zeolite membranes prepared by in situ method. Chau and coworkers[101] has demonstrated that pre-seeding the support with colloidal zeolites can significantly reduce the influence of the support. For the silicalite-1 (Sil-1)/porousSS-316L membranes, this simple method had led to better reproducibility in both the deposited microstructure and separation properties of the membrane.

The synthesis gel for making zeolites is usually composed of water, a precursor for tetrahedral framework atoms such as Si and Al, and a structure directing agent.

Because of the high alkalinity of the gel and the high reaction temperature, the alumina support can dissolve into the reactive solution, altering the gel composition. Therefore, when using alumina supports for synthesizing zeolite membrane, we need to consider its effect in membrane formation.[102] During in-situ crystallization, zeolite crystals nucleate and grow on the support surface by placing the support in direct contact with the alkaline precursor gel under hydrothermal conditions. In order to reduce the number and size of inter-crystalline voids, most zeolite membranes are prepared with more than one hydrothermal synthesis layer.

Zeolite membrane synthesis is influenced by numerous factors, such as synthesis gel/solution composition, ageing and pH of the gel, hydrothermal temperature, time, chemical and structural nature of the support, position of the support, and nature of the autoclave. Zeolite membranes are often prepared under conditions similar to zeolite powder synthesis, and these conditions might not be optimal for membrane formation. For membrane synthesis, the critical problem is not forming a zeolite film, but controlling film thickness, orientation of crystals, and the number and size of defects.

Recently, microwave heating for synthesizing zeolite seeds[103] and zeolite membranes[104] has been studied. Microwave heating enables a direct and fast energy input into zeolite reaction mixtures, thus drastically reducing the crystallization time.[105] All the studies reported demonstrate that microwave syntheses take considerably less time than conventional hydrothermal techniques, to well over an order of magnitude shorter.[106]

By tailoring the chemistry and structure of the materials used to prepare them, synthetic zeolites can be modified to provide a wide range of desired adsorption

characteristics or selectivities. In order to improve the performance of zeolites as molecular sieves, several techniques have been developed to change the zeolite pores by modifying the zeolite framework,[107] using cation exchange,[108] or pre-adsorbing strongly adsorbed molecules.[109] Pore modification of the widely used zeolites could be one good way to achieve high separation selectivities for small size molecules.[110] Post-synthetic silylation and coking have been used to block defects in zeolite membranes.[111] Ion exchange on NaX and NaY zeolites could tune their adsorptive properties for carbon dioxide.[112] The CO_2/N_2 separation selectivity increased when NaY membranes were exchanged with K+, Rb+, and Cs+, and the selectivity decreased when a NaY membrane was exchanged with Li+.

In zeolite membranes, both molecular sizes relative to the pore size,[113] and the relative adsorption strengths[114] determine the faster permeating species in a binary mixture. Poshusta et al. identified three separation regimes where both components are able to diffuse through the zeolite pores.[19] The first regime covers differences in diffusivity, where there is a difference in the size of molecules, but both molecules have similar adsorption strengths and the higher selectivity will be observed for the smaller molecule. The second regime is competitive adsorption, in which both molecules have similar sizes, but differ in their adsorption strengths. The molecules will be competing for the same adsorption site within the zeolite pore. The strongly adsorbing molecule will not spare many adsorption sites for the weakly adsorbing molecule, and thus the higher membrane selectivity will be observed for the strongly adsorbed molecule in this regime. The third regime is combined differences in diffusivity and competitive adsorption.

Carbon dioxide strongly adsorbs on zeolites because it has the strongest electrostatic quadrupolar moment (4.30×10^{-26} esu· cm^2), which significantly contributes to its attraction to polar surfaces.[115] CO_2 preferentially permeates in CO_2/N_2, CO_2/CH_4, and CO_2/H_2 mixtures at low temperatures, because CO_2 adsorbs more strongly on zeolites than the other gases. For the CO_2/N_2 and CO_2/CH_4 mixtures, CO_2 is smaller in size and thus permeates faster and separated by the third regime at lower temperatures, where differences in diffusivity and competitive adsorption combine to enhance the separation factor. At higher temperatures, the CO_2/N_2 or CO_2/CH_4 mixture is separated by the first regime, due to only differences in diffusivity. A tradeoff exists between flux and selectivity, and as additional zeolite layers are added to a membrane to seal defects, the membrane has more transport resistance.

Because CO_2 (~0.33 nm kinetic diameter) is smaller than CH_4 (~0.38 nm), small-pore zeolites, whose pore sizes are close to that of CH_4 molecules, can effectively separate CO_2/CH_4 mixtures.[116] In particular, silicoaluminophosphates such as SAPO-34 with pore size of ~0.38 nm,[18] aluminosilicates such as zeolite Linde type T with pore size of ~0.41 nm,[117] silicalite-1 with pore size of ~0.55 nm[118] and DD3R with pore size 0.36 x 0.44 nm[119] can be used to separate CO_2 from CH_4. These small-pore zeolite membranes have high CO_2/CH_4 selectivities due to a combination of differences in diffusivity and competitive adsorption.

Table 2.1. Comparison of the zeolite membranes for CO_2/CH_4 gas separations

Membrane	CO_2/CH_4 selectivity	CO_2 permeance $(x10^7)$ $(mol/m^2.s.Pa)$	Reference
Polymeric	---	---	Figure 2.6[73]
FAU (NaY)	20	1.0	Kusakabe et al. 1997[120]
FAU (KY)	40	7.0	Hasegawa et al. 2002[121]
Linde type T	400	0.4	Cui et al. 2004[117]
DD3R	500	0.6	J. Van den Bergh et al. 2008[119]
Silicalite-1	23	7.0	Guo et al. 2006[118]
SAPO-34	30	0.2	Poshustaet al. 1998[122]
SAPO-34	67	1.6	Li et al. 2004[18]
SAPO-34	115	4.0	Li et al. 2006[20]
SAPO-34	171	18.0	Carreonet al. 2008[21]

The separation performance of relevant membranes for CO_2/CH_4 gas mixtures is summarized in Table 2.1. As shown in Figure 2.4, the polymeric membranes performance is lower than the upper bound of the Robinson plot.[73] Zeolite NaY,[120] KY[121] and silicalite-1[118] membranes showed either low CO_2/CH_4 selectivity or low CO_2 permeance. Zeolite T[117] and DD3R[119] membranes showed very high selectivities, but very poor permeances. SAPO-34 showed average CO_2/CH_4 separation performance initially[18, 122, 20] and extensive research resulted in high CO_2/CH_4 selectivities and CO_2 permeances[21]

compared to the other zeolite and polymeric membranes. To the best of our knowledge, SAPO-34 is known to be the best zeolite material available for CO_2/CH_4 separation.
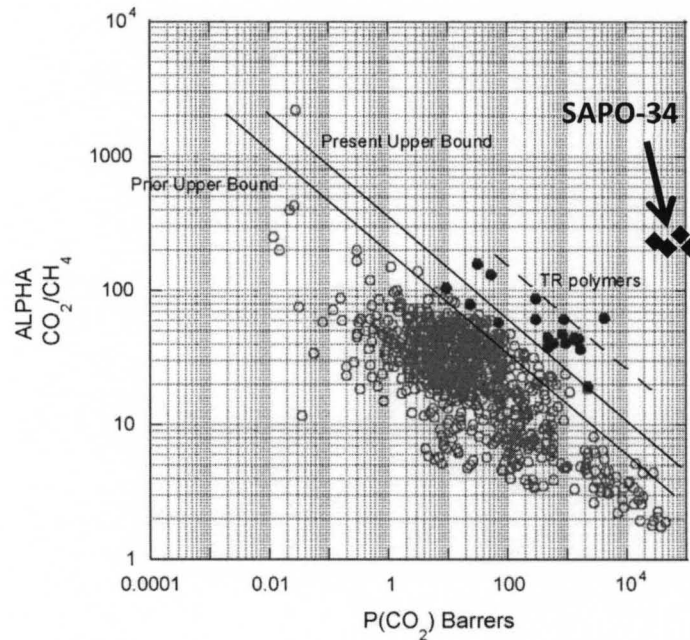
Figure 2.6. Comparision of SAPO-34 membranes with the reported polymeric membranes.

The first composite membrane using SAPO-34 zeolite was synthesized in 1997.[123] In 1998, pure SAPO-34 membrane was prepared using alumina supports.[122] In later studies, the SAPO-34 membranes were synthesized using different supports and their ability to separate CO_2/CH_4, CO_2/N_2, N_2/CH_4, H_2/CH_4, H_2/CO_2, and H_2/N_2 binary mixtures was reported. The effect of impurities[124], temperature[22] and humidity on the stability of SAPO-34 membrane[125] was studied and reported that SAPO-34 membrane is stable under extreme and industrial conditions. As shown in Figure 2.6, SAPO-34 membranes perform much better than any existing polymeric membranes for CO_2/CH_4 separation.[23]

Extensive work has been published on SAPO-34 membranes for the separation of CO_2 from various light gases. In 1997, Zhang *et al.* synthesized for the first time SAPO-34 membranes on alumina disks and reported CO_2/N_2 and H_2/N_2 separation performance.[123] Most of the relevant work done on SAPO-34 membranes for CO_2 separation has been reported by Falconer and Noble research groups.[122,20,21,124,22,23,126-131] In particular, these groups have demonstrated the successful synthesis of high performance SAPO-34 membranes able to efficiently separate CO_2/CH_4 gas mixtures. Recently independent research groups have reported SAPO-34 membranes for CO_2 purification, prepared via microwave,[132] on macroporous supports,[133] as mixed matrix membranes[134] and on tubular supports.[135] Because SAPO-34 membrane is an inorganic oxide and the underlying support is ceramic or metal, these membranes are far more robust than conventional polymeric membranes and can be usable in high-pressure environments.

2.4.2.2. Metal and Metal Oxide membranes

Metal oxide ceramic membranes have a greater chemical stability, since they are resistant to organic solvents, chlorine, and extremes of pH, to which organic membranes may be susceptible.[136] Different types of metal and metal oxide membranes, such as carbon molecular sieves, alumina, silica, palladium etc., have been reported for gas separation.

Carbon molecular sieve membranes have a very long history. As early as 1955 Barrer and Strachan produced a pioneering work on the adsorption and the diffusion of gases in microporous plugs made of compressed, high specific surface carbon powder,

evidencing the importance of surface flow for the most polarizable species.[137] Extensive studies were carried out on the preparation of carbon molecular sieve membranes from both rubbery and glassy polymers. One major disadvantage that hinders their commercialization is their brittleness, making them require a careful handling. This may be prevented to a certain degree by optimizing precursors and preparation methods. Other disadvantages are aging and pore blocking by higher organics. Hinds et al. reported the synthesis of free-standing and silicon-chip supported vertically aligned carbon nanotubes membranes by complex multistep synthesis procedures.[138] The use of single-walled carbon nanotubes (SWNT) with smaller diameter as membranes is particularly interesting because, in addition to fast transport rates, the 4-12 Å pore openings might be size-selective for gas mixtures.[138] However, alignment to the penetrant stream is a challenge.

Mesoporous alumina membranes have been also widely used for gas separation applications.[139] The mesoporous structure of alumina dictates that transport within the membranes takes place by a Knudsen diffusion mechanism. Since selectivity in this regime is limited, and the rate of diffusion is controlled by molecular weight, alumina membranes are of limited use in the separation of gases. With mixtures such as CO_2/N_2, where the gases have similar mass, and CO_2/H_2, where selectivity toward the heavier component is required, alumina is undesirable as a membrane material.

Silica is considered a viable starting material in the fabrication of CO_2 selective membranes, primarily because of its innate stability and flexibility in structure modification.[140] Unlike alumina, which tends to undergo phase transition at relatively low temperatures, or carbon, which can exhibit substantial changes in pore size in oxidizing environments, silica shows exceptional thermal, chemical, and structural stability in both

oxidizing and reducing environments. Generally, microporous silica membranes are prepared by deposition of a silica layer onto a porous support by either the sol-gel method,[141] or chemical vapor deposition (CVD) technique,[142] or phase separation method.[143]

The most studied metal membrane for gas separation is palladium. Pd membranes have been prepared by depositing palladium on a porous support. These palladium membranes are highly selective to hydrogen.[144] Therefore, these membranes have applications in the separation of carbon dioxide and hydrogen. Besides Pd and its alloys, other metals such as tantalum, niobium, and vanadium also have high selectivities.[61] The disadvantages of this type of membranes are high cost, low permeabilities, brittleness, and susceptibility to poisoning. The low permeability across the dense inorganic membranes limits its intended applications, compared to porous inorganic membranes.

2.4.2.3. Mixed matrix membranes

Nonporous polymeric membranes give high selectivity but poor permeability. On the other hand, porous inorganic membranes give high permeability but poor selectivity. For better results, both selectivity and permeability in a membrane should be balanced. Hybrid materials in which polymers and ceramics are dispersed at a molecular level have been investigated as gas separation membranes.[145] Mixed matrix materials, typically, comprised of molecular sieving materials embedded in a polymer matrix, have potential to provide economical, high performance gas separation membranes if defects at the molecular sieve/polymer interface can be eliminated.[61] A combination of the sol-gel reaction and polymerization is used to synthesize the hybrid material. Resulting hybrid

materials present the advantages of each material; for example, the flexibility and selectivity of polymers and thermal stability of ceramics. Among these hybrid materials, polyimide-silica materials have received the most attention for the gas permeation studies. Additionally, careful matching of the intrinsic permeability and selectivity of the support matrix and the molecular sieve domains is necessary.

Jia et al. were the first to investigate zeolite-filled rubbery polymer membranes composed of PDMS, a rubbery polymer, and a hydrophobic zeolite, silicalite-1.[146] It was concluded that the silicalite played the role of molecular sieve in the membrane by facilitating the permeation of smaller molecules but hindering the permeation of larger ones, although its pore openings were larger than the size of the permeating gases. It was suggested that the shape-selective effect was not only inherent in the equilibrium adsorption of gas molecules, but also in the kinetic adsorption and diffusion. Kulprathipanja et al. found that mixed matrix membranes comprised of cellulose acetate and silicalite-1 have improved characteristics as the silicalite content increases.[147] They obtained the CO_2/H_2 separation as high as 10 from the mixed matrix membranes for an equimolar feed of CO_2 and H_2. CO_2 molecules have the ability to interact with the polar surface of zeolite during permeation and, hence, CO_2 permeability and permselectivity increase considerably with increasing zeolite loadings in the mixed matrix membranes. Okui et al. prepared porous hybrid membranes from monoalkyltrimethoxysilane using the sol-gel technique.[148] They introduced some functional groups, such as methyl, propyl, 3-chloropropyl, octadecyl, 3,3,3-trifluoropropyl, and phenyl, to study the effect of CO_2 permeability properties of the resulting materials. The permeance of gases increased with increasing temperature and, therefore, the permeation of hybrid membranes was governed

by the dissolution-diffusion mechanism through the polymeric zone in the membrane. While hybrid membrane research has been considerably more limited than that on the other types of membranes discussed, interesting results have been achieved particularly in the separation of CO_2/CH_4 mixtures.

2.5. Metal organic framework membranes

In the last years a new class of porous crystalline materials namely, metal-organic frameworks (MOFs), have attracted the attention of the scientific community. Metal organic frameworks are crystalline materials that can be tailored to specific applications through varying the metals, ligands, and linkers.[149] They can be synthesized inexpensively, relatively easy, in high purity, and in a highly crystalline form. These materials cover a much wider range of pore sizes than zeolites, even bridging micro and mesoporous materials. The combination of organic and inorganic building blocks offers an almost infinite number of variations, enormous flexibility in pore size, shape, andstructure, and myriad opportunities for functionalization and grafting.

MOFs can be considered as three-dimensionally structured coordination metal complexes, in which the metal ions are connected to the ligands through covalent coordination bonds.[149] The key to their success is the appropriate design of molecular building blocks to obtain the desired structure and properties. MOFs and zeolites alike are produced almost exclusively by hydrothermal or solvothermal techniques. The main properties of MOFs are ordered structures, the presence of channels or cavities with defined shapes and dimensions, a large surface area, and in some cases, peculiar lattice flexibility. Due to these properties, MOFs are very attractive materials for their potential

applications[150] in catalysis, gas storage, ion exchange, separation, and polymerization, as compared to "classic" porous materials, such as zeolites and active carbons.

A variety of studies are available examining gas adsorption and storage in MOFs, particularly for carbon dioxide, methane and hydrogen.[151] These materials have the highest adsorption capacities, specific surface areas, and pore volumes compared to zeolites and other inorganic materials.[152] Their thermo-stability is sometimes unexpectedly high, reaching temperatures above 400C. There is tremendous interest in these new materials, but the major studies deal with synthesis, while the majority of applications focus on adsorption, separation, sensors and storage.

If one thinks in terms of membranes, the highly accessible porosity infers high fluxes, while the wide range of pore sizes would make it possible to tackle classical, extremely important separations[153] such as the separation of hydrogen from other gases, the removal of CO_2, the separation of alkanes from alkenes, linear from branched alkanes, and mixtures of aromatic isomers, as well as the separation of larger molecular isomers. The development of MOF-based membranes is challenging, and recently the first gas-mixture separations were achieved.[154] The main problem in synthesizing these membranes is the intergrowth between the support and the crystals. Modification of the interaction needs to be done to get highly robust and selective membranes.[155] High flexibility will impose limits on the molecular sieving, but, on the other hand, may be more forgiving towards differences in thermal expansion between support and selective layer, thus precluding crack formation at elevated temperatures.[153] Future applications of MOF membranes will also depend on the reproducibility of the synthesis and on the applicability of the conditions to the preparation of other MOF topologies. Robust

synthetic strategies can be developed that will allow the facile synthesis of continuous MOF membranes.
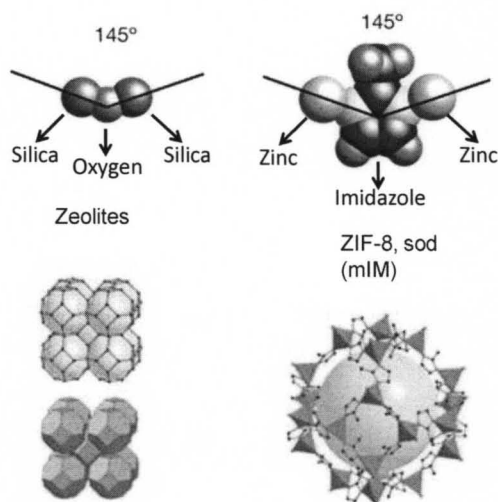
Figure 2.7. Comparision between zeolites and zeolitic imidazolate frameworks and examples of their structures.

Zeolite imidazolate frameworks (ZIFs), a subclass of MOFs, have emerged as a novel type of crystalline porous material which combines highly desirable properties from both zeolites and MOFs, such as crystallinity, microporosity, high surface areas, and exceptional thermal and chemical stability,[156-160] as described in Chapter 1. In ZIFs, metal atoms such as Zn, Co, and Cu are linked through N atoms by ditopic imidazolate (Im) or functionalized Im links to form neutral frameworks and to provide tunable nanosized pores formed by four-ring and six-ring ZnN_4, CoN_4, and CuN_4 clusters.[161,162,156-159, 163,164] The framework of ZIF compounds closely resemble the framework of zeolites, i.e the T-O-T bridges (T = Si, Al, P) in zeolites are replaced by M-Im-M bridges (M = Zn, Co, Cu) and coincidentally, their bond angles in both structures are 145° as shown in Figure 1.11.[162] Emerging functional applications of ZIFs in gas separations,[165-168] catalysis,[169,170] and sensing[171] have been recently reported.

In particular, ZIF-8 is one of the most studied prototypical ZIF compounds,[163,164,165,166] due to its potential functional applications in gas storage, catalysis and gas separations.[167-171] ZIF-8 has large pores of 11.6 Å which are accessible through small apertures of 3.4 Å and it has cubic space group (I-43m) with unit cell dimensions of 16.32 Å. It has sodalite (SOD) zeolite-type structure with about two times larger pore sizes than the corresponding SOD zeolites. Due to its highly porous open framework structure, large accessible pore volume with fully exposed edges and faces of the organic links, pore apertures in the range of the kinetic diameter of several gas molecules and high CO_2 adsorption capacity, ZIF-8 is highly attractive for gas separation applications. Several studies revealed that ZIF-8 with hetero-links have pores that can affect exceptional selective capture and storage of CO_2 and it shows the highest adsorption selectivity for capture of CO_2 from binary mixtures with methane, nitrogen, and oxygen. Based on all these properties, ZIF-8 is an appealing material for natural gas purification and landfill gas separation. ZIFs, based on an imidazolate linker and metallic centers, can form symmetrical porous structures analogous to zeolites. Thermally and chemically stable ZIF-8 particles have been synthesized by solvothermal methods and synthesis times up to 1 month,[163] 1 day[161] and 1 hr,[164] employing diverse gel compositions and synthesis conditions. ZIF-8 crystals with narrow particle size distribution and sizes from microns (~150 μm)[161] to nanometers (~ 50 nm)[164] and surface areas in the 900 – 1600 m²/g [161] range have been reported. So it is important to study the formation mechanism of ZIF-8 in order to understand its growth and to improve its properties for different applications.

CHAPTER 3

EXPERIMENTAL APPROACH

One of the main goals of this work is to decrease the crystal size of SAPO-34

seeds and improve its carbon dioxide adsorption capacity. In principle, small crystals

with high carbon dioxide adsorption capacity will result in thinner membranes able to

selectively separate CO_2 from light gases. We employed two main techniques to prepare

small SAPO-34 seeds displaying narrow size distribution: crystal growth inhibitors and

microwave hydrothermal treatment. To increase the CO_2 adsorption capacity, SAPO-34

was functionalized with organic amino cations. The SAPO-34 membranes were tested for

CO_2/CH_4 and CO_2/N_2 gas separation. Another main objective of this work is to develop

new materials to be prepared as membranes. A particular type of metal organic

framework, ZIF-8 (zeolitic imidazolate framework-8) was prepared as seeds and

membranes. In this chapter, we describe in detail the synthesis procedure of SAPO-34

and ZIF-8 seeds and membranes as well as techniques employed to characterize and

evaluate these seeds and membranes. Finally we present the separation performance of

the resultant membranes for CO_2/CH_4 and CO_2/N_2 gas mixtures.

3.1. SAPO-34 seeds employing crystal growth inhibitors

Aluminum isopropoxide ($Al(i-C_3H_7O)_3$, >99.99% metal basis, Aldrich),

phosphoric acid (85 wt% aqueous solution, Sigma-Aldrich), and Ludox (40 wt%

insuspension, Sigma-Aldrich) were used as the inorganic precursors.

Tetraethylammonium hydroxide (35 wt%, Sigma-Aldrich) and dipropylamine (99 wt%, Aldrich) were used as the primary and secondary structure-directing agents (SDA) respectively. The crystal growth inhibitors (CGI) used in the synthesis was polyethylene glycol-600 (Alfa Aesar), polyoxyethlene lauryl ether (Acros Organics) and methylene blue (Sigma-Aldrich), as shown in Figure 3.1. In a typical synthesis, aluminum isopropoxide, phosphoric acid and H_2O were mixed and stirred for about 2hr to form a homogeneous solution. Then Ludox was added and the resulting solution was stirred for another 2 h. The primary and secondary templates were added to the precursor solution and stirring continued for another 30 min before crystal growth inhibitors were added in the desired molar ratio. The composition of the gel was $1Al_2O_3:1H_3PO_4:0.3SiO_2$: $1TEAOH:1.6DPA:77H_2O$: xCGI, where $0.037 < x < 0.2$. The final resulting gel was aged for 3 days while stirring at 50^0C, since aging improves control over zeolite nucleation by depolymerizing ludox and forming the germ nuclei or even complete nuclei.[172] The homogeneous gel was transferred to a Teflon lined stainless steel autoclave (Parr Instrument Company) and heated under autogenous pressure in static condition in conventional oven at 220^0C for 24 hr as shown in Figure 2.2.

Polyethylene Glycol
$H(OCH_2CH_2)_nOH$
Size ~ 3.93 nm

Brij-35
$C_{12}H_{25}(OCH_2CH_2)_nOH$
Size ~ 4 nm

Methylene Blue
$C_{16}H_{18}N_3ClS$
Size ~ 1.6 x 0.7 x 0.37 nm
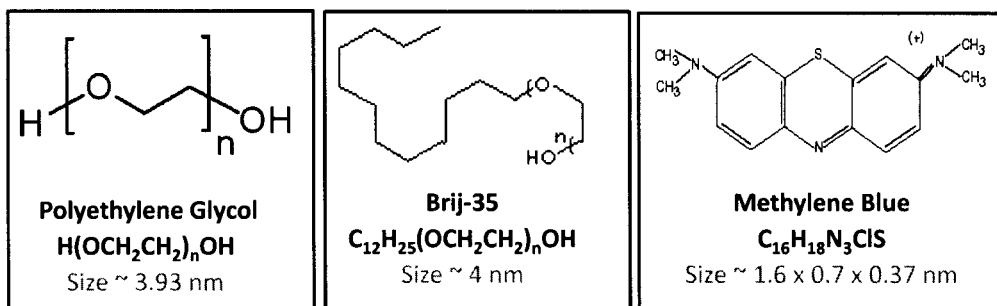
Figure 3.1. The crystal growth inhibitors (CGI) used for SAPO-34 seeds synthesis

Alternatively, hydrothermal treatment was also done using controlled temperature ramp. After the gel was cooled to room temperature, it was centrifuged at 4000 rpm for 20 min to separate the seeds from the mother liquor. The resultant precipitate was washed with water. The centrifugation-washing process was repeated 3 times. The resultant precipitate was dried overnight at 60^0C. The as-synthesized samples were calcined at 550^0C for 5 hrs with heating and cooling rates of 1^0 and 10^0C/min respectively to remove both the structure-directing agents and the retained crystal growth inhibitors.
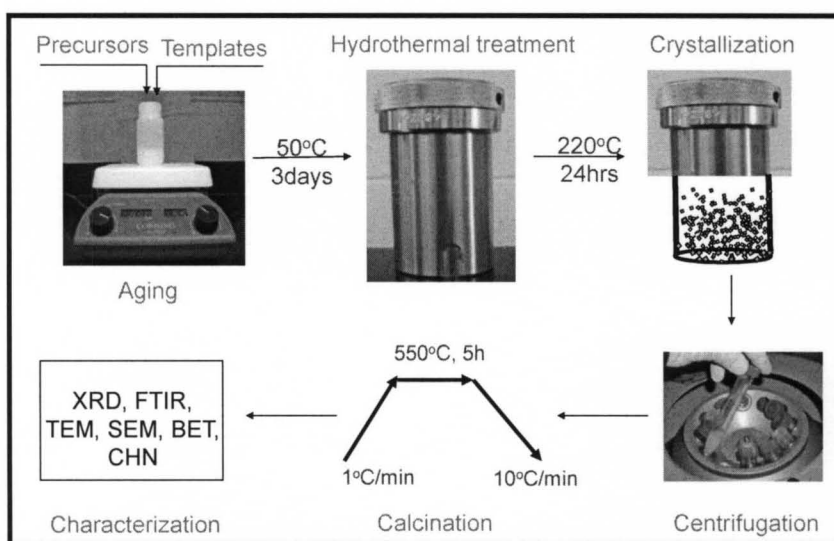
Figure 3.2. SAPO-34 seeds synthesis procedure using hydrothermal method

The SAPO-34 seeds were synthesized with two different molar ratios for each CGI to study the effect on the structural properties of SAPO-34. One reference SAPO-34 was also synthesized without CGI. All the samples were prepared hydrothermally at 220^0C for 24 hrs in conventional oven. Hydrothermal synthesis for some samples was done using a temperature controlled furnace i.e. increasing temperature at 1^0C/min from room temperature to 125^0C and holds it for 5 h at 125^0C, then increased to 220^0C at 1^0C/min and holds it for 15 h. It is well known that the size of the final crystal size

46

depends on the nucleation process. In principle, holding the gel temperature at 125^{0}C, favors the formation of more nuclei; then the increase in temperature results in smaller crystals.

3.2.   Synthesis of SAPO-34 seeds using microwave heating

An alternative approach to decrease the SAPO-34 crystal size is to direct the synthesis via microwave heating. The synthesis gel composition was 1Al$_2$O$_3$:1H$_3$PO$_4$:0.3SiO$_2$:1TEAOH:1.6DPA: 77H$_2$O, which is prepared using the same method as above. The gel was transferred to a glass tube and MW heating for different times was carried out with continuous stirring in a computer controlled MW oven (Mars 5, CEM corp.) at 150°C and 250 psi. After cooling, the product was separated using centrifugation and dried overnight at 60°C. The dried samples were calcined at 550°C for 5 h with heating and cooling rates of 1°C/min to remove the organic templates.

3.3.   Synthesis of SAPO-34 membranes

SAPO-34 membranes were prepared by secondary seeded growth inside tubular porous stainless steel supports (0.1 grade, 0.27-μm pores, Mott Corporation). The synthesis gel preparation and molar ratios were the same we employed for SAPO-34 seeds synthesis. The membranes were prepared by rubbing the inside surface of porous supports with dry, calcined SAPO-34 seeds using cotton swabs. The rubbed porous supports, with their outside wrapped with Teflon tape, were then placed vertically in an autoclave and filled with synthesis gel. The hydrothermal treatment was carried out at 493 K for 24 h. The resulting membranes were washed with deionized water and dried overnight at 343 K. The membranes were calcined using a computer-controlled muffle furnace at 673 K for 8 h in atmospheric air to remove the organic templates from the

SAPO-34 framework. The calcination heating and cooling rates were 0.7 K/min and 0.9 K/min respectively. The calcined membranes were stored at 473 K.

3.4. Functionalization of SAPO-34 seeds and membranes

The SAPO- 34 seeds were functionalized via ion-exchange with ethylene diamine (ED), hexylamine (HA) and octylamine (OA). The ion-exchange step was performed refluxing the corresponding amine in toluene. Specifically, the toluene with a known amount of amine was placed in a 50 ml flask and heated using a hot plate to 378 K while stirring. Then 0.5 g of SAPO-34 were added. In the case of membranes, the support was immersed in the amine-toluene solution. The exchange was performed under vigorous stirring at 378 K for 18 h under refluxing conditions.

3.5. Synthesis of ZIF-8 seeds

3.5.1. Room temperature synthesis

In a typical synthesis, 0.3 g of zinc nitrate hexahydrate, $(Zn(NO_3)_2 \cdot 6 \, H_2O$, Fluka, $\geq 99\%)$ were dissolved in 11.3 g of methanol (Acros Organics, extra dry, water <50 ppm). A solution consisting of 0.66 g of 2-methylimidazole $(C_4H_6N_2$, Aldrich, 99%) and 11.3 g of methanol was added to the Zn based solution and vigorously stirred for different times. This gel composition corresponds to that reported earlier.[164] The resultant particles were separated from the gel by centrifugation at 4000 rpm and washed with methanol. This procedure was repeated 3 times. The resultant ZIF-8 powder was dried overnight at 75°C.

3.5.2. Solvothermal synthesis

The same composition synthesis gel as above was used for the solvothermal synthesis of ZIF-8 seeds. After adding the zinc salt and imidazole to methanol solvent, the solution was transferred to a Teflon lined stainless steel autoclave and treated

solvothermally at 150°C for 5 hrs. The resultant particles were separated by centrifugation at 4000 rpm and washed with methanol and dried overnight at 75°C.

3.6.   Synthesis of ZIF-8 membranes

ZIF-8 membranes were prepared inside tubular α-alumina supports (0.2 μm pores, US Filter) by secondary seeded growth. Before synthesis, about 1 cm on each end of the supports was glazed (Duncan 1001N) to prevent membrane bypass and to provide a sealing surface for O-rings. The permeate area was ~5.1 cm^2. The glazed supports were calcined at 900°C for 30 min with controlled heating and cooling rates of 1°C/min and boiled at 100°C for 1 hr and dried overnight at 100°C. Membranes were prepared by rubbing the inside surface of the support with dry ZIF-8 seeds and outside wrapped with teflon tape. The supports were then placed in a teflon lined stainless steel autoclave and filled with the synthesis gel and treated hydrothermally at 150°C for 5 hr.

Glazing
the supports

Rubbing
with seeds

Outside wrapped
with teflon

Membrane

Hydrothermal synthesis
At 150°C for 5 h
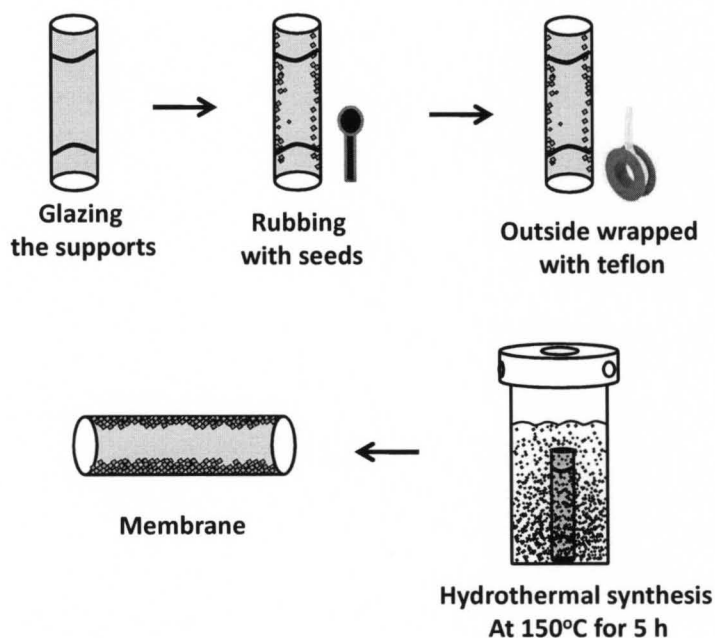
Figure 3.3. Procedure for the synthesis of ZIF-8 membranes using α-alumina supports

After solvothermal treatment, the membrane was washed with deionized water and dried for 2 hrs at 100°C. A second layer was applied similarly by placing the support in opposite direction for uniformity. Then, the double layered membrane was washed with deionized water, dried and stored at 100°C before separation experiments. Multiple layers were applied to form continuous membranes. Figure 3.3 shows the schematic of the synthesis of steps for the preparation of ZIF-8 membranes. The separation performance of the ZIF-8 membranes for equimolar CO_2/CH_4 gas mixture was measured in a separation system shown in Figure 4.1. In all separation experiments, the pressure drop was 40 KPa, permeate pressure was 99.5 KPa (atmospheric pressure) and the feed pressure was 139.5 KPa. The total feed flow rate was 200 mL/min.

3.7. SAPO-34 and ZIF-8 seeds and membrane characterization

Powder X-ray diffraction patterns were collected using a Bruker D8-Discover diffractometer at 40 kV, 40mA with Cu Kα radiation. The particle size of SAPO-34 and ZIF-8 was determined using FE-SEM (FEI Nova 600) with an acceleration voltage of 6 kV. TEM images and diffraction patterns were taken on a Technai F20 FEI TEM using a field emission gun, operating with an accelerating voltage of 200 kV. ZIF-8 is highly sensitive in the TEM electron beam. For this study, low-dose imaging conditions were employed using increased spot size and diverged beam to reduce the radiation damage. Fourier-transform infrared spectra of samples were measured using BX FTIR (Perkin-Elmer) system. The surface area and adsorption-desorption isotherm measurements were carried out on MicromeriticsTristar 3000 porosimeter at 77 K using liquid nitrogen as coolant and the samples were degassed at 135 °C for 3 h before the measurements. The CO_2 and CH_4 adsorption isotherms were studied at room temperature using water as the coolant. TGA profiles were collected on a TA 2050 series thermal gravimetric analyzer (TA Instruments) with a heating rate of 5°C/min under continuous-

flow of nitrogen. The quantitative analysis of elemental carbon, hydrogen, and nitrogen were carried out using a model 440 CHN/O/S analyzer (Exeter analytical, MA). The ICP analysis was carried out on an Applied Research Laboratories ARL3410+ ICP-OES.

3.8. Separation performance
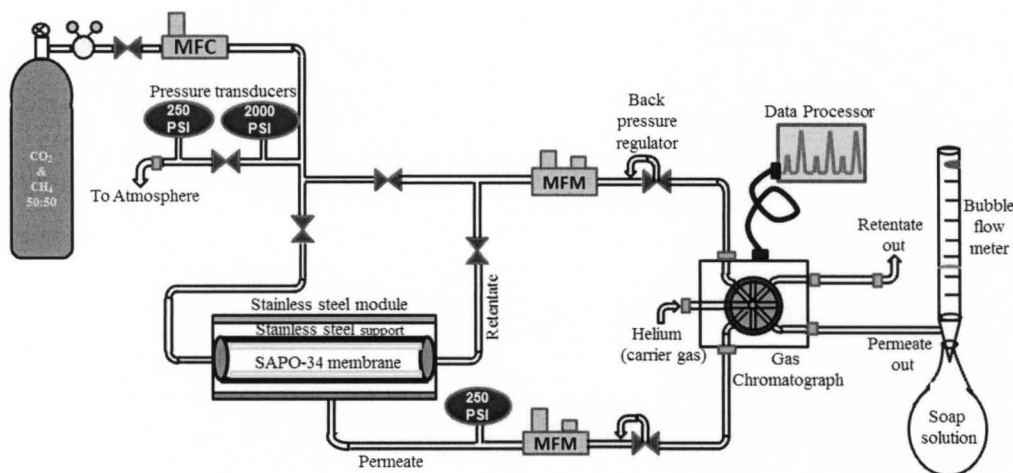
Figure 3.4. Separation system used for CO_2/CH_4 and CO_2/N_2 gas separation experiments

The separation performance of the SAPO-34 and ZIF-8 membranes for equimolar CO_2/CH_4 and CO_2/N_2 gas mixtures was evaluated in a separation system shown in Figure 3.4 and Figure 3.5. The supports used for the synthesis of SAPO-34 and ZIF-8 membranes are shown Figure 3.6. Mass flow controllers were used to mix pure CO_2, CH_4 and N_2 gases. The membranes were mounted in a stainless steel module with silicone O-rings as seals on both ends. The pressure on each side of the membrane was independently controlled. The driving force across the membrane was provided by pressure drop. In all separation experiments, the pressure drop was 138 KPa and the permeate pressure was 99.5 KPa (atmospheric pressure). The gas flux was measured by a soap film bubble flow meter. The total feed flow rate was 100 mL/min. The compositions of the feed, retentate, and permeate streams were measured, after attaining the steady

51

state, using a gas chromatograph (SRI instruments, 8610C) equipped with a thermal conductivity detector and HAYESEP-D packed column. The oven, injector and detector temperatures in the GC were kept at 65°C, 100°C and 150°C respectively. Because one component preferentially permeates through the membrane in the cross-flow configuration, the partial pressures in the feed and retentate are quite different. Therefore, a logarithm of the mean partial pressure drop was used to calculate the driving force. The separation selectivity was determined as the ratio of the permeances. The permeances were calculated as the fluxes divided by the partial pressure driving forces. The permeate pressure was 99.5 KPa.
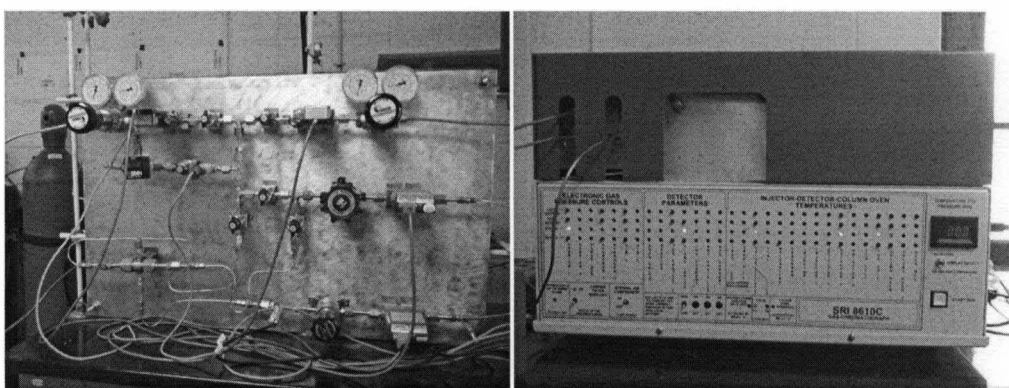
Figure 3.5. Gas separation system coupled with a gas chromatograph employed for the evaluation of SAPO-34 and ZIF-8 membranes.
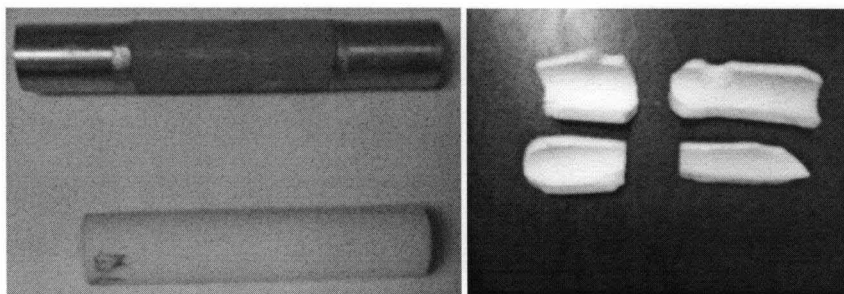
Figure 3.6. The stainless steel and alumina tubular porous supports used for the preparation of membranes and the membrane on inside surface of the support

SYNTHESIS OF SAPO-34 SEEDS USING CRYSTAL

GROWTH INHIBITORS AND MICROWAVE REACTOR

Here we describe the successful synthesis of SAPO-34 crystals by using polyethylene glycol (PEG), polyoxyethylene lauryl ether (Brij-35) and methylene blue (MB) as crystal growth inhibitors. The use of these additives resulted in higher surface area and smaller SAPO-34 crystals with narrow crystal size distribution. The influence of crystal growth inhibitors in the adsorption capacities of SAPO-34 crystals on CO_2 and CH_4 is discussed. Also, this work was to synthesize SAPO phases displaying small crystal size and narrow particle size distribution using MW heating to considerably decrease the synthesis time. Interestingly, a phase transition from SAPO-5 to SAPO-34 with prolonged MW heating time was observed. To the best of our knowledge, this is the first evidence of the preparation of SAPO-34 by phase transformation from SAPO-5 using MW assisted synthesis.

4.1. SAPO-34 seeds synthesized with crystal growth inhibitors

4.1.1. Crystal structure of SAPO-34

The BET surface area and average crystal size of SAPO-34 crystals synthesized employing crystal growth inhibitors (CGI) are shown in Table 4.1. The samples synthesized with CGI displayed higher surface areas, most likely due to their smaller

crystal size and due to the incorporation of extra microporosity in the SAPO-34 framework. Specific surface areas in the 540-700 m^2/g range were obtained when CGI were incorporated in the synthesis gel, while surface areas of ~ 500 m^2/g were obtained in the absence of CGI. With controlled heating and cooling rates of hydrothermal treatment, the surface area increased compared to the conventional heating. The highest surface area is observed for the SAPO-34 sample synthesized with Brij-35 and the increase is about 40% compared to the SAPO-34 sample synthesized without crystal growth inhibitors.

Table 4.1. BET specific surface area and average crystal size of SAPO-34 crystals synthesized using different CGI

Sample ID	Crystal Growth Inhibitor (CGI)	Mole ratio of CGI	Specific Surface Area (m^2/g)	Average Crystal Size (μm)
1	Polyethylene Glycol	0.1	645	0.7 ± 0.1
2	Polyethylene Glycol	0.2	622	0.7 ± 0.2
3	Brij-35	0.056	698	0.6 ± 0.1
4	Brij-35	0.112	633	0.7 ± 0.1
5	Methylene blue	0.037	540	0.9 ± 0.1
6	Methylene blue	0.075	563	0.9 ± 0.1
7	Methylene blue	0.075	700	0.6 ± 0.2
8	Without CGI	---	496	1.4 ± 0.2

XRD patterns of the calcined SAPO-34 samples synthesized using PEG, Brij-35, MB as CGI and without CGI respectively are shown in Figure 4.1. All XRD patterns correspond to chabazite structure,[173] which is the typical structure of SAPO-34. The

intensity and peak positions are in agreement with previously reported SAPO-34 XRD spectra.[21] Except for the sample synthesized using Brij-35, all samples were composed of pure SAPO-34. The sample synthesized with Brij-35 showed a peak at $2\theta \sim 23°$ (Figure 4.1.b) which tentatively is assigned to $AlPO_4$-18. The $AlPO_4$-18 framework has a three-dimensional pore system with a pore diameter of ~0.38 nm which is essentially the same as SAPO-34.[23]
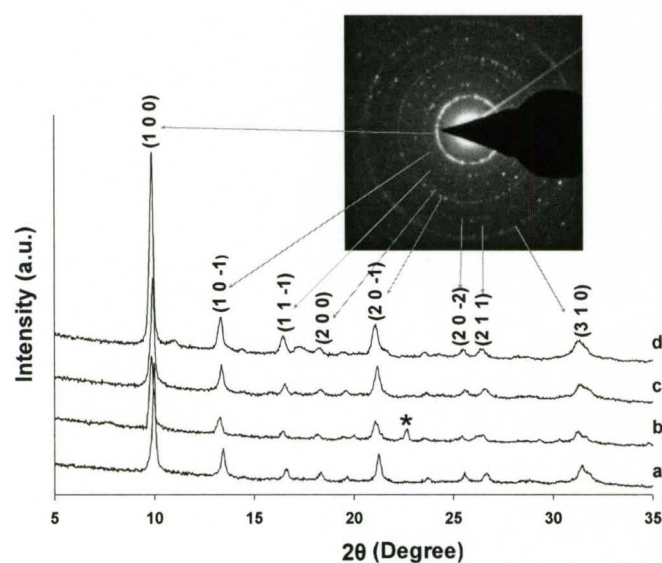
Figure 4.1. XRD patterns of SAPO-34 crystals synthesized using a) PEG b) Brij-35 c) MB as CGI and d) without CGI. Inset shows the SAPO-34 diffraction pattern. * indicates the peak of $AlPO_4$-18 crystals. *hkl* Miller indexes are assigned based on chabazite structure.

The interplanar spacing calculated using the Bragg's law from the reflections at different 2θ values and TEM diffractograms are in good agreement with reported literature data for SAPO-34.[21] Absorption FTIR spectra revealed the lattice vibration regions and their respective IR frequencies of all SAPO-34 samples as shown in Figure 4.2. Here the main peak around 1100 cm^{-1} corresponds to the asymmetric stretching of the

tetrahedral bonds (TO$_4$, where T = Al, Si, P), confirming the formation of SAPO-34 zeolite. The other peaks around 650 and 1600 corresponds to the TO bonding and –OH bonding in the SAPO-34 framework. These spectra correspond to SAPO-34 with chabazite (CHA) structure as reported in literature.[174] XRD and FTIR spectra suggest that the crystal structure of SAPO-34 is not affected by the incorporation of the CGI.
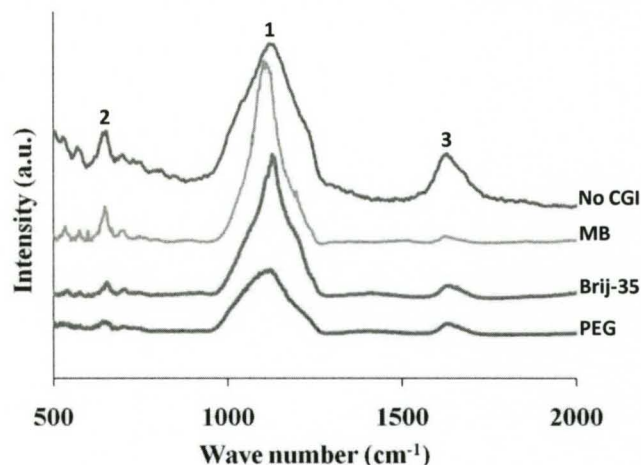
Figure 4.2. FTIR spectra of the SAPO-34 samples synthesized using PEG, Brij-35, MB and without CGI. 1 = Tetrahedra bonding (TO$_4$), 2 = TO bonding, 3 = -OH bonding.

4.1.2. Morphology and size of SAPO-34 seeds

The sample prepared without CGI shows cubic morphology displaying well-developed crystals in the size range of 1.5-2 μm with homogeneous crystal size distribution as shown in Figure 4.3. Figure 4.4 shows the SEM images of SAPO-34 crystals exhibiting a pseudo-cubic plate-like morphology, which is typical of SAPO-34. The average crystal size of these samples was in ~0.6-0.9 μm range. Also, some smaller crystals of ~0.2μm - 0.5μm were also observed, indicating bimodal size distribution of these samples. Figure 4.4a shows crystals of ~0.8μm size and thickness of ~0.25μm, synthesized employing PEG as CGI. The crystal size decreased to ~0.7μm with ~0.2μm

56

thickness, using Brij-35 as CGI (Figure 4.4b). When MB was employed as CGI, the crystal size and thickness were ~0.9μm and ~0.2μm, respectively as shown in Figure 4.4c. Interestingly, regular sized ~0.15μm nano-cubes were also observed when MB was used as CGI. Figure 4.4d shows the TEM image of SAPO-34 prepared with Brij-35 as CGI, confirming the plate-like morphology and ~ 0.7 μm in size crystals.
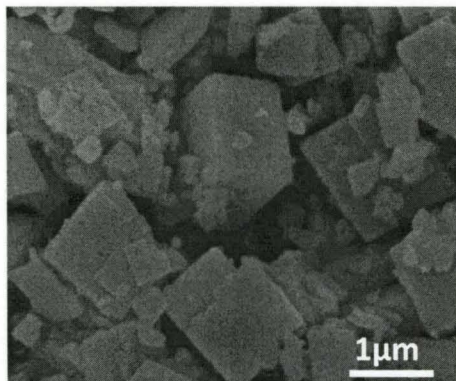
Figure 4.3. SEM of the SAPO-34 crystals synthesized without any CGI
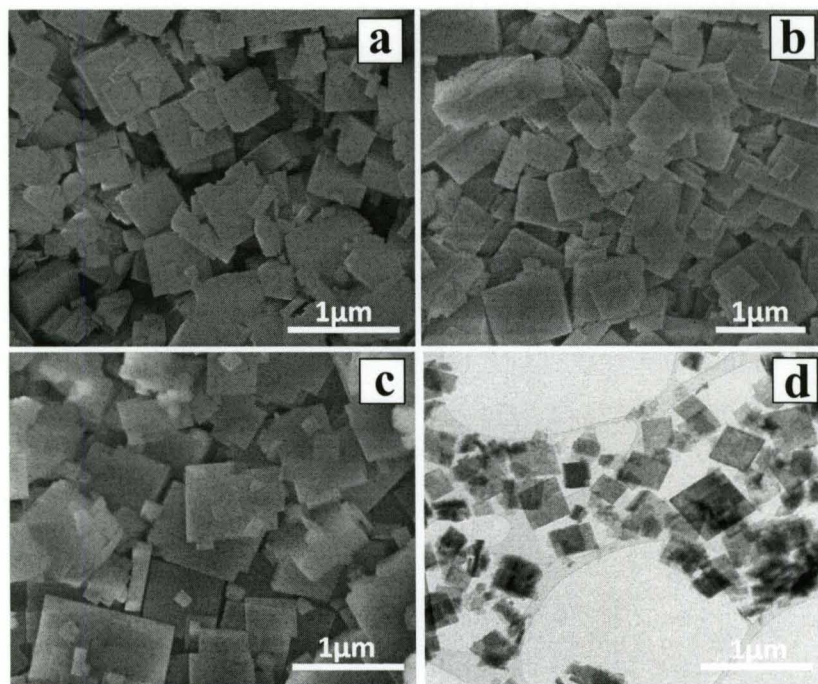
Figure 4.4. SEM images of SAPO-34 crystals synthesized using a) PEG b) Brij-35 c) MB as CGI and d) TEM image of SAPO-34 crystals synthesized with Brij-35 as CGI.

4.1.3. Surface properties of SAPO-34
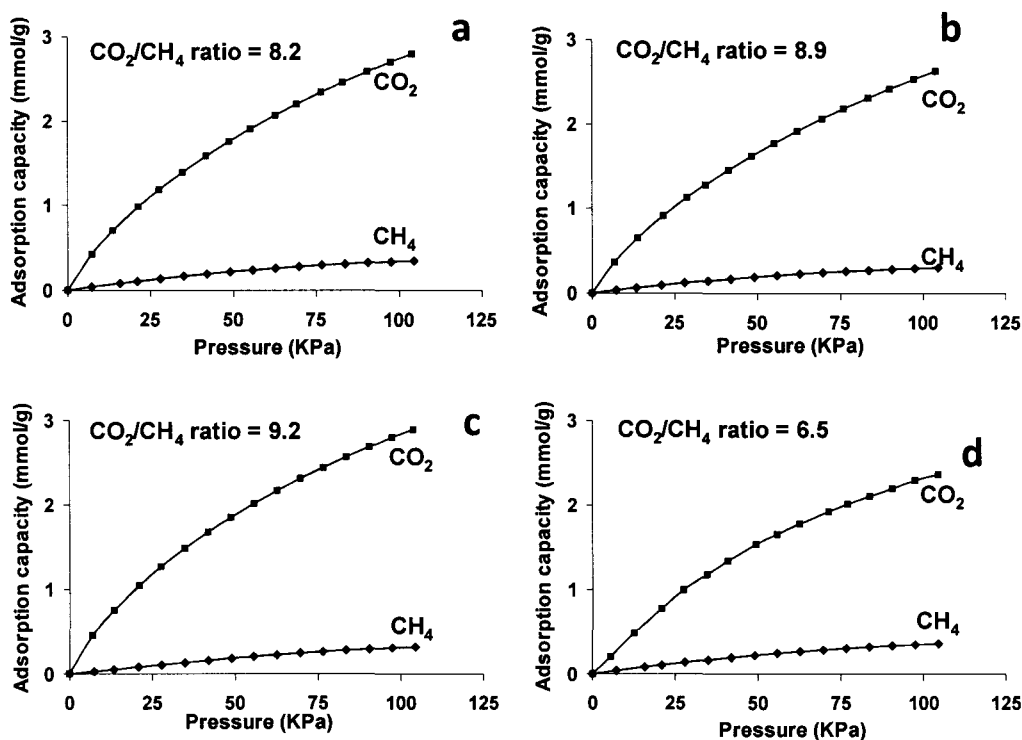
Figure 4.5. CO_2 and CH_4 adsorption isotherms of SAPO-34 crystals synthesized using a)PEG b) Brij-35 c) MB as CGI and d) without CGI.

CO_2 and CH_4 were chosen as the probe molecules to study the adsorption capacity of SAPO-34 due to their energy and environmental importance and relevance in gas separations. To study the adsorption capacity of SAPO-34, CO_2 and CH_4 isotherms were collected at room temperature using water as the coolant. The adsorption isotherms of SAPO-34 crystals synthesized with and without CGI are shown in Figure 4.5. The SAPO-34 crystals adsorbed preferentially CO_2 over CH_4. To evaluate the effect of CGI on the CO_2 and CH_4 adsorption properties, a reference material was synthesized without using any CGI. At 1 atm pressure, the SAPO-34 crystals synthesized using CGI adsorbed ~8-9 times more CO_2 than CH_4. For the reference material (without CGI), the CO_2/CH_4

adsorption ratio was only ~ 6.5 as shown in Figure 4.5d. The high CO_2/CH_4 adsorption

capacities observed for samples prepared with CGI make these crystals attractive for

CO_2/CH_4 mixtures separation since it is known that the higher the CO_2/CH_4 adsorption

ratio, the higher the CO_2/CH_4 separation selectivity. Since both CO_2 (0.33 nm) and CH_4

(0.38 nm) molecules are able to enter the porous structure of SAPO-34, the CO_2/CH_4

separation selectivity will depend on the preferential adsorption of CO_2 even though it

diffuses faster than CH_4.
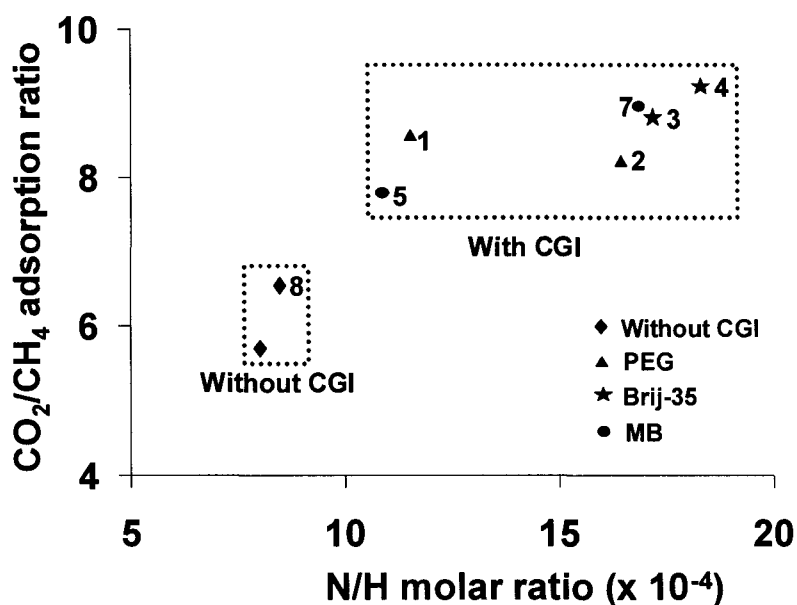
Figure 4.6. CO_2/CH_4 adsorption ratio as a function of N/H molar ratio

Figure 4.6 shows the effect of N/H molar ratio on the CO_2 and CH_4 adsorption

capacities. The CHN analysis revealed that more nitrogen was retained or incorporated in

the SAPO-34 framework when CGI were employed in the synthesis gel. The N/H molar

ratios of the SAPO-34 crystals synthesized using CGI were in the range of 11×10^{-4} -

18×10^{-4}. But it was only ~ 8×10^{-4} for the samples synthesized without CGI. Furthermore,

the N/H molar ratio increased with the amount of CGI. For instance, The N/H molar ratio

increased from 11.5×10^{-4} to 16.5×10^{-4} for the SAPO-34 crystals synthesized employing 2 and 4 g of PEG as CGI respectively. The same trend was observed for Brij-35 and MB. Interestingly, the higher the N/H molar ratio, the higher the CO_2/CH_4 adsorption ratio. Therefore, in principle, one may fine-tune the CO_2 and CH_4 adsorption capacities of the crystals by simply adjusting the N/H content.

4.1.4. Crystal growth inhibition mechanism
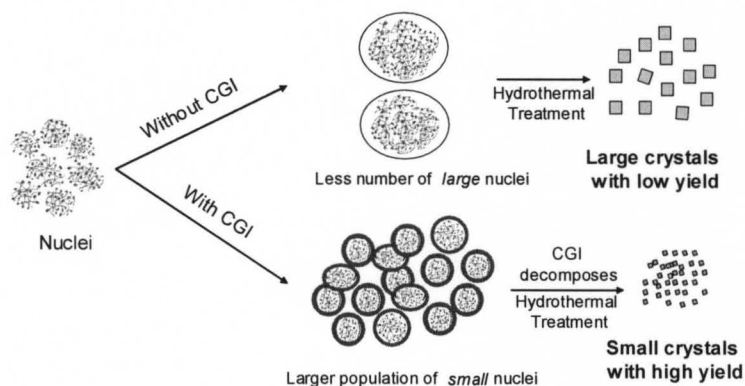
Figure 4.7. Proposed route for the formation of SAPO-34 crystals in the presence of CGI.

The formation of zeolite nanocrystals requires conditions that favor nucleation over crystal growth in the initial stages of the process. Nucleation in zeolite precursor solution occurs because of the supersaturation. In the initial stages of hydrothermal treatment, the amorphous zeolite phase forms. During the induction period CGIs potentially interact with reactive sites of the inorganic precursors in solution, shortening the nucleation period and thereby resulting in a larger number of smaller nuclei.[175]

The crystal grow on these primary building units at the expense of surrounding amorphous gel until it consumed completely by solution mediated transport. At this stage, CGI separates these nuclei by adsorbing onto its surface, minimizing the rate transport of

60

the amorphous gel on these nuclei, there by inhibiting the growth rate of the zeolite crystals, resulting in smaller crystals. Then, the adsorbed CGI decomposed at high temperature in later stages of the hydrothermal treatment. Therefore, a larger population of small nuclei after the induction period explains the production of smaller crystals as shown in Figure 4.7. A similar mechanism has been suggested for synthesis of pure-silica-zeolite MFI nanocrystals employing MB as CGI.[176] The events in the early stages are of critical importance in determining crystallization process. Therefore, a detailed understanding of these phenomena is highly desirable in order to improve structural and morphological control of these important materials.

The incorporation of CGI in the synthesis gel also increased the pH of the resultant solution. The pH of the synthesis gel prepared without any CGI was 9.7 and increased to ~10 when PEG, Brij-35 and MB were incorporated. It is well known that alkalinity promotes the secondary nucleation at initial stages of the hydrothermal treatment and quick transformation to stable phase in later stages leading to smaller crystals.[172] It is clear that CGI did not act as structure-directing agents (SDA), since the kinetic diameters of these molecules are large enough to fit in the pore size of SAPO-34 (~ 0.38 nm). For instance, MB molecule has a rectangular parallelepiped shape[177] with dimensions of 1.6 x 0.7 x 0.37 nm^3, which is much larger than the pore size of SAPO-34 as shown in Figure 3.1. Similarly, the micellar size of Brij-35 and PEG in water is ~4 nm[178] and ~0.69-3.93 nm[179] respectively. Due to their larger molecular size, CGI can only adsorb on the surface of the nuclei and do not enter into the porous system of SAPO-34, supporting the proposed mechanism.

4.2. SAPO-34 seeds synthesized using microwave reactor

The synthesis times were increased from 30 to 500 min, since, no crystalline phase was detected before 30 min and pure SAPO-34 was observed at 500 min. From Table 4.2, it can be observed that the surface area of the SAPO samples increased with increasing the synthesis time and the ICP Si/Al and Al/P ratios in the SAPO framework are in well agreement with the synthesis gel compositions, except for samples B and D. SAPO phases with different ICP compositions as compared to the synthesis compositions have been observed previously in literature[180] and this difference may be related to the silicon substitution mechanism during nucleation and crystallization steps.[181]

Table 4.2. Synthesis time, relative amounts, surface area and ICP elemental composition of SAPO-34 and SAPO-5 phases

Sample ID*	Synthesis time (min)	SAPO-34 relative amount (%)	Surface area (m^2/g)	ICP composition	
				Si/Al	Al/P
A	30	0	224	0.1498	0.9759
B	60	23	283	0.1121	0.9391
C	120	35	319	0.1448	0.9941
D	300	56	338	0.1606	0.4950
E	420	81	411	0.1607	1.0026
F	500	100	447	0.1687	0.9621

4.2.1 Phase transformation of SAPO-5 to SAPO-34

XRD was used to follow the structural evolution of SAPOs as the synthesis time progressed (Figure 4.8). Pure SAPO-5 was formed after the gel was treated for 30 min under MW heating as shown in Figure 4.8a. The XRD pattern corresponding to SAPO-5 with AFI structure agrees well with the reported literature.[23,182] After 60 min, XRD revealed the presence of a reflection at $2\theta \sim 9.9°$, which tentatively was assigned to the (1 1 0) plane of SAPO-34, indicating the coexistence of the two phases. As the time progressed, the characteristic peaks corresponding to SAPO-34 increased, while SAPO-5 peaks decreased. Pure crystalline SAPO-34 was observed at 500 min of MW treatment. Longer synthesis times led to a more template concentrated gel, favoring the formation of CHA over AFI. Jhung et. al. reported that CHA amount increases over AFI with increasing the template concentration.[183] The percentage of relative phases (Table 4.3) were determined from the sum of the area under the curve for the most prominent peaks of SAPO-34 (plane (1 1 0) at $2\theta \sim 9.5°$) and SAPO-5 (plane (1 0 0) at $2\theta \sim 7.5°$).
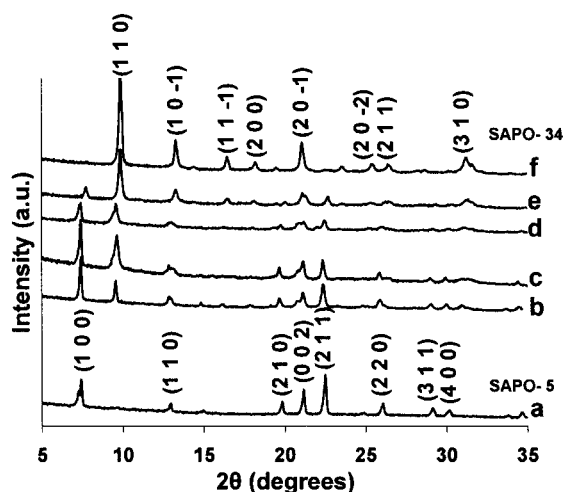
Figure 4.8. XRD patterns of SAPO phases synthesized by microwave assisted approach after a) 30; b) 60; c)120; d) 300; e) 420; and f) 500 min
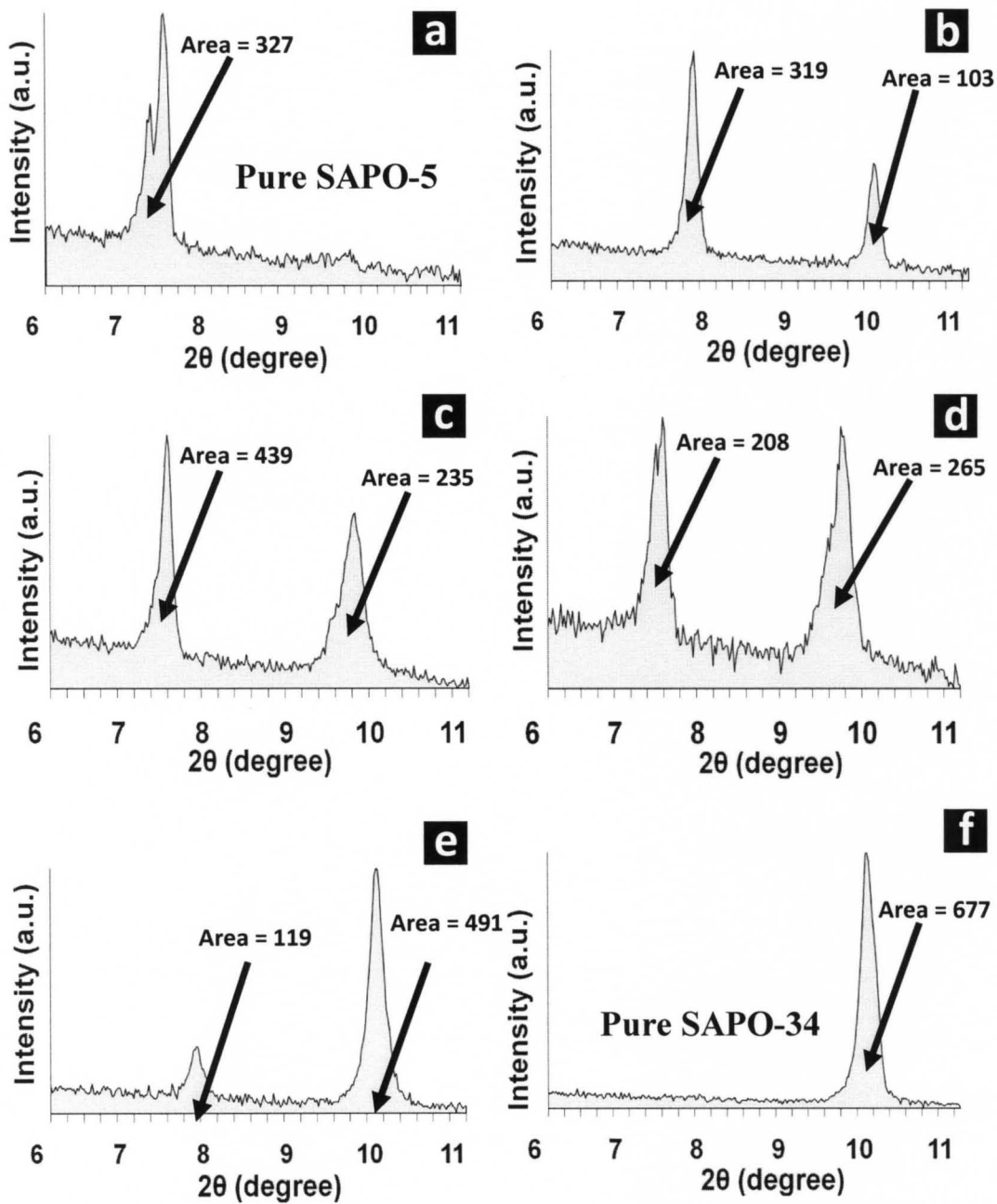
Figure 4.9. Calculation of the area under the most prominent XRD peaks of SAPO-5 and SAPO-34 synthesized using microwave assisted approach after a) 30; b) 60; c) 120; d) 300; e) 420; and f) 500 min.

The SAPO-5 to SAPO-34 phase transition was followed by determining the relative amounts of SAPO phases by using XRD patterns as shown in Figure 4.9. Results are summarized in Table 4.3. The most prominent peak for SAPO-5 is present at 2θ ~7.4° and for SAPO-34 is present at 2θ ~9.9°. The area under the curve for these two peaks was quantified using origin software, after baseline correction, to determine the relative amounts of SAPO-34. They were calculated by the ratio of the area under the curve for the 2θ ~9.9° reflection over the total area (under 2θ ~7.4° and 2θ ~9.9°). As an example for sample B: % relative amount of SAPO-34 is $(103/(103 + 319)) \times 100 = \sim 24\%$.

Table 4.3. Relative amounts of SAPO phases as a function of microwave synthesis time

Sample	Synthesis time (min)	Area under the Curve		SAPO-34 Relative amount (%)
		2θ ~7.4° (1 0 0)	2θ ~9.9° (1 1 0)	
A	30	327	0	0
B	60	319	103	24
C	120	439	235	35
D	300	208	265	56
E	420	112	491	81
F	500	0	677	100

Figure 4.10 shows the FTIR spectra of the samples synthesized for different times. The lattice vibrations of SAPO-5 are 683, 1035, 1302, and 1633 cm^{-1}, which are in well agreement with the literature[184,185] and clearly shifted to typical lattice vibrations of SAPO-34 at 641, 1124 and 1626 cm^{-1},[186,187] with increased times. The peak around 650 is assigned to the vibration of double-6 rings and the bending of T-O tetrahedra. The

main peak which is present around 1100 is due to the asymmetric stretching of T-O tetrahedra. The peak around 1630 and 1300 are more intense in SAPO-5 due to the presence of remained templated and adsorbed water even after calcination, which are typical for SAPO-5[188] and they are almost disappeared in SAPO-34. The frequency of the peak around 1100 shifts slightly because of the differences in bond lengths and angles of highly strained and not yet thoroughly cross-linked unstable SAPO-5 lattices compared to the stable lattices of SAPO-34.[185] The FTIR spectra of the SAPO-34 and SAPO-5 clearly showed that structure changes have taken place during the phase transformation.
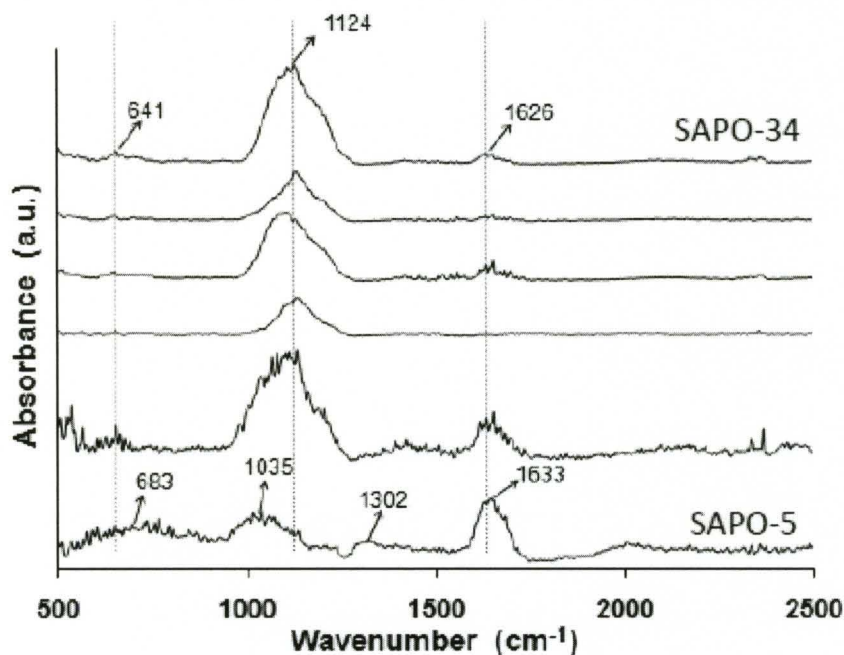
Figure 4.10. FTIR spectra of SAPO-34 formation by phase transformation of SAPO-5.

4.2.2. Morphological changes of SAPO phases
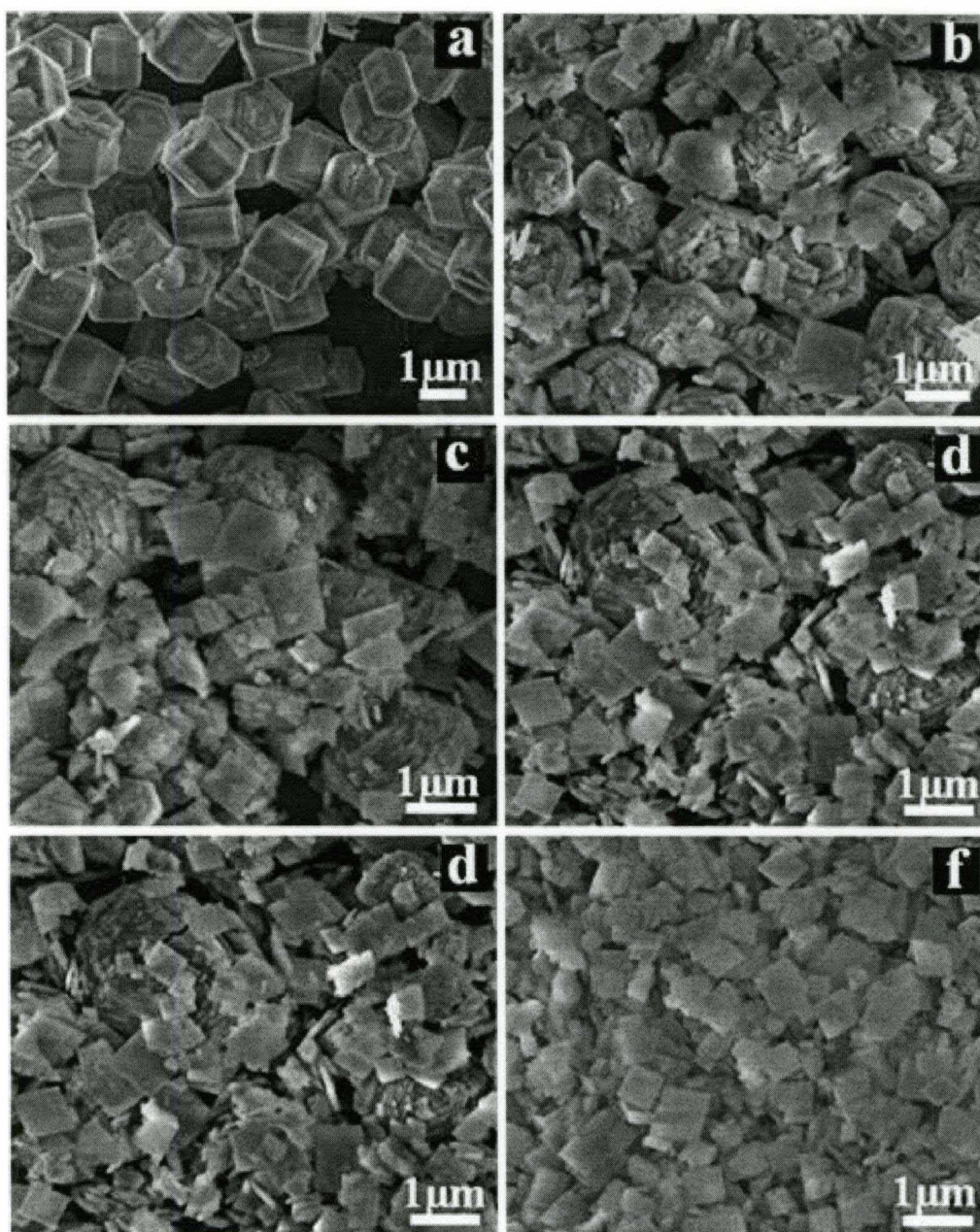
Figure 4.11. SEM pictures of SAPO phases synthesized by microwave assisted approach after a) 30; b) 60; c) 120; d) 300; e) 420; and f) 500 min
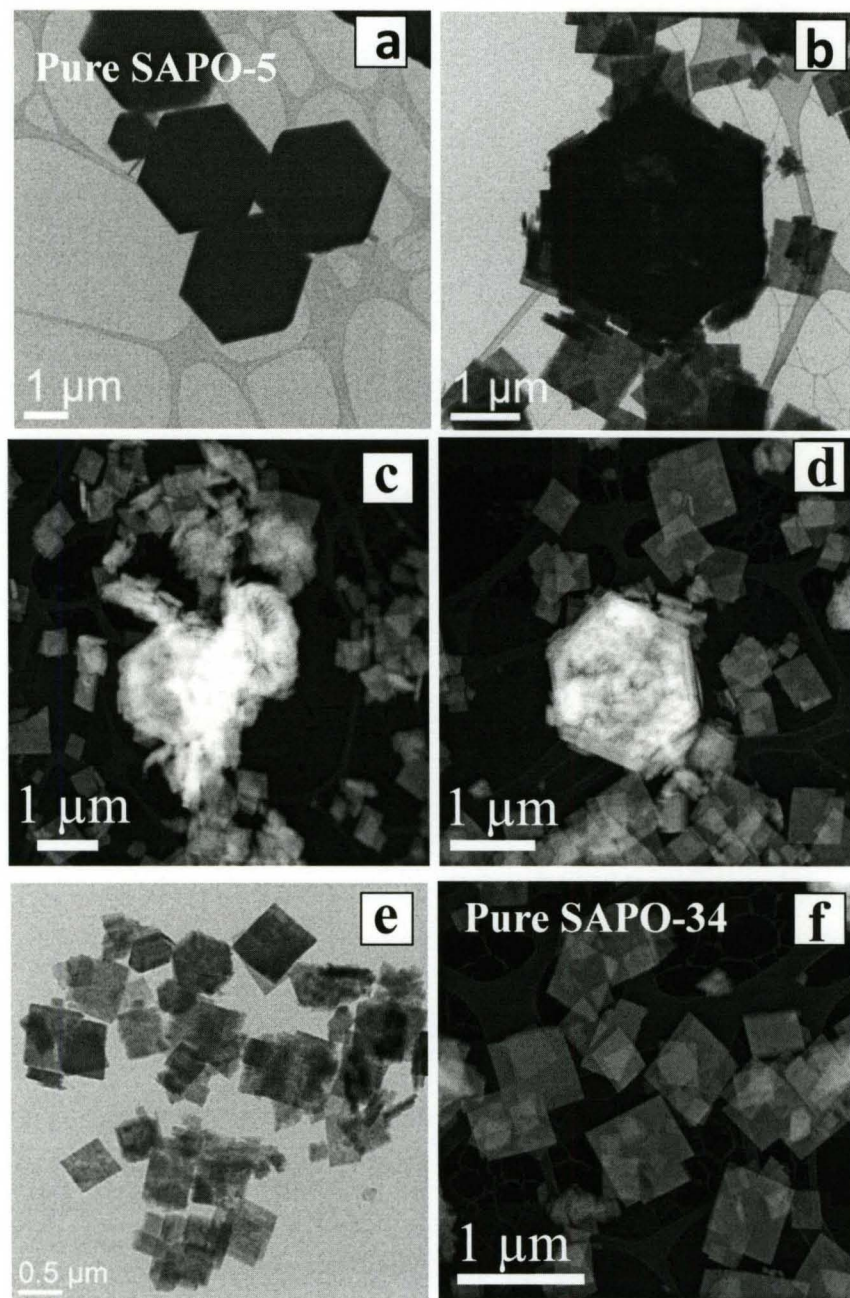
Figure 4.12. TEM images of the silicoaluminophosphate phases synthesized using microwave assisted approach after a) 30; b) 60; c) 120; d) 300; e) 420; and f) 500 min.

The morphological features of these phases were inspected by SEM and TEM to follow the SAPO-5 to SAPO-34 phase transformation. Homogeneous hexagonal crystals of ~2.5 μm were observed after 30 min of MW treatment as shown in Figure 4.11a and 4.12a. It is well known that hexagonal shapes are typical for SAPO-5 phases.[183] As the MW heating time increased, the hexagonal crystals of pure SAPO-5 ripened and formed characteristic cubic crystals of SAPO-34 phase.[23] Both phases coexisted at 60, 120, 300 and 420 min of MW synthesis treatment as shown in Figure 4.11c-4.11e. The longer the time, the more cubic crystals corresponding to SAPO-34 appeared. At 500 min of MW treatment, all the SAPO-5 crystals were transformed to ~0.5 μm SAPO-34 crystals as shown in Figure 4.11f and confirmed by XRD (Figure 4.9). The phase transition of SAPO-5 to SAPO-34 was also confirmed using TEM (Figure 4.12). Therefore, it can be concluded that SAPO-5 was completely transformed to SAPO-34 at 500 min.

4.2.3. Surface properties of SAPO-5 and SAPO-34

The SAPO-5 transition to SAPO-34 was also confirmed by the experimentally measured surface areas of the synthesized SAPO phases and presented in Table 4.2. Typical surface areas of SAPO-5 are in the ~200-280 m^2/g range[189] and for SAPO-34 are in the ~400-500 m^2/g range.[23] The surface areas of the synthesized samples increased with increasing time of MW treatment confirming the formation of SAPO-34 by the transformation of SAPO-5. The adsorption capacity of the synthesized SAPO phases was studied by choosing CO_2 and CH_4 as the probe molecules due to their energy and environmental importance and relevance in gas separations. The adsorption isotherms of CO_2 and CH_4 were collected at room temperature using water as the coolant. The CO_2/CH_4 adsorption ratios were calculated at 100 KPa. The CO_2/CH_4 adsorption ratio

was ~ 8 for the pure SAPO-5 sample as shown in Figure 4.13a. In general, this ratio increased as the synthesis time increased. The adsorption ratio of the pure SAPO-34 sample obtained after 500 min of MW treatment was ~29 as shown in Figure 4.13f.
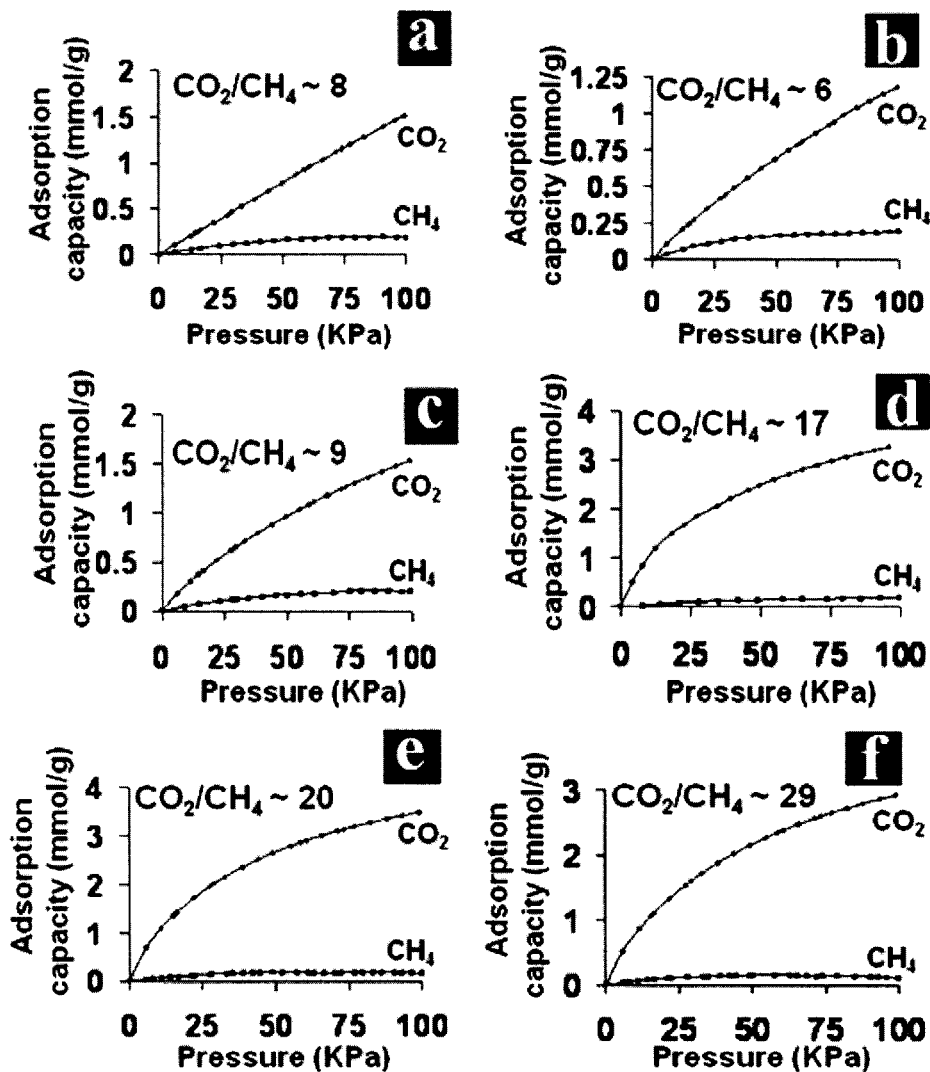
Figure 4.13. CO_2 and CH_4 adsorption isotherms of the SAPO phases synthesized by microwave assisted approach after a) 30; b) 60; c)120; d) 300; e) 420; and f) 500 min.

The high CO_2/CH_4 adsorption capacity observed for pure SAPO-34 may be attributed to the significant decrease in the crystal size (~ 0.5 μm). The high CO_2/CH_4 adsorption capacities may be due to the different distribution mechanism of silicon in the SAPO-34 framework compared to the conventional synthesis. Also, higher surface of SAPO-34 framework is available for smaller crystals, which preferentially adsorb the CO_2. We found that as the crystal size decreased, the CO_2/CH_4 adsorption ratio increased. The effect of crystal size of SAPO-34 phase on CO_2/CH_4 adsorption capacities is shown in Figure 4.14. The increase in the relative amount of SAPO-34 as the synthesis time increased may also contributed to the increase in the CO_2/CH_4 adsorption ratio, since it is well known that SAPO-34 adsorbs more preferentially CO_2 over CH_4 than SAPO-5. The smaller crystal size with narrow particle size distribution and higher CO_2/CH_4 adsorption capacities of the samples prepared by MW assisted approach make these phases highly attractive to synthesize SAPO-34 membranes for CO_2/CH_4 mixture separations, since it is well known that the higher the CO_2/CH_4 adsorption ratio, the higher the CO_2/CH_4 separation selectivity of the membranes.
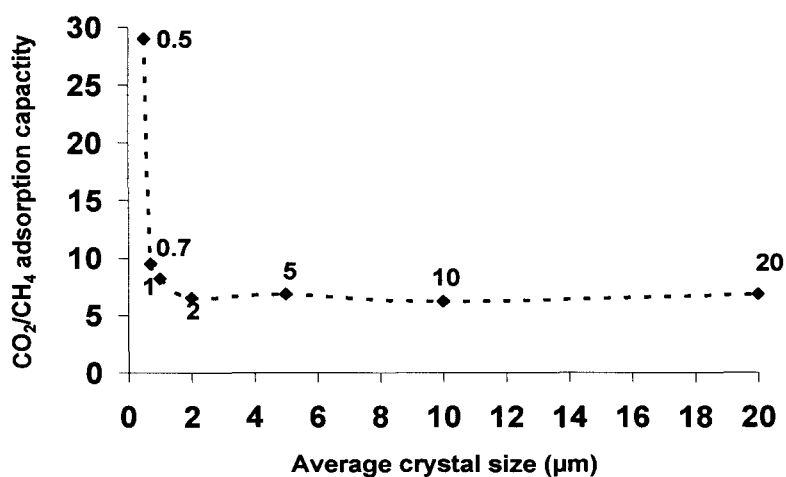
Figure 4.14. Effect of crystal size of SAPO-34 on CO_2/CH_4 adsorption capacity

Zeolite synthesis is governed by the occurrence of successive phase transformations. Thermodynamically, the least favorable phase crystallizes first, and is replaced by more stable phases.[190] In our case, the formation of SAPO-5 favors under the MW heating because SAPO-5 is least stable as compared to SAPO-34. According to "Ostwald Ripening mechanism",[191] it is likely that the highly strained and not yet thoroughly cross-linked unstable SAPO-5 lattices formed at the initial stages of MW heating, redissolved in the gel by releasing some strain energy leading to lattice restructuring to SAPO-34 crystals. The phase transformation of SAPO-5 to SAPO-34 can also be explained by the higher solubility of AFI,[192] small crystallite size of AFI[193] and may indicate that CHA is more stable than AFI at the employed reaction conditions. Under the MW heating, the higher solubility of the AFI structure is further enhanced by increasing the rate of solubility through the formation of so-called "active water molecule" by the breakage of hydrogen bonds.[59]

The carbon, hydrogen and nitrogen content of silicoaluminophosphate phases were presented in Table 4.4. The CHN analysis of the synthesized SAPO phases revealed that some residues of carbon, nitrogen and hydrogen remained in the samples even after calcination, which is not unusual. In fact, it has been shown for calcined SAPO-34 that carbon, nitrogen and hydrogen from the amino group of the template(s), may form very stable surface compounds bonded to the zeolite framework.[145]

Table 4.4. CHN analysis of SAPO phases as a function of microwave synthesis time

Sample ID	Synthesis time (min)	Amounts in mg/ 30mg of sample		
		Carbon	Hydrogen	Nitrogen
A	30	0.02	2.02	0.00
B	60	0.04	1.90	0.01
C	120	0.03	1.64	0.00
D	300	0.04	1.79	0.00
E	420	0.04	1.92	0.01
F	500	0.05	1.27	0.00

4.3. Difference between conventional heating and microwave heating

The smaller crystal size of the SAPO-34 under the microwave heating compared to the conventional heating can be attributed to the rapid increase in the temperature of the synthesis gel, superheating of the gel, fast dissolution of the gel, changes in the growth mechanism, condensation rate.[58,59] The composition of these zeolites can also be varied under microwave heating by changing the association between the species within the synthesis mixture.

Microwave radiation results in a rapid heating throughout the material with reduced thermal gradient compared to the conventional heating. The formed zeolite crystals are more uniform in microwave reactor. Two different views were reported to explain their homogenity. Some suggests that more rapid nucleation of the initial crystallites[194-197] and others explained using more uniform growth process.[198-200] Rapid

crystallization occurs in the microwave reactor because of the fast dissolution of the gel, which in turn depends on the polarization effects of the water and template molecule under microwave irradiation. Because of the formation of more active molecules, which have a higher potential to dissolve the gel, in the microwave reactor compared to conventional heating, fast dissolution occurs. Microwave irradiation also changes the condensation rate of the tetrahedral bonding to give a special structure, which may be different from conventional heating.[201]

Generally two types of nucleation occur during the formation of zeolites. They are homogeneous nucleation and heterogeneous nucleation. Homogenous nucleation occurs uniformly throughout the parent phase. Heterogeneous nucleation occurs the surface of some different substance, such as a dust particle, the wall of the container, grain boundaries, dislocations, acts as the center upon which the first atoms, ions, or molecules of the crystal become properly oriented.[202] In microwave reactor, homogeneous nucleation occurs throughout the gel because of uniform heating of the SAPO-34 synthesis gel. Growth of the crystal begins once the zeolite nucleus exceeds its critical radius. In conventional heating, heat transfers to the synthesis gel from the walls of the reactor. So the initial nuclei form at the walls of the reactor and growth of new nuclei at the center occurs on the already formed nuclei, resulting in heterogeneous nucleation. In the nucleation process, where new solid phase nucleates from the reaction solution, two competing effects determine the free energy of this new phase. The creation of new volume increases the free energy while formation of an interface decreases it. The nuclei with sizes below the critical size dissolve back into the solution while nuclei with sizes

bigger than the critical size grow to become crystals. The crystals grow until they reach equilibrium with the solution.

The reasons for the decreased synthesis time or the reduction in overall reaction rate under microwave radiation can be explained by separately analyzing the induction, nucleation and crystal growth steps. Thermal lag always presents in the conventional synthesis, which is not presented in the microwave. Stirring is one of the main effect in the synthesis of SAPO-34. There is no stirring in the conventional synthesis of SAPO-34. But the synthesis gel was stirred during the synthesis. Rapid stirring in hydrothermal synthesis resulted in faster reaction rates which are comparable with microwave heating, but the morphology is poorer.[203,204]

Besides many advantages of microwave effect, it also results in different membrane morphology, orientation and composition. So these membranes show different permeation properties compared to conventional heating.

4.4.   Conclusions

SAPO-34 crystals displaying BET surface areas up to $700m^2/g$, enhanced CO_2/CH_4 adsorption ratios, and crystal sizes in the ~0.6-0.9 µm range, with narrow particle size distribution employing PEG, Brij-35 and MB as crystal growth inhibitors were synthesized. The relatively high N/H molar ratios observed in the SAPO-34 crystals prepared with CGI, led to high CO_2/CH_4 adsorption capacities. SAPO-34 has also been successfully synthesized by the transformation of SAPO-5 using microwave hydrothermal reactor. The synthesized SAPO-5 and SAPO-34 phases displayed small and narrow particle size distribution with crystallites of ~ 2.5 and ~ 0.5 µm respectively. The

synthesized SAPO-34 displayed high CO_2/CH_4 adsorption ratio (~ 29), making it highly attractive for CO_2/CH_4 gas separations. The short synthesis time, smaller crystal size and narrow particle size distribution of the synthesized SAPO phases, make the MW heating an attractive and useful approach for the potential preparation of the thinner membranes for practical gas separation applications. Due to its small crystal size, narrow particle size distribution, higher surface area and preferential CO_2 adsorption capacities over CH_4, these crystals represent ideal phases to prepare thin supported membranes for CO_2/CH_4 separations.

CHAPTER 5

AMINO-FUNCTIONALIZED SAPO-34 MEMBRANES FOR CO$_2$/CH$_4$ AND CO$_2$/N$_2$ SEPARATION

As explained in the introduction, a key factor influencing the separation selectivity in any membrane is the competitive adsorption between the molecular species. In this respect it is highly desirable to enhance the preferential adsorption of a particular gas molecule to improve gas selectivity. Therefore, in order to design high CO$_2$ selective membranes, herein we propose the functionalization of SAPO-34 seeds and membranes by the incorporation of functional groups that promote selective CO$_2$ adsorption. Specifically, SAPO-34 membranes were functionalized using ethylenediamine, hexylamine and octylamine as organic amino cations. The surface functionalized SAPO-34 membranes were evaluated in the separation of CO$_2$ from CH$_4$ and N$_2$.

5.1. Functionalized SAPO-34 seeds characterization

The XRD patterns of the calcined SAPO-34 seeds before and after ethylene diamine (ED) functionalization are shown in Figure 5.1. The XRD patterns of the nonfunctionalized SAPO-34 phase corresponds to the chabazite topology as shown in Figure 5.1a, which is the typical structure of SAPO-34.[23] The intensity and peak positions are in agreement with previously reported SAPO-34 XRD spectra.[23] The crystalline

structure of SAPO-34 was preserved after the amine functionalization with ED (Figure 5.1b-5.1c). However, as the ED loading increased, the intensity of the different planes decreased, suggesting a decrease in the extent of crystallinity, as confirmed by the reduction in the intensity of the XRD reflections.
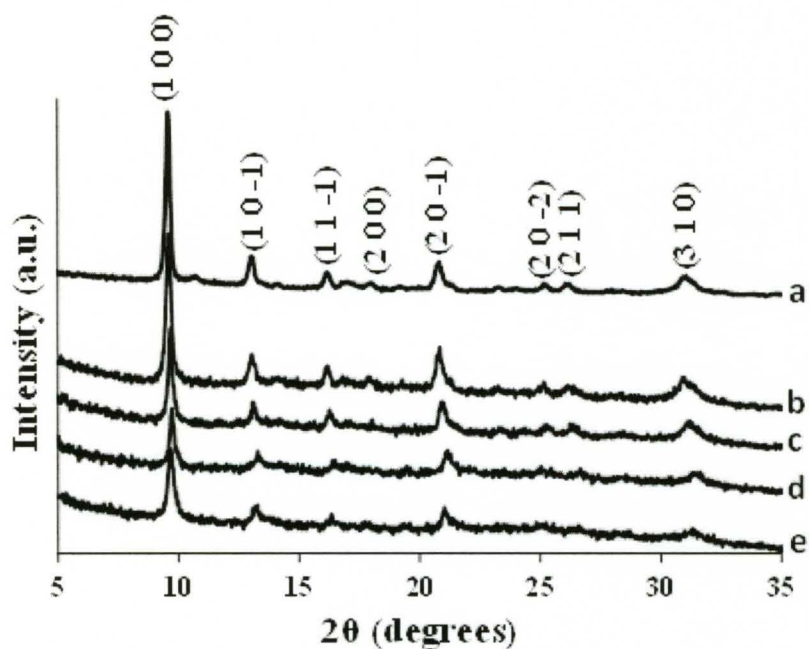
Figure 5.1. XRD patterns of the SAPO-34 seeds a) nonfunctionalized; and functionalized with ethylene diamine: b) 0.15mmol; c) 0.33 mmol; d) 1.66 mmol; and e) 8.32 mmol.
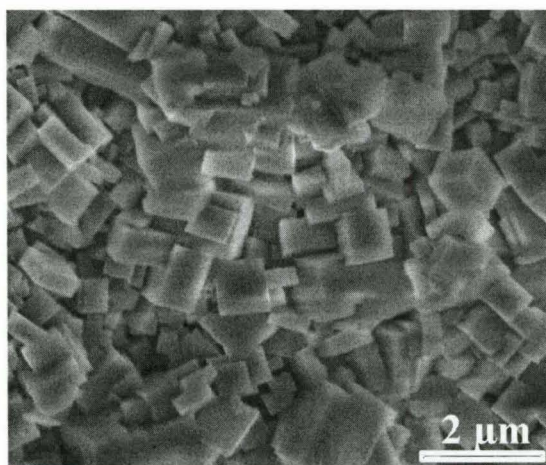
Figure 5.2. SEM image of the nonfunctionalized SAPO-34 seeds

The SEM image of the nonfunctionalized SAPO-34 seeds is shown in the Figure 5.2. Figure 5.3a-d shows the SEM images of SAPO-34 seeds functionalized with different loadings of ED. Figure 5.3a shows the SAPO-34 seeds functionalized with 0.15 mmol of ED displaying pseudocubic plate-like morphology, which is typical of SAPO-34. The average crystal size of these seeds was ~0.6μm. Figure 5.3b shows the presence of some nonhomogeneous crystals for the sample prepared with 0.33 mmol of ED. As the ED concentration increased, the SAPO-34 morphology became more heterogeneous and less crystalline (Figure 5.3c-5.3d), in agreement with the reduction in the intensity of XRD reflections (Figure 5.1b-5.1e).
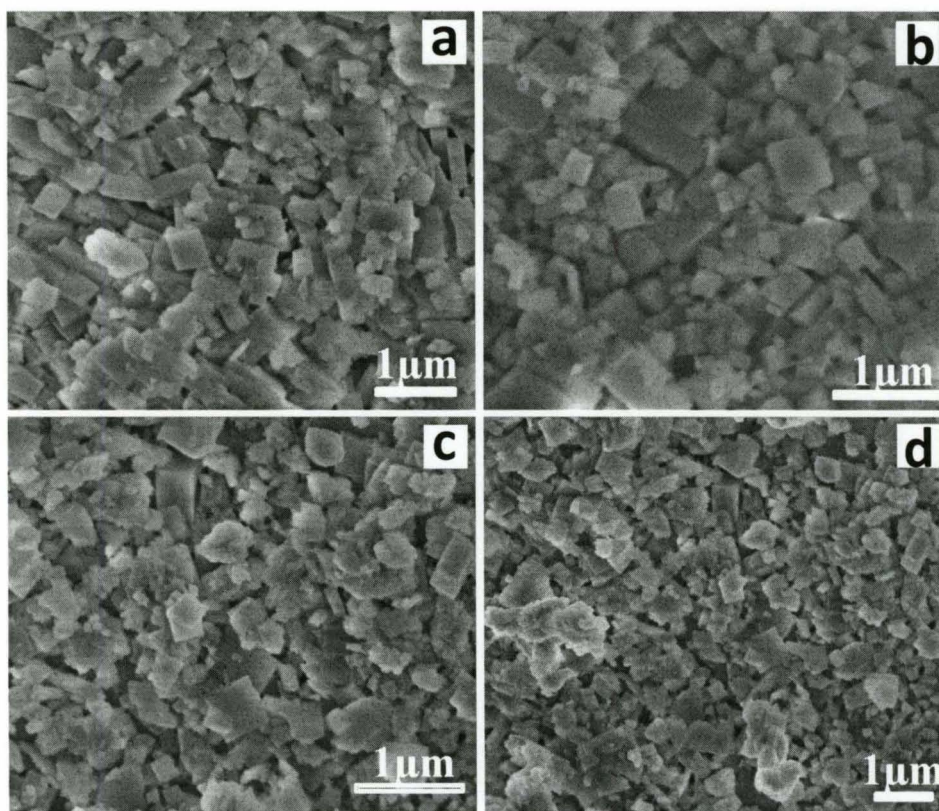
Figure 5.3. SEM images of the SAPO-34 seeds functionalized with ethylene diamine: a) 0.15mmol; b) 0.33 mmol; c) 1.66 mmol; and d) 8.32 mmol.

The N_2 adsorption isotherms at 77K of the nonfunctionalized and ED-functionalized SAPO-34 seeds are shown in the Figure 5.4. All samples displayed type I adsorption isotherms typical of microporous phases as defined by IUPAC. The BET surface area of the nonfunctionalized SAPO-34 was 487 m^2/g. The surface area of the functionalized SAPO-34 decreased to 368, 302, 113 and 81 m^2/g with ED loadings of 0.15, 0.33, 1.66 and 8.52 mmol respectively. The decreased in surface area due to amine group grafting on porous materials is well known.[205]
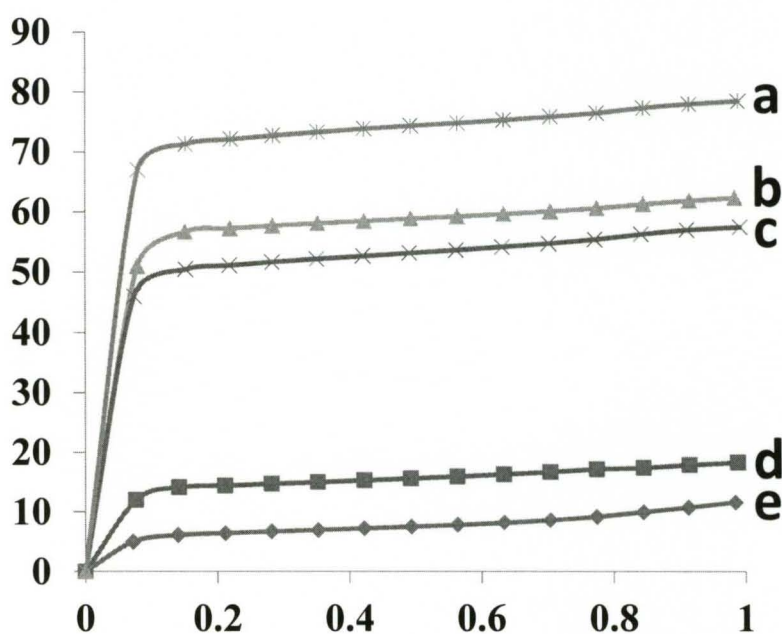
Figure 5.4. N_2 adsorption isotherms of SAPO-34 seeds: a) nonfunctionalized and functionalized with ethylenediamine: b) 0.15 mmol; c) 0.33 mmol; d) 1.66 mmol and e) 8.52 mmol.

The successful grafting of ED in the SAPO-34 framework was confirmed by FTIR spectra as shown in Figure 5.5. Figure 5.5a displays the FTIR spectra of the nonfunctionalized SAPO-34 sample, which show significant bands at 3450, 1617, 1094

and 642 cm⁻¹, which are related to O-H stretching vibrations, H-O-H bend, T-O-T asymmetric stretching vibrations and the vibrations in the double ring ((Si,Al)-O$_4$, PO$_4$) region, respectively.[174] FTIR spectra for the functionalized phases are presented in Figure 5.5b-5.5e. For all functionalized samples, the characteristic vibrations of the SAPO-34 framework were not affected. The important characteristic vibrations of amines are well evident in these spectrums. A strong absorption at ~ 3000 and 3500 cm⁻¹ was assigned to the N- H stretch mode of primary amines.[206]
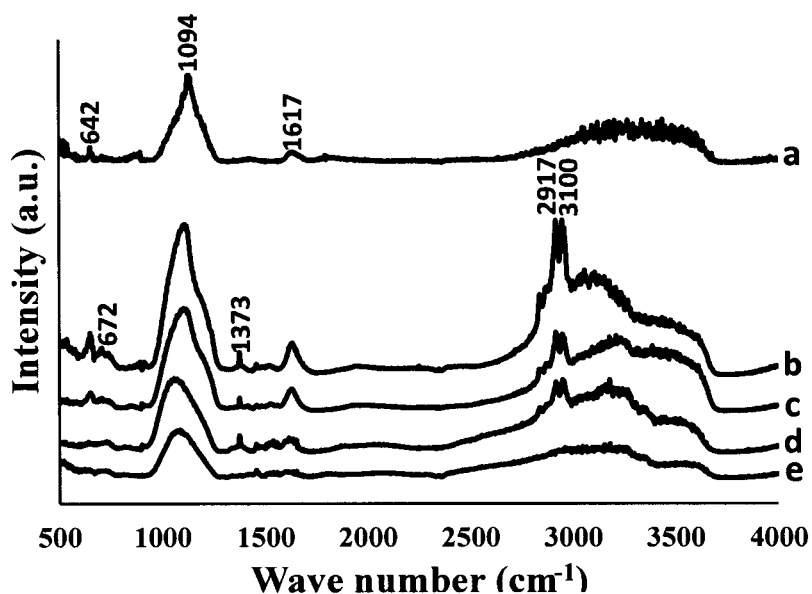
Figure 5.5. FTIR spectra of the SAPO-34 seeds a) nonfunctionalized; and functionalized with ethylene diamine: b) 0.15 mmol; c) 0.33 mmol; d) 1.66 mmol; and e) 8.32 mmol.

The C-N stretching at 1373 cm⁻¹ can also be identified. The 2917 and 3100 cm⁻¹ peaks can be assigned to sp^2 CH$_2$ stretching vibrations originating from the organic part of ethylene diamine.[206] The 672 cm⁻¹ can be tentatively assigned to Al-N bond.[207] The presence of these vibrations in FTIR spectra confirm that ED has been grafted on the surface of SAPO-34 seeds. Interestingly, the intensity of the N-H, C-N, sp^2 CH$_2$ and Al-N

bonds decreased as the amount of ED increased, suggesting that high amine loadings lead to poor grafting.

Figure 5.6 shows a general schematic of functionalized SAPO-34 and its role in preferential CO_2 adsorption. One of the amino groups of ED first adsorbs at the Bronsted acid bridging -OH groups of SAPO-34. It is well known that SAPO-34 surface is rich on unsaturated –OH groups.[208,209] Then, it coordinates to tetrahedral metal atoms of the SAPO-34 framework. The most likely coordination as suggested by FTIR is Al-N. The other amino group of ED, in principle may be available for the preferential adsorption of CO_2. Polymeric membranes containing amino groups have been successfully employed for effective CO_2 capture.[210,211,212] Selective adsorption of carbon dioxide along with the molecular sieving property of SAPO-34 in principle may enhance the separation performance of the membranes for CO_2/CH_4 and CO_2/N_2 mixtures.
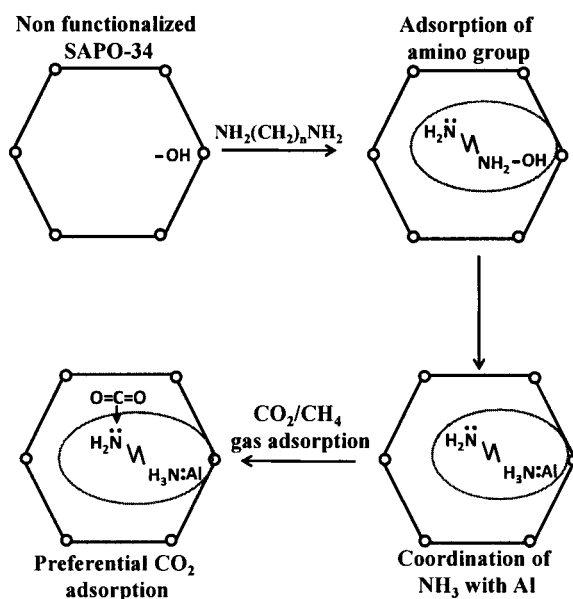
Figure 5.6. Schematic of ethylene diamine functionalized SAPO-34 and its role in promoting CO_2 adsorption.

5.2. SAPO-34 membranes

Single layer SAPO-34 membranes were prepared on tubular stainless steel supports using secondary seeded growth. The synthesized membranes were employed to separate CO_2/CH_4 and CO_2/N_2 gas mixtures. The average thickness of the membranes was ~ 6 μm as shown in Figure 5.7. Table 5.1 shows the separation performance of SAPO-34 membranes as a function of ED loadings for equimolar CO_2/CH_4 gas mixtures. CO_2 permeance did not change significantly by the incorporation of ED.
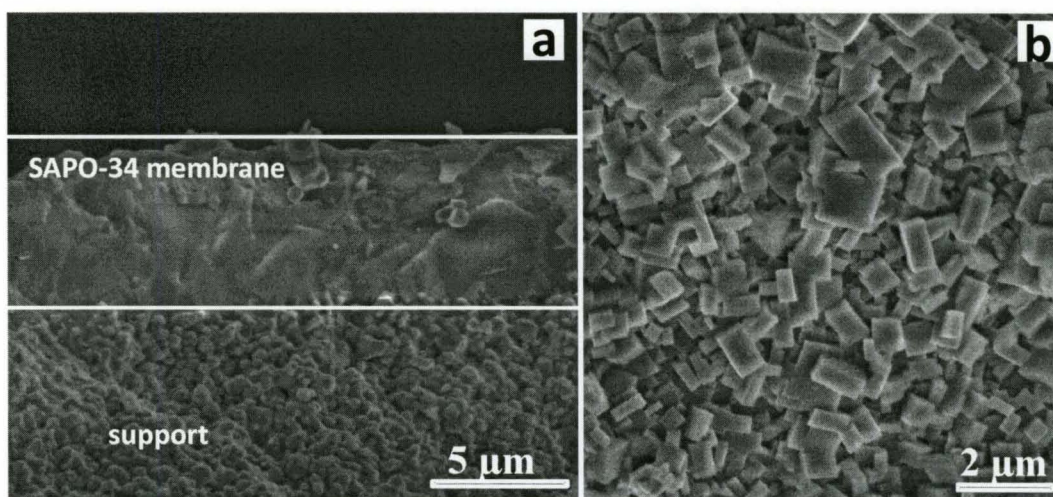
Figure 5.7. SEM images of SAPO-34 membranes: a) Cross-sectional and b) top view

5.2.1. CO_2/CH_4 separation performance of SAPO-34 membranes

However, as expected the CO_2/CH_4 separation selectivity was affected by the incorporation of the amino group. In particular for low ED loadings (0.15, 0.33, 1.66 mmol), the CO_2/CH_4 selectivity was higher as compared to the nonfunctionalized membrane. At high amine loadings (8.32 mmol), the separation selectivity decreased considerably. As shown in Table 5.1, both the CO_2/CH_4 selectivity and separation index (π) increased at lower ED loadings and decreased at higher ED loadings.

Table 5.1. CO$_2$/CH$_4$ separation performance of SAPO-34 membranes at 295 K and 138 KPa

Sample ID	P$_{CO2}$ x 10^7 (mol/m^2 s Pa)	P$_{CH4}$ x 10^9 (mol/m^2 s Pa)	CO$_2$/CH$_4$ Selectivity	Separation index*
Non-functionalized	4.6	2.9	159	7.3
0.15 mmol ED	4.9	2.0	245	12.0
0.33 mmol ED	4.4	1.9	233	10.3
1.66 mmol ED	4.4	2.7	164	7.1
8.32 mmol ED	5.3	5.8	92	4.8

$*\pi$ = (CO$_2$ permeance × (selectivity −1)) x permeate pressure
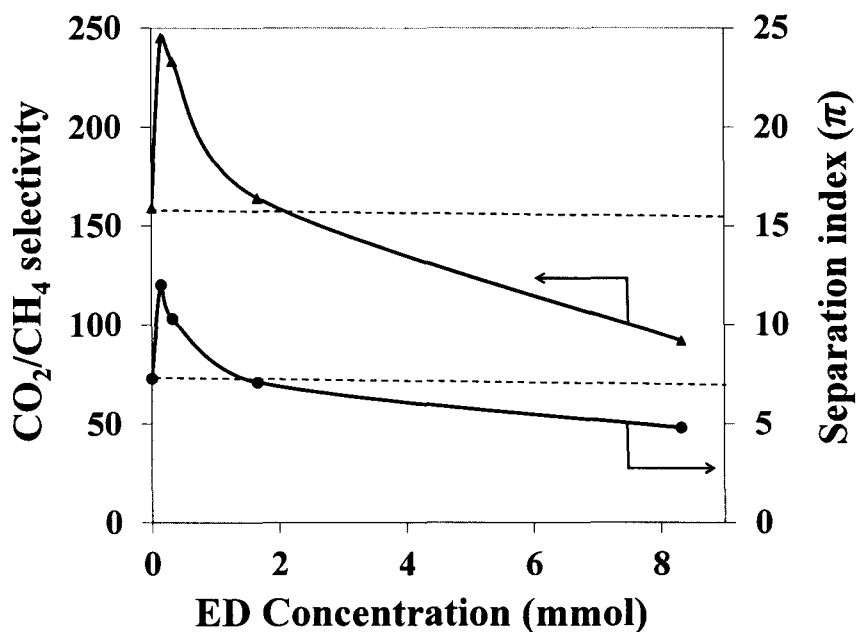
Figure 5.8. Effect of ethylene diamine concentration on CO$_2$/CH$_4$ selectivity and separation index. The dotted line is shown as reference (nonfunctionalized membrane)

The optimum ethylene diamine concentration for superior separation performance was 0.15 mmol (Figure 5.8), which corresponded to ~0.5 wt% of nitrogen in the SAPO-34 framework (determined by CHN analysis). An increase of ~ 54% in CO_2/CH_4 selectivity and ~ 40% increase in separation index were observed for this membrane as compared to the nonfunctionalized SAPO-34 membrane. The enhanced CO_2/CH_4 separation performance of this sample is related to the preferential CO_2 adsorption promoted by one of the amino groups of ED. CO_2, a Lewis acid molecule, adsorbs preferentially on a nitrogen-rich basic surface. This is supported by CO_2 and CH_4 gas adsorption experiments which confirm that the CO_2/CH_4 adsorption capacity for the 0.15 mmol ED functionalized membrane was higher (9.3) than that of the nonfunctionalized membrane (6.5) as shown in Figure 5.9. The poor CO_2/CH_4 separation performance for membranes with high ED loadings may be related to structural features such as loss of crystallinity (Figure 5.1d-5.1e) and the presence of less homogeneous crystals (Figure 5.3c-5.3d) for these particular samples.
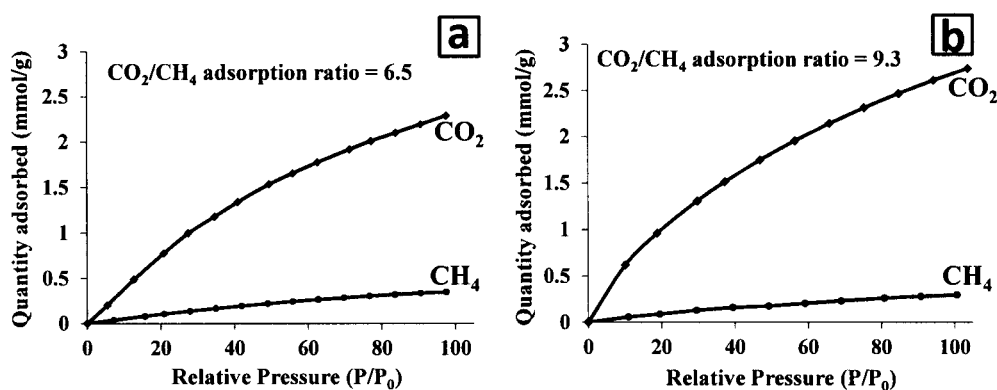
Figure 5.9. CO_2/CH_4 adsorption isotherms: a) nonfunctionalized SAPO-34 and b) 0.15 mmol ED functionalized SAPO-34

Table 5.2. Comparison of CO_2/CH_4 separation performance of SAPO-34 membranes

Membrane support	Temperature (K)	CO_2 permeance $(mol/m^2 \, s \, Pa)$	CO_2/CH_4 selectivity	Reference
Alumina	300	2.0×10^{-8}	30	122
Alumina	300	3.3×10^{-8}	36	19
Stainless steel	297	1.6×10^{-7}	67	18
Stainless steel	297	1.4×10^{-7}	87	124[a]
Stainless steel	297	8.4×10^{-8}	95	126
Stainless steel	297	1.2×10^{-7}	170	20
Stainless steel	295	6.4×10^{-8}	95	22
Stainless steel	295	7.8×10^{-8}	118	127[b]
Alumina	295	1.8×10^{-6}	171	21
Stainless steel	295	3.6×10^{-7}	227	23
25 cm long stainless steel	295	7.1×10^{-7}	130	128[c]
Stainless steel	295	5.1×10^{-7}	252	129[d]
Alumina	295	2.3×10^{-7}	75	130[e]
Stainless steel net	-	2.8×10^{-6}	9	131
Stainless steel	295	4.9×10^{-7}	245	**This work**

[a]Effect of impurities on separation; [b]Effect of Ion exchange on separation; [c]Scale up of membranes; [d] CO_2/CH_4 selectivities up to 283 were reported, but at lower CO_2 permeances $(2.4 \times 10^{-7} \, mol/m^2 \, s \, Pa)$; [e]High pressure CO_2/CH_4 separations (4.6MPa)

86

Table 5.2 summarizes the relevant work up-to-date reported on SAPO-34 membranes for CO_2/CH_4 separation. Remarkable improvement in separation performance has been achieved since the first report demonstrating the ability of SAPO-34 membranes to separate CO_2/CH_4 mixtures.[122] To date, the most efficient SAPO-34 membranes to separate CO_2/CH_4 gas mixtures have been prepared by a) employing multiple templates during synthesis on stainless steel[23] and alumina porous supports,[21] b) blocking non-zeolite pores (defects) with oligosaccharide molecules,[129] and c) removing the templates in the presence of nitrogen or under vacuum.[130] As shown in Table 5.2, the separation performance of our best ED functionalized membrane compares with the so far best SAPO-34 membrane reported.[129]

5.2.2. CO_2/N_2 separation performance of SAPO-34 membranes

The synthesized SAPO-34 membranes were also evaluated for the separation of CO_2 from N_2. Table 5.3 shows the separation performance of SAPO-34 membranes as a function of ED loadings for equimolar CO_2/N_2 gas mixtures. The CO_2 permeance was slightly increased by the incorporation of ED. Similar to the CO_2/CH_4 separation selectivity; the CO_2/N_2 selectivity was also increased by the incorporation of ED. The selectivity of the SAPO-34 membranes for CO_2/N_2 gas mixture is low compared to the CO_2/CH_4 because of the smaller difference in kinetic diameters between CO_2 (0.33 nm) and N_2 (0.364 nm) molecules as compared to CH_4 (0.38 nm). The CO_2/N_2 selectivity increased considerably at low ED loadings as compared to the nonfunctionalized membrane. As shown in Table 5.3, both the CO_2/N_2 selectivity and separation index (π) increased at lower ED loadings and decreased at higher ED loadings. The optimum

ethylene diamine concentration for superior CO_2/N_2 separation performance was 0.15 mmol (Figure 5.10).
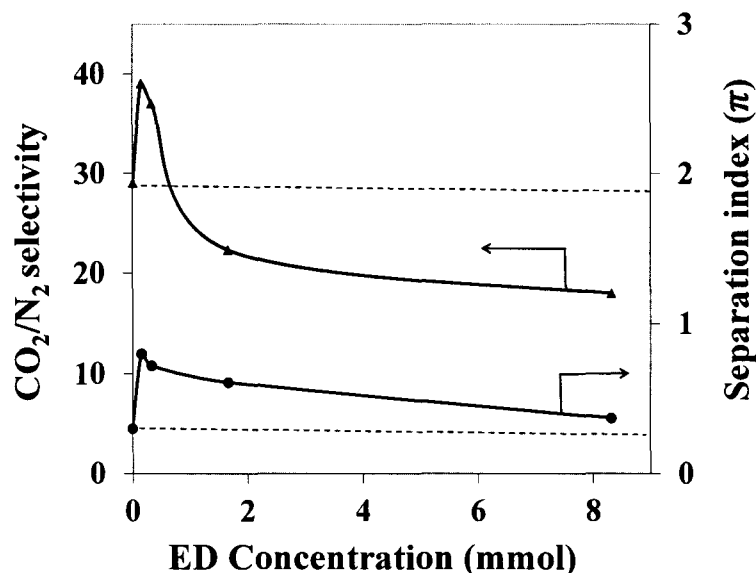
Figure 5.10. Effect of ethylene diamine concentration on CO_2/N_2 selectivity and separation index. The dotted line is shown as reference (nonfunctionalized membrane).

The CO_2/N_2 selectivity for this membrane was increased by ~ 35% and the separation index was increased by ~ 167% as compared to the nonfunctionalized SAPO-34 membrane. Similar to the CO_2/CH_4 separation, the enhanced separation performance for CO_2/N_2 can be attributed to the preferential CO_2 adsorption promoted by the amino group. The limited CO_2/N_2 separation performance for functionalized membranes at high ED loadings may be related to the loss of crystallinity and the presence of less homogeneous crystals. The functionalized membranes with low ED loadings have great potential for CO_2 capture in flue gas treatment because of their relatively high CO_2 permeance and moderate CO_2/N_2 selectivities.

Table 5.3. CO_2/N_2 separation performance of SAPO-34 membranes at 295 K and 138 KPa

Sample ID	P_{CO2} x 10^7 (mol/m^2 s Pa)	P_{N2} x 10^9 (mol/m^2 s Pa)	CO_2/N_2 Selectivity	Separation index*
Non-functionalized	1.1	3.8	29	0.30
0.15 mmol ED	2.1	5.4	39	0.80
0.33 mmol ED	2.0	5.5	37	0.72
1.66 mmol ED	2.9	13.4	22	0.61
8.32 mmol ED	2.2	12.7	18	0.37

*π = CO_2 permeance x (selectivity -1)) x partial pressure

5.3. Hexylamine and Octylamine functionlized membranes

We extended the grafting approach employing other amino organic cations such as hexylamine (HA) and octylamine (OA). We employed the optimum conditions found for ED (0.015 mmol) for the functionalization of SAPO-34 membranes with HA and OA. The SEM images show that the morphology of the seeds was not affected by the functionalization as shown in Figure 5.11. Table 5.4 shows the CO_2/CH_4 separation performance of HA and OA functionalized membranes and compared to the nonfunctionalized membrane. CO_2 permeance decreased with the incorporation of HA and OA, while CO_2/CH_4 selectivities increased significantly. However, the overall CO_2/CH_4 separation performance was improved only for the HA functionalized sample. Octylamine (OA) is a bulkier molecule that led to a huge decrease in CO_2 permeance, most likely associated with pore blockage.
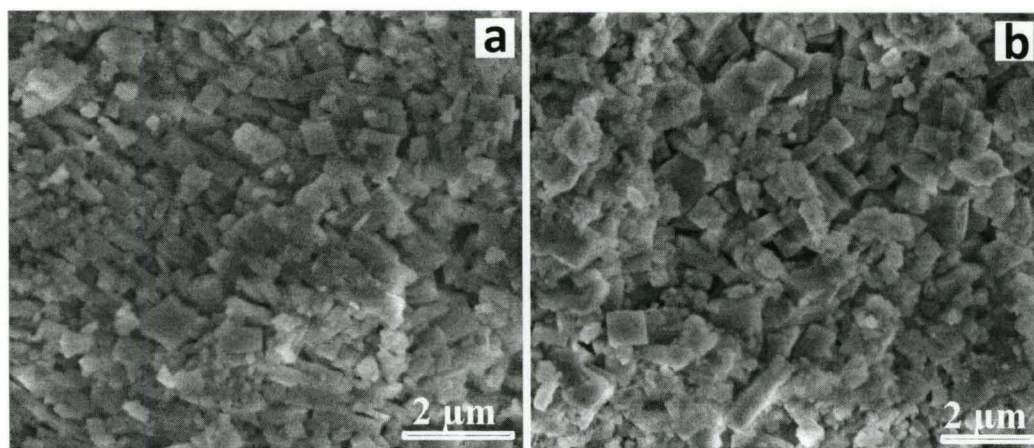
Figure 5.11. SEM images of SAPO-34 seeds functionalized with: a) Hexylamine and b) Octylamine.

Table 5.4. CO_2/CH_4 separation performance of hexylamine and octylamine functionalized SAPO-34 membranes at 295 K and 138 KPa.

Sample ID	P_{CO2} x 10^7 (mol/m^2 s Pa)	P_{CH4} x 10^9 (mol/m^2 s Pa)	selectivity	Separation index*
Non-functionalized	4.6	2.9	159	7.3
0.15 mmol HA	3.7	1.5	238	8.72
0.15 mmol OA	1.9	0.8	229	4.31

*π = (CO_2 permeance x (selectivity -1)) x permeate pressure

Table 5.5 shows the CO_2/N_2 separation performance for the HA and OA functionalized versus nonfunctionalized membranes. As in the CO_2/CH_4 case, the overall separation index (π) was only improved for the HA functionalized membrane. When comparing the three organic amino cations employed to functionalize the membranes, it is clear that ED led to high higher separation performance for both CO_2/CH_4 and CO_2/N_2

mixtures. The presence of the two amino groups in ED, as explained in Figure 5.6,

enhanced in greater extent the preferential CO_2 adsorption as compared to the other two

amino organic molecules (HA and OA).

Table 5.5. CO_2/N_2 separation performance of hexyl amine and octyl amine

functionalized SAPO-34 membranes at 295 K and 138 KPa.

Sample ID	P_{CO2} x 10^7 (mol/m^2 s Pa)	P_{N2} x 10^9 (mol/m^2 s Pa)	selectivity	Separation index*
Non-functionalized	1.1	3.8	29	0.3
0.15 mmol HA	2.1	5.8	36	0.75
0.15 mmol OA	1.2	4.1	30	0.37

*π = (CO_2 permeance x (selectivity -1)) x Permeate pressure

5.4. Model equations

Selectivity is defined as the ratio of CO_2 permeance over CH_4 permeance:

$$\text{Selectivity} = \alpha_{CO_2/CH_4} = \frac{J_{CO_2}}{J_{CH_4}} = \frac{CO_2 \text{ Permeance}}{CH_4 \text{ Permeance}} \quad \text{-------- Equation (5.1)}$$

In general, the diffusion of gas molecules through the membrane takes place by

two prominent phenomena. They are Knudsen diffusion and surface diffusion. Knudsen

diffusion occurs in the gas phase through the pores in the membrane layer having

diameters smaller than the mean free path dimensions of the molecules in the gas mixture

either by concentration or by pressure gradients.[74] As a result, the movement of

molecules inside the narrow pore channels takes place through collision of the diffusing

molecules with the surface rather than with each other. Surface diffusion is the adsorption

of a component on a site and hop from one site to another through strong interaction.[13]

Surface diffusion rates and mechanisms are affected by a variety of factors including the

strength of the surface-adsorbant bond, orientation of the surface lattice, attraction and

repulsion between surface species and chemical potential gradients. Therefore, the total

permeance of a component is the sum of the Knudsen diffusion and surface diffusion

assuming that both diffusion mechanisms are independent of each other.

$$\text{Knudsen diffusion coefficient} = D_k = \frac{d\,u}{3\,\tau} \qquad \text{-------- Equation (5.2)}$$

Where, d = diameter of the pore, u = average gas velocity, τ = tortuosity factor (τ =1,

since the pores of SAPO-34 are cylindrical and straight).

$$\text{u = average molecular speed} = \sqrt{\frac{8RT}{\pi\,m}} \qquad \text{-------- Equation (5.3)}$$

where, R= universal gas constant, T = temperature, m = molecular weight of the gas.

$$\text{Therefore, } D_k \text{ can be expressed as: } \quad D_k = \frac{d}{3}\sqrt{\frac{8RT}{\pi\,m}} \qquad \text{-------- Equation (5.4)}$$

Flux in Knudsen regime of component i is given by,

$$J_{ik} = \frac{n\pi d^2 P\, D_k}{4RTL} \qquad \text{-------- Equation (5.5)}$$

$$\text{Substituting } D_k \text{ from equation 4.4., } \quad J_{ik} = \frac{nd^3 P}{6L}\sqrt{\frac{2\pi}{RTm_i}} \qquad \text{-------- Equation (5.6)}$$

Where n is the surface concentration of pores, L is the thickness of the membrane, P is

the log mean pressure drop across the membrane.

Pressure drop is the driving force for the separation of gases and is calculated using;

$$\Delta P_{ln,i} = \frac{\left(P_{f,i}\, x_{f,i} - P_{p,i}\, x_{p,i}\right) - \left(P_{r,i}\, x_{r,i} - P_{p,i}\, x_{p,i}\right)}{ln\left[\dfrac{\left(P_{f,i}\, x_{f,i} - P_{p,i}\, x_{p,i}\right)}{\left(P_{r,i}\, x_{r,i} - P_{p,i}\, x_{p,i}\right)}\right]}$$ ------- Equation (5.7)

Where, f, p and r are the feed, permeate and retentate respectively. $P_{f,i}$, $P_{p,i}$, and $P_{r,i}$ are the partial pressure of the component i in feed, permeate and retentate respectively and $x_{f,i}$, $x_{p,i}$, and $x_{r,I}$ are the fraction of component i in feed, permeate and retentate respectively.

For a gas passing through the small pores of SAPO-34 in the Knudsen regime, the number of molecules that pass through the pore is proportional to the pressure and inversely proportional to its molecular weight. It is therefore possible to separate a gas mixture if the components have different molecular weight.

Maxwell-stefan equations (M-S equations) have been widely used to calculate the surface diffusion in an ideal gas mixture. The summarized form of Maxwell-stefan equations for a mixture of two gas components diffusing through a membrane is,

$$-\rho\, \frac{q_i}{RT}\, \frac{d\mu_i}{dL} = \frac{q_j J_i - q_i J_j}{q_j^{sat}\, D_{ij}} + \frac{J_i}{D_{is}}$$ -------- Equation (5.8)

Where, ρ is the density of the gas, q_i and q_j is the surface of the pores covered with component i and j respectively, μ_i is chemical potential, L is the thickness of the membrane, J_i and J_j are the fluxes of component i and j through the membrane, D_{is} and D_{ij} is the surface diffusion coefficient of the component i and diffusion coefficient of the mixture.

The driving force for diffusion is the chemical potential gradient on the left hand side of the M-S equation. First term on right hand side represents the interactions

between adsorbed molecules and second term represents the interaction between a molecule and the pore wall. Interaction between adsorbed molecules can be neglected by assuming that the adsorbed molecules are independent. This assumption is valid since the isotherms of SAPO-34 followed the Langmuir model. Also, in small pore zeolites like SAPO-34 (0.38 nm), the inter-cage jumps of adsorbed species are random, so binary exchange coefficient can be taken as infinite. The chemical potential gradient can be related to the gradient in the surface coverage by a matrix of thermodynamic factors. Taking all these into account, the M-S equation can be simplified as

$$\text{Surface diffusion flux, } J_{is} = \frac{\rho \, D_{is} \, q^{sat}}{L} \, e^{-E/RT} \, ln\left(\frac{1-\theta_p}{1-\theta_f}\right) \quad \text{-------- Equation (5.9)}$$

According to Langmuir theory of adsorption,

$$\text{Fractional coverage, } \theta_i = \frac{q_i}{q^{sat}} = \frac{K_i \, P}{1+ K_i P} \quad \text{-------- Equation (5.10)}$$

$$\text{Adsorption equilibrium constant, } K_i = K_0 \, e^{\left[\frac{-\Delta H_{ads}}{RT}\right]} \quad \text{-------- Equation (5.11)}$$

Sustituting θ_p and θ_f (fractional coverage on permeate and feed side) in equation 4.9,

$$J_{is} = \frac{\rho \, D_{is} \, q^{sat}}{L} \, ln\left(\frac{1+K_i P_f}{1+K_i P_p}\right) \quad \text{-------- Equation (5.12)}$$

Where, D_{is} is the surface diffusion coefficient, ΔH_{ads} is the heat of adsorption, P_f and P_p are the pressure on feed and permeate side.

The relation for surface diffusion coefficient (D_{is}) is more complicated than that for Knudsen diffusion because D_{is} and K_i depends on the fraction of the adsorption sites occupied by species i. This is due to the fact that there is usually a distribution function

94

for the heats of adsorption rather than a single value. The total permeance can be evaluated by adding the equations 4.6 and 4.9.

$$J_{total} = J_{ik} + J_{is}$$ -------- Equation (4.13)

$$J_i = \frac{nd^3 P}{6L} \sqrt{\frac{2\pi}{R T m_i}} + \frac{\rho \, D_{is} \, q^{sat}}{L} \, ln\left(\frac{1 + K_i P_f}{1 + K_i P_p}\right)$$ -------- Equation (4.14)

Taking ideal conditions for CO_2/CH_4 separation, we calculated the CO_2 and CH_4 permeances and selectivities for the synthesized SAPO-34 membranes. At 20 psi of feed pressure and 3 mmol/g of adsorption capacity, the CO_2 permeance is 6.2×10^{-7} mol/m^2.Sec. Pa. The permeance is calculated using the typical values of K_i and D_{is} for porous materials as 0.0084 /KPa and 9.9×10^{-11} m^2/sec. The experimental value of the CO_2 permeance for the SAPO-34 membrane with around the same adsorption capacity is 4.6×10^{-7} mol/m^2.Sec. Pa. The change in permeance of CO_2 is around 1.6×10^{-7} mol/m^2.Sec. Pa. Similar results were obtained for CH_4 permeance. The calculated and experimental permeances of CH_4 are 5.2×10^{-9} mol/m^2.Sec. Pa. and 2.0×10^{-9} mol/m^2.Sec. Pa.

The fluxes of CO_2 increases with increase in the pressure drop across the membrane. The fluxes of a component increased with increase in the quantity of the CO_2 adsorbed on SAPO-34 framework. With the incorporation of ethylene diamine content, the CO_2 adsorption on SAPO-34 is increased and it is 9.5 times higher than the CH_4. But, for non-functionalized membrane it is only 6.5. Therefore, the surface diffusion dominates significantly with the incorporation of ethylene diamine content, while the Knudsen diffusion is constant at constant pressure and temperature. As the pressure increases, the CO_2 adsorption increases at higher rate compared to the CH_4 up to certain

pressure and stay constant at higher pressures. These suggest that for the more strongly adsorbed gases, the permeation mechanism through functionalized membrane is strongly based on surface diffusion of the adsorbed species. As the permeance of CO_2 increased, the selectivity also increased considerably. These facts show that the CO_2 adsorbed on the membrane micropores, occupying most of the surface and inhibiting the diffusion of CH_4 due to the existence of a competitive adsorption. The flux is also strongly depends on the temperature. As temperature increases, flux increased due to the activated diffusion. But as temperature increases, the CO_2 adsorption on the SAPO-34 surface decreases, resulting in lower fluxes. The maximum flux can be obtained by carefully selecting the temperature by compensating both effects. It can be concluded that permeances and selectivities of the CO_2 in a gas mixture are the result of a complex equilibrium governed by factors, such as their potential of adsorption and interactions between species and pressure drop across the membrane.

5.5. Conclusions

In summary, SAPO-34 seeds and membranes were functionalized with several organic amino cations. The successful incorporation of the amino groups in the SAPO-34 framework was confirmed by FTIR. The chabazite structure of SAPO-34 was preserved after the functionalization step. The resultant SAPO-34 membranes effectively separated CO_2/CH_4 and CO_2/N_2 gas mixtures. An optimum concentration of ethylenediamine led to highly CO_2 selective membranes. CO_2/CH_4 selectivities as high as 245 with CO_2 permeances of ~ 5 x10^{-7} mol/m^2 s Pa at 295 K and 138 KPa, were observed for an optimum ethylenediamine functionalized membrane, which corresponded to a ~ 40% increase in separation index as compared to the nonfunctionalized SAPO-34

membrane. Similarly, CO_2/N_2 separation performance was highly improved with the incorporation of ethylenediamine. CO_2/N_2 selectivities as high as 39 with CO_2 permeances of ~ 2.1 x10^{-7} mol/m^2 s Pa at 295 K and 138 KPa, were observed for an optimum ethylenediamine functionalized membrane, which corresponded to a ~ 167% increase in separation index as compared to the nonfunctionalized SAPO-34 membrane. The presence of amino groups in the SAPO-34 structure led to higher CO_2/CH_4 and CO_2/N_2 selectivities mainly due to preferential adsorption of CO_2

CHAPTER 6

STRUCTURAL EVOLUTION OF ZEOLITIC

IMIDAZOLATE FRAMEWORK-8

A fundamental understanding on the formation mechanisms of zeolitic imidazolate frameworks is highly important in order to improve structural and morphological control in the synthesis of these novel materials. To our best knowledge, almost nothing is known about the nucleation, growth, and crystallization events on this particular type of metal organic frameworks. Herein, we present the entire process from gel formation, nucleation, crystallization and growth of ZIF-8 at room temperature.

6.1. Crystal evolution of ZIF-8

Figure 6.1 shows the structural evolution of ZIF-8 as a function of time. As shown in Figure 6.1, the most prominent peak for ZIF-8 corresponding to the plane (011) increased as time progressed. The area under the curve of this peak was quantified using origin software, after baseline correction, to determine *the relative crystallinity of ZIF-8 phase* as shown in Figure 6.2 and Table 6.1, which can be related to the phase transformation rate. Similar analysis has been used to determine the relative amount of phases/crystallinity in porous frameworks.[213,214] Even at short synthesis times (20

98

minutes), the presence of sharp peaks suggests that ZIF-8 likely evolves from a metastable phase.
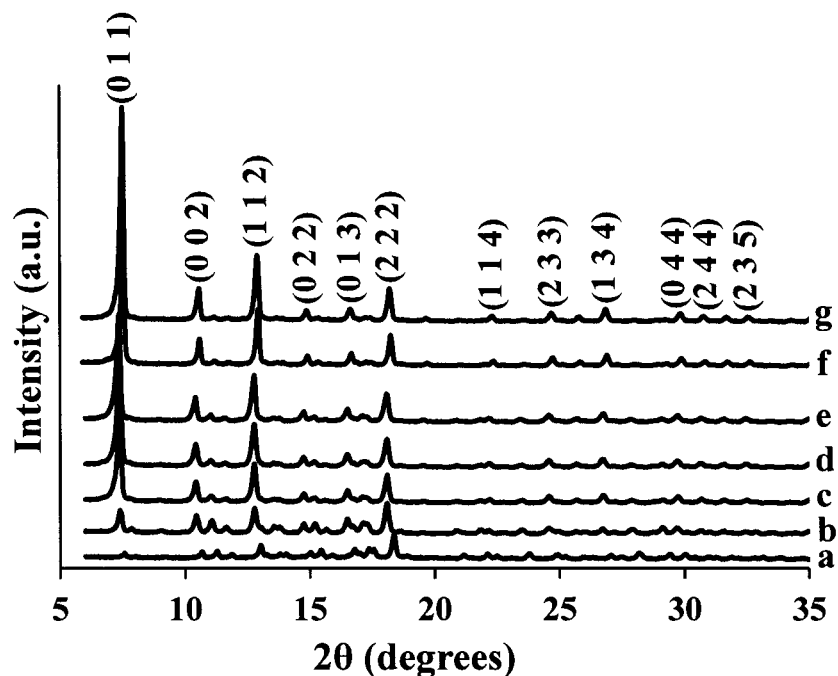
Figure 6.1. XRD patterns illustrating the structural evolution of ZIF-8 as a function of synthesis time : a) 20 min; b) 30 min; c) 40 min; d) 50 min; e) 60 min; f) 12 hrs and g) 24 hrs.

As shown in Figure 6.1 and Figure 6.2, the relative crystallinity of ZIF-8 increases slowly at short synthesis times. Then a rapid increase is observed in the 30 to 40 minutes range. Finally, after 50 min the *relative crystallinity of ZIF-8* remained practically constant (above 90 %), reaching a maximum of 100% at 24 hr. Since longer synthesis times (48 hr) did not change the area under the curve of the (011) peak of ZIF-8 as compared to the 24 hr sample, it is reasonable to assume that the ZIF-8 relative crystallinity achieves its maximum at 24 hr. It is important to mention that small particles were observed at 10 min, however due to its extremely small yield, we were not able to

record the XRD pattern. Nevertheless, TEM revealed that ~50 nm particles, some of them already faceted, evolved at 10 min. The formation of ZIF-8 is also observed using FTIR as shown in Figure 6.3.
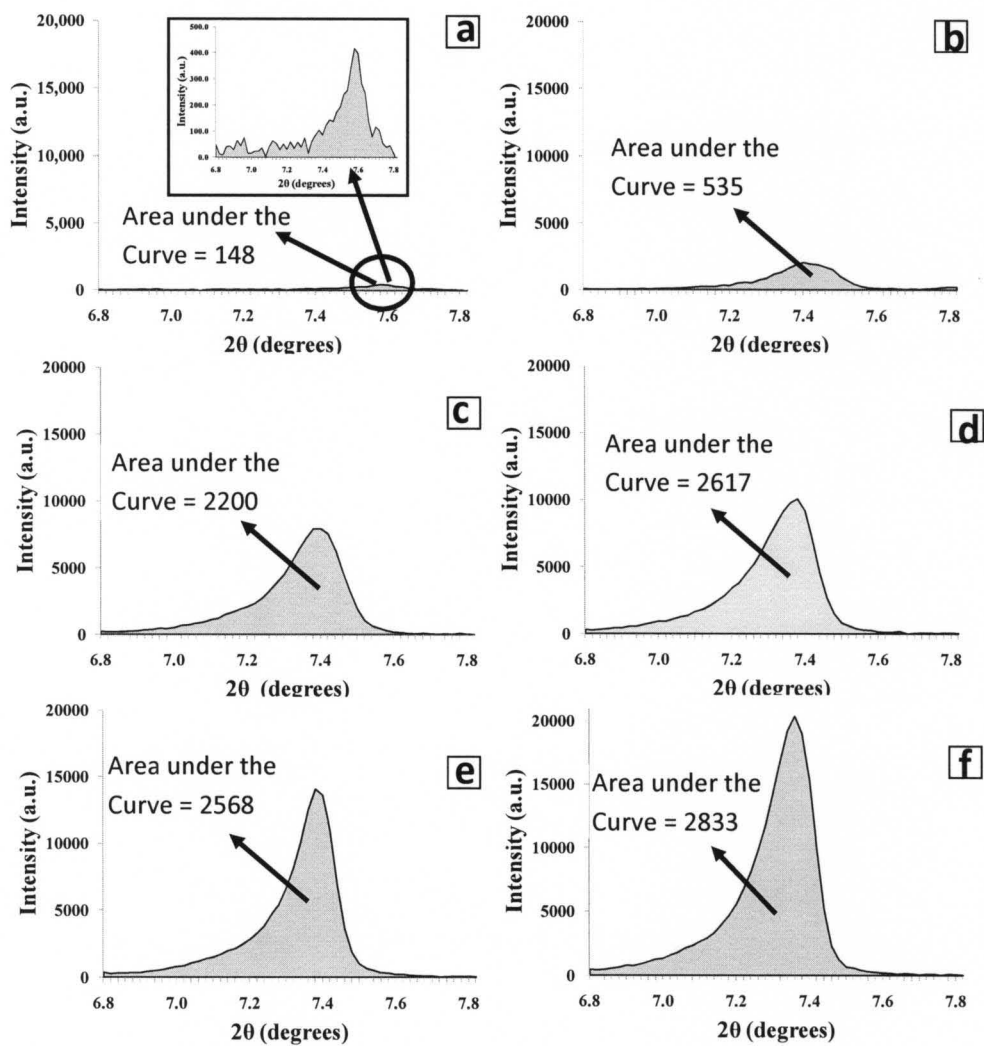
Figure 6.2. Calculation of the area under the curve for the most prominent XRD peak (0 1 1) of ZIF-8 synthesized at: a) 20 min; b) 30 min; c) 40 min; d) 60 min; e) 12 hrs; and f) 24 hrs.

The ZIF-8 relative crystallinity was calculated with the following expression:

$$\text{ZIF-8 relative crystallinity} = \frac{\text{Area under the curve (0 1 1)plane at time "t"}}{\text{Area under the curve (0 1 1)plane at 24 hr}}$$

-------- Equation (6.1)

Table 6.1. ZIF-8 relative crystallinity as a function of synthesis time

Synthesis time	Area under the curve	% crystallinity	Surface area (m^2/g)
20	148	5.2	180
30	535	18.8	193
40	2200	77.6	489
50	2618	92.4	613
60	2617	92.3	744
720	2568	90.6	814
1440	2833	100	798
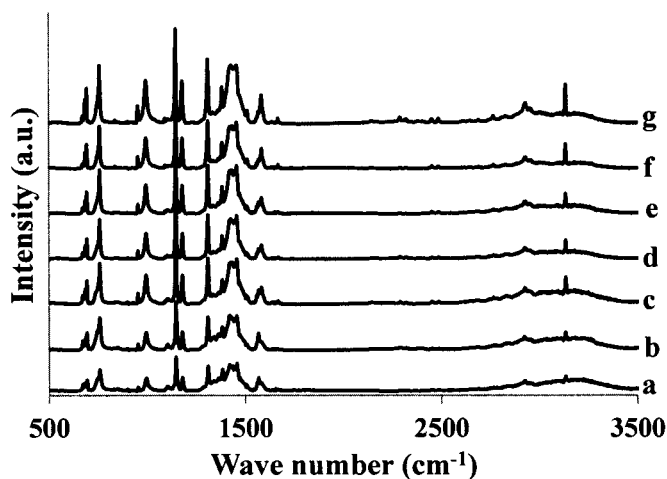
Figure 6.3. FTIR study of the structural evolution of ZIF-8 as a function of synthesis time: a) 20 min; b) 30 min; c) 40 min; d) 50 min; e) 60 min; f) 12 hrs and g) 24 hrs.

101

6.2. Kinetics of ZIF-8 formation

I - Nucleation, II- Growth phase, III- Stationary phase
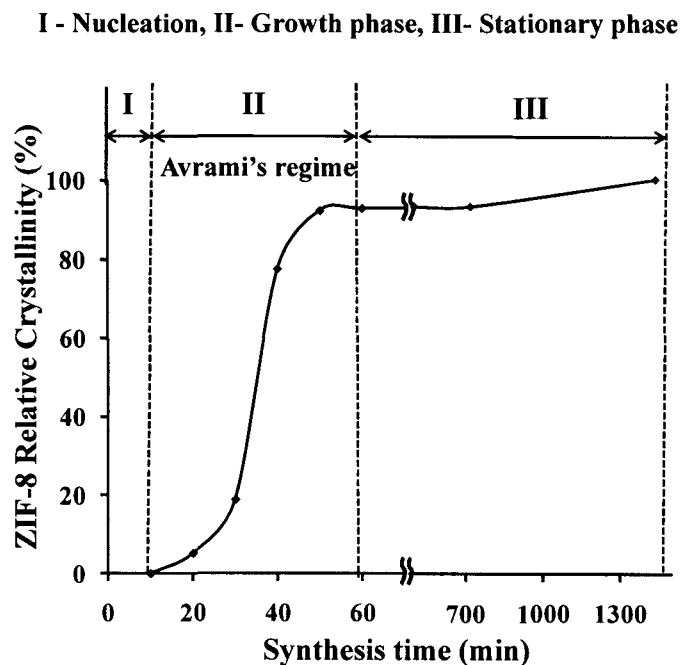
Figure 6.4. Kinetics of transformation of ZIF-8 as a function of time.

As shown in Figure 6.4, the structural evolution of ZIF-8 as a function of time can be divided in three stages. Initially, below 10 minutes, there is an incubation time required to nucleate the ZIF-8 phase, corresponding to the nucleation stage (I). Once nucleated, there is an increase in the relative crystallinity of ZIF-8 with time (II). In this region, a maximum in crystallinity is achieved at ~60 minutes. Interestingly, in this sigmoidal regime, the kinetics of transformation followed Avrami's classical model;[215,216] therefore, the relative crystallinity of ZIF-8 as a function of time in this region can be expressed as y=1-exp [-kt^n]; where k is a scaling constant, and n is the Avrami's constant. For our case, k = 5.1 x10^{-7}, and n ~ 4 as shown in Figure 6.5. In particular, n gives useful information regarding the nucleation process, and shape of the growing entities. Typically a value of 4 suggests that the phase nucleates randomly in the parent phase

102

(homogeneous nucleation), and that the growing entities adopt spherical shapes.[217,218]

Finally, the ZIF-8 relative crystallization rate remains relatively constant above 60

minutes, due to the consumption of the metastable phase (III).
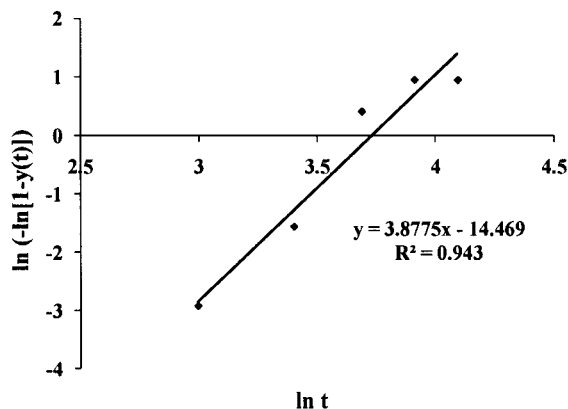
Figure 6.5. Calculation of rate of formation of ZIF-8 crystals

Avrami's Equation : $1 - y(t) = e^{Kt^n}$ -------- Equation (6.2)

LinearAvrami's Equation: $\ln(-\ln[1 - y(t)]) = \ln K + n \ln t$ -------- Equation (6.3)

t = synthesis time

y (t) = ZIF-8 relative crystallinity as a function of time

k = scale constant

n = Avrami's constant

The initial pH of the solution was 7.8. The pH decreased to 7.5, 7.4, and 7.3 at 10,

20 and 40 minutes respectively. At 50 minutes and above, the pH remained practically

constant at 7.2 as shown in Figure 6.6, and correlates with the ZIF-8 relative crystallinity,

suggesting that a reduction in the pH may promote the crystallization of the framework.

At equilibrium, protonated and neutral forms of the imidazole linker coexists in

solution.[195]. Based on the correlation between the solution pH and the evolution of the

ZIF-8 relative crystallinity, it is likely that the concentration of the deprotonated linker decreased as pH decreased, resulting in the stabilization of the neutral form of the linker, which ultimately limited *the rate of phase transformation* as confirmed by the late stages of Avrami's regime and the stationary region of Figure 6.4.
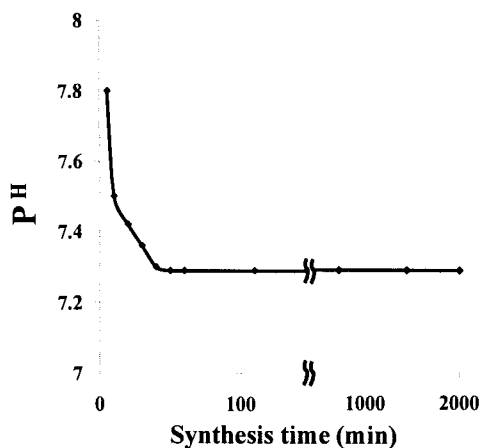
Figure 6.6. Solution pH as a function of synthesis time

6.3.   Morphological evolution of ZIF-8

The formation and growth of ZIF-8 was confirmed by TEM images as shown in Figure 6.7. The sample synthesized at 10 minutes reveals small ~50 nm spherical (consistent with Avrami's model) and faceted particles displaying narrow size distribution. The presence of some faceted particles indicates initial stages of crystallization. At 30 minutes, the particle size increased to 230 ± 40 nm (Figure 6.7b). Furthermore, some crystals show facets. As shown in Figures 6.7c and 6.7d, the size of the crystals remained practically constant at 40 and 60 minutes; however more homogeneous faceted crystals were observed. In particular, homogeneous ~230 nm ± 20nm crystals were observed at 60 minutes. At 12 hrs, the crystal size increased to 500 ± 40 nm and became less homogeneous (Figure 6.7e).
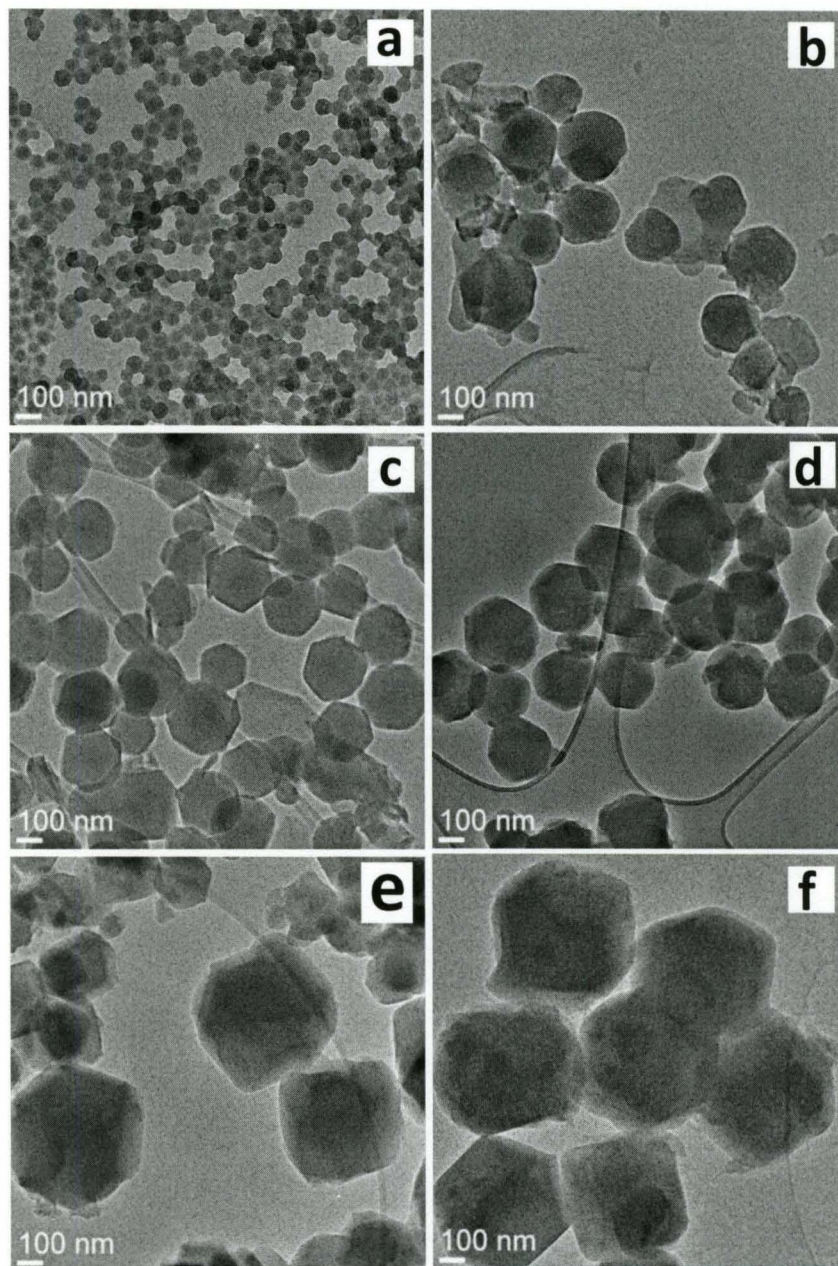
Figure 6.7. TEM images of ZIF-8 as a function of synthesis time: a) 10 min; b) 30 min; c) 40 min; d) 60 min; e) 12 hrs; and f) 24 hrs.

Finally, Figure 6.7f shows ~500 nm crystals displaying relative narrow size distribution. The TEM images revealed that while increasing the crystallization time from

10 minutes to 24 hrs, the average particles size increased significantly, most likely due to the Ostwald ripening. In this spontaneous, thermodynamically-driven process, small particles disappear at the expense of growing larger ones, which are energetically favored.

6.4. SAED patterns of ZIF-8 evolution
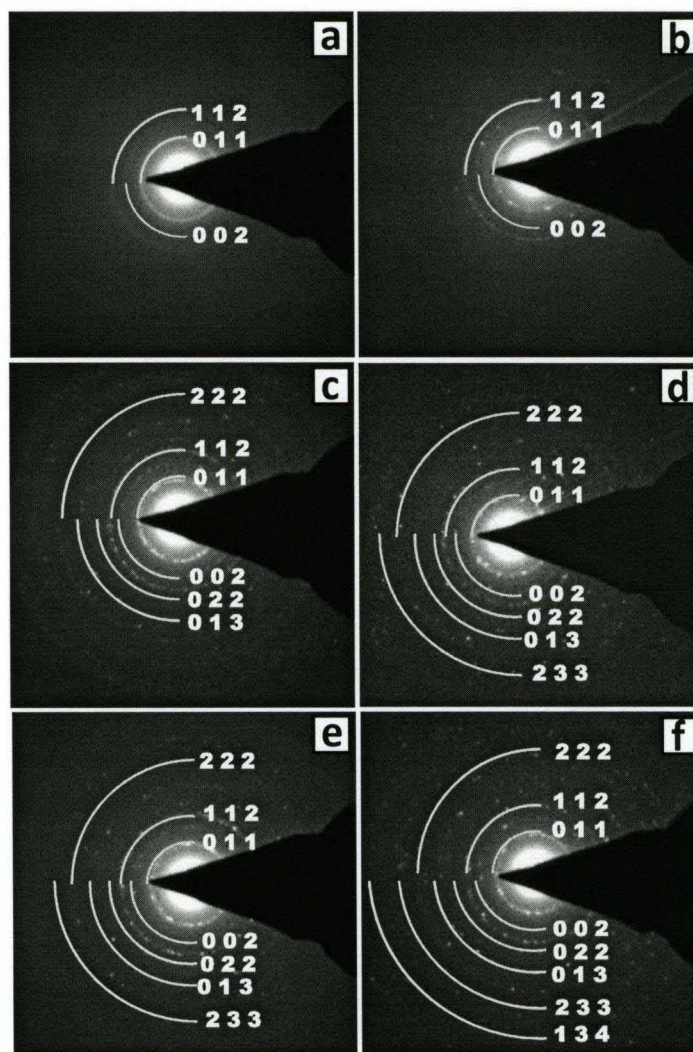
Figure 6.8. TEM diffractograms of ZIF-8 as a function of synthesis time: a) 10 min; b) 30 min; c) 40 min; d) 60 min; e) 12 hrs; and f) 24 hrs

Figure 6.8 shows the selected area electron diffraction patterns (SAED) as a function of synthesis time. As shown in Figure 6.8a, the starting of the formation of crystal planes of ZIF-8 is observed. The well-defined ring nature of SAED pattern confirms the formation of crystallites of ZIF-8. Because of relatively small crystallite size the rings are diffuse. With the increase of the synthesis time, the average crystal size increases and the SAED rings become more "spotty". The d-spacing of the (0 1 1) plane calculated from the SAED patterns is ~11.95 Å, in agreement with its XRD pattern and reported d-spacing values for crystalline ZIF-8 particles. The cubic lattice parameter of these crystals is 16.87 Å.
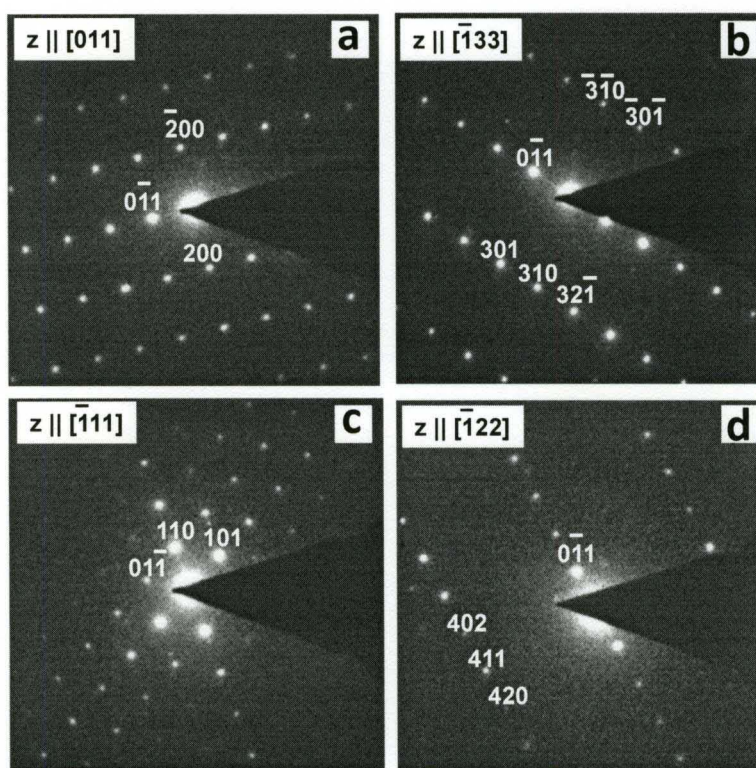
Figure 6.9. SAED patterns of the ZIF-8 crystals synthesized at 12 h taken from four crystals oriented close to: a) [0 1 1]; b) [-1 3 3]; c) [-1 1 1]; and d) [-1 2 2] zone axis. The indexing of the patterns is consistent with the bcc crystal structure of ZIF-8.

Figure 6.9 shows single crystal SAED patterns from a few randomly selected crystals of sample synthesized for 12 hrs. All these patterns were consistently indexed using bcc crystal structure. Moreover, the lattice parameter obtained from these patterns agrees within the experimental error with the one expected for ZIF-8.

The nitrogen adsorption-desorption isotherms displayed type I isotherms, typical of microporous phases (Figure 6.10). Interestingly, the BET surface areas correlated with the ZIF-8 relative crystallinity i.e. low surface areas were observed at 20 and 30 minutes, then increased rapidly in the 40-60 minutes range, and remained practically constant above 60 minutes as shown in Table 6.1. The CHN analysis of the pure crystalline ZIF-8 sample showed that the percentage of these elements is C- 41.11, H - 4.62, and N - 24.86 (Ash - 26.5), which are closely in agreement with the theoretical components.[195]
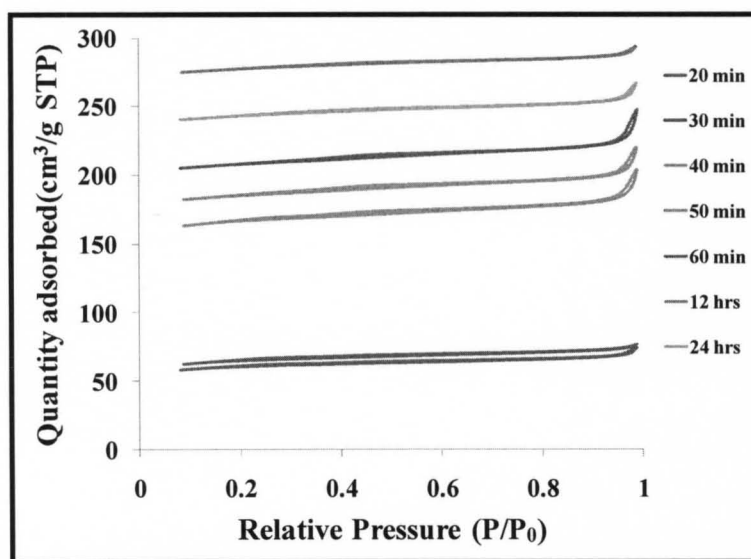
Figure 6.10. Nitrogen adsorption-desorption isotherms of ZIF-8 as a function of synthesis time.

6.5. Particle growth mechanism

Figure 6.11 shows a schematic of the potential events that may take place during the formation of ZIF-8 crystals. Our XRD analysis and TEM studies support the proposed formation pathway. The homogenized gel solution led to ~50 nm particles after 10 minutes. As time progressed, tiny ZIF-8 crystallites grew at the expense of the surrounding spherical gel agglomerates, most likely as a result of supersaturation within the gel particles. This phenomena has been observed during the formation of various types of zeolites, including zeolite A,[219] Y[220] and Si-MFI.[221,222] At this point, ZIF-8 and a metastable phase coexist. The fraction of ZIF-8 phase increases until the nutrient pool (remaining metastable phase) is totally exhausted leading to a fully crystalline ZIF-8 phase. Based on XRD analysis, one may assume that the ZIF-8 structure fully develops at synthesis times above 50 min. Finally, the "small" crystals to attain a lower energy state need to transform into "larger" crystals via Ostwald ripening mechanism.[223]

ZIF-8 +
metastable phase

Larger crystals of ZIF-8 +
metastable phase

30 min

10 min

60 min

24 hrs

Larger ZIF-8
crystals

Homogeneous pure
crystalline ZIF-8
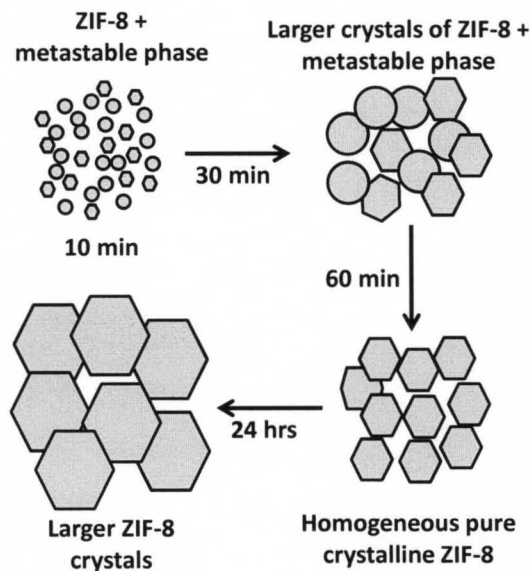
Figure 6.11. Proposed formation pathway of ZIF-8 as a function of synthesis time.

As suggested for several zeolite systems,[224] the medium range order (low relative crystallinity) observed in ZIF-8 may be related to weak Vanderwaals intermolecular interactions established in the synthesis gel before the development of long range order of the crystal, leading to fully crystalline phase. This strongly suggests that species in solution participating in the formation of the ZIF-8 may form a structure with medium range order and then turn to long range order by solution transport or solid state (supported by Avrami's kinetics) transformation mechanisms or by a combination of both.

6.7.   Conclusions

In summary, we have followed the structural evolution of ZIF-8 as a function of time at room temperature. We have identified the different stages of ZIF-8 formation: nucleation, crystallization, growth, and stationary periods; and elucidated its kinetics of transformation. We hypothesize that the observed semicrystalline to crystalline transformation may take place via solution and solid mediated mechanisms as suggested by the observed phase transformation evolution and Avrami's kinetics respectively. We found that the reduction in solution P^H played an important role as the driving force for the crystallization process. A fundamental understanding of ZIF-8 structural evolution demonstrated in this study would facilitate the preparation of novel functional materials. For instance, this study will help in developing ZIF-8 membranes to be used for molecular separations at different synthesis times, which in principle will allow us to effectively control crystal size and membrane thickness, which are critical parameters in the preparation of efficient membranes.

CHAPTER 7

HIGHLY PERMEABLE ZEOLITIC IMIDAZOLATE FRAMEWORK-8 MEMBRANES FOR CO_2/CH_4 SEPARATION

In this chapter, we present the synthesis, characterization and CO_2/CH_4 gas separation performance of tubular alumina supported ZIF-8 membranes using hydrothermal process. To the best of our knowledge, this is the first example of the preparation of continuous and reproducible ZIF-8 membranes for a functional gas separation application. The synthesized ZIF-8 membranes displayed unprecedented high CO_2 permeances and relatively high separation indexes for equimolar mixtures of CO_2 and CH_4.

7.1. Structural studies of ZIF-8

The XRD pattern of the hydrothermal synthesized ZIF-8 seeds is shown in Figure 7.1. The XRD pattern corresponds to SOD structure, which is the typical structure of ZIF-8. The relative intensity and peak positions of the XRD pattern are in agreement with previous reports,[161,164] confirming the formation of pure crystalline ZIF-8 phase. The interplanar spacing calculated using Bragg's law from the reflections at different Bragg's angles are presented in Table 7.1 and agrees well with literature.[161,164] The average crystal size was ~ 40 ± 5 nm, calculated using the Scherrer's equation from the

broadening of the XRD peaks. Absorption FTIR spectra revealed the typical lattice

vibration frequencies of the bonds between zinc and imidazole in ZIF-8 structure (Figure

7.2). The d-spacing values are calculated using the Bragg's equation.
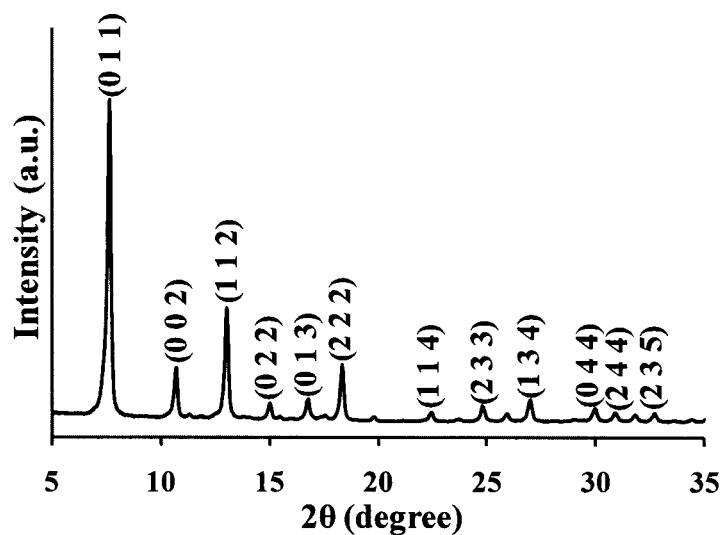
Figure 7.1. XRD patterns of ZIF-8 seeds employed for membrane synthesis
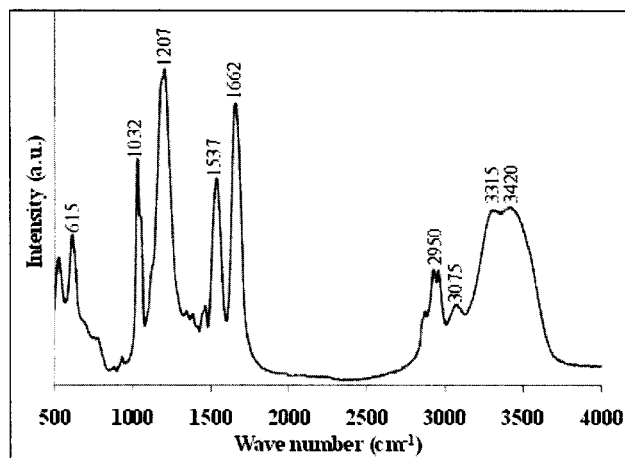
Figure 7.2. FTIR spectra of ZIF-8 seeds employed for membrane synthesis.

Table 7.1. Calculation of d-spacing using XRD and comparing with SAED patterns

Peak number	θ	Intensity	d-spacing	d-spacing /11.54	Diameter of SAED rings	Diameter /5.1	Planes
1	.65	27828	11.54	1	5.1	1	(0 1 1)
2	0.7	4903	8.26	0.71	6.7	0.76	(0 0 2)
3	3.0	10028	6.78	0.58	8.7	0.58	(1 1 2)
4	5.0	1883	5.89	0.51	10.2	0.5	(0 2 2)
5	6.7	2229	5.27	0.45	11.3	0.45	(0 1 3)
6	8.3	5164	4.83	0.41	12.4	0.41	(2 2 2)
7	2.4	1087	3.96	0.34	14.2	0.35	(1 1 4)
8	4.7	1660	3.58	0.31	14.9	0.34	(2 3 3)
10	7.0	2166	3.29	0.28	16.8	0.30	(1 3 4)
11	0.0	1429	2.97	0.25	17.5	0.29	(0 4 4)
12	0.9	1091	2.89	0.25	18.1	0.28	(3 3 4)
13	1.8	908	2.80	0.24	20.4	0.25	(2 4 4)

The morphological features of ZIF-8 crystals were inspected under HRTEM (Figure 7.3a). Sharp faceted and homogeneous ~ 55 nm crystals were observed. The morphology was also inspected by SEM as shown in Figure 7.3b. The formation of ZIF-8 was also confirmed by collecting the TEM SAED patterns and comparing it with XRD patterns. The diffraction rings of the different planes, shown in Figure 7.3c, are in well agreement with the XRD peaks of ZIF-8 as shown in Table 7.1 and corresponds to a body centered cubic structure with a unit cell parameter of 16.48 °A. Column 5 and Column 7

in Table 7.1 show the normalized values of *d*-spacing, calculated using the XRD peaks and the TEM SAED patterns respectively. They are in well agreement with each other. The corresponding planes are also given in Table 7.1.
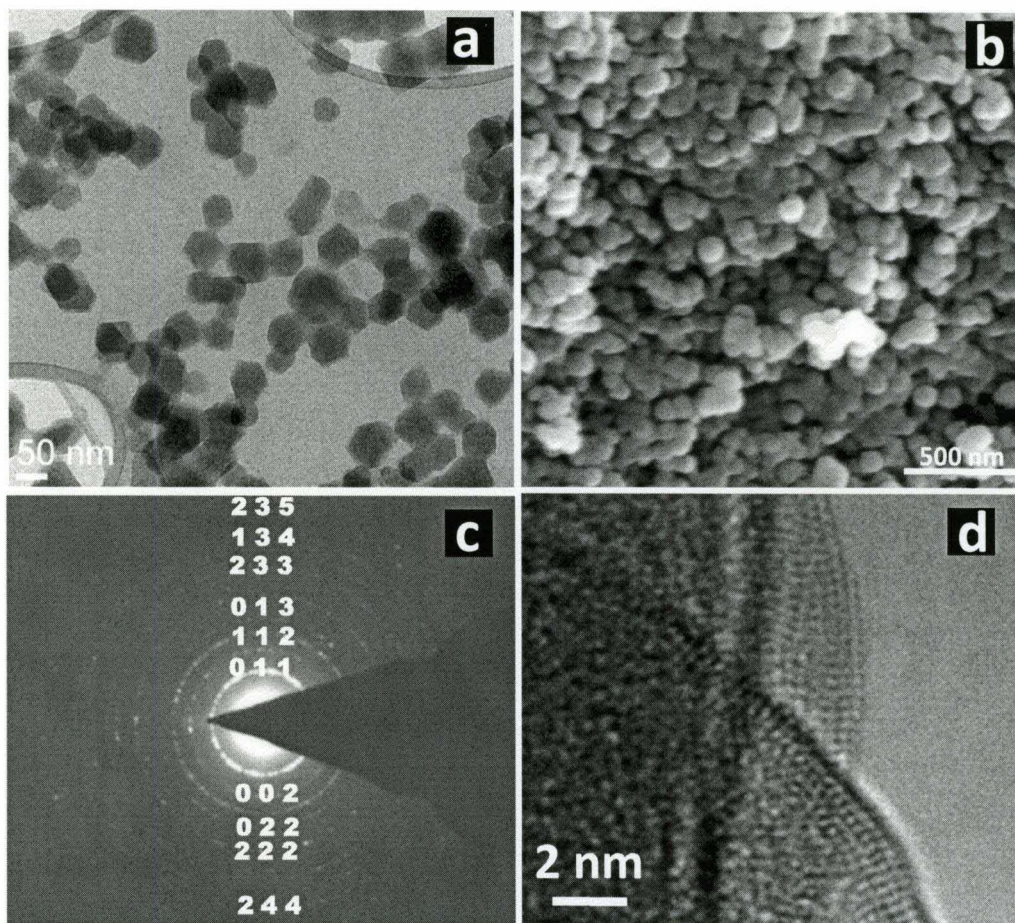
Figure 7.3. ZIF-8 seeds employed for membrane synthesis; a) TEM image; b) SEM image; c) SAED patterns; d) Magnified image of the HRTEM image.

A magnified image of the HRTEM of the hexagonal-like particles reveals the spacing of the lattice fringes matching with the *d*-spacing of the (2 2 2) planes (Figure 7.3d). These lattice fringes were taken with minimum TEM beam exposure time because of the fast amorphization of the crystals. The CHN analysis revealed the carbon,

hydrogen and nitrogen contents in the ZIF-8 framework, C – 41.7%, H - 4.5% and N - 24.4% (ash ~ 29.4%), which are in good agreement with the calculated theoretical amounts (C - 42.2%, H -4.4% and N - 24.6%).[164]

The apparent surface area and micropore volume of the ZIF-8 nanocrystals were 1072 m^2/g and 0.53 cm^3/g respectively, using BET and DR methods and taking the data points on the nitrogen branch in the range of P/P_0 of 0.01– 0.3. Type I isotherms (Figure 7.4a) were observed indicating the microporous nature of the ZIF-8 crystals. The adsorption isotherms of CO_2 and CH_4 on ZIF-8 were collected at room temperature using water as the coolant. The ZIF-8 crystals adsorbed CO_2 preferentially over CH_4. At 100 KPa, the ZIF-8 crystals adsorbed ~14 times more CO_2 than CH_4 as shown in Figure 7.4b. The nonpolar nature of CO_2 molecules favored its binding and preferential adsorption on polar ZIF-8 walls.[162] The preferential adsorption of CO_2 over CH_4 makes ZIF-8 crystals highly attractive for CO_2 purification from natural gas.
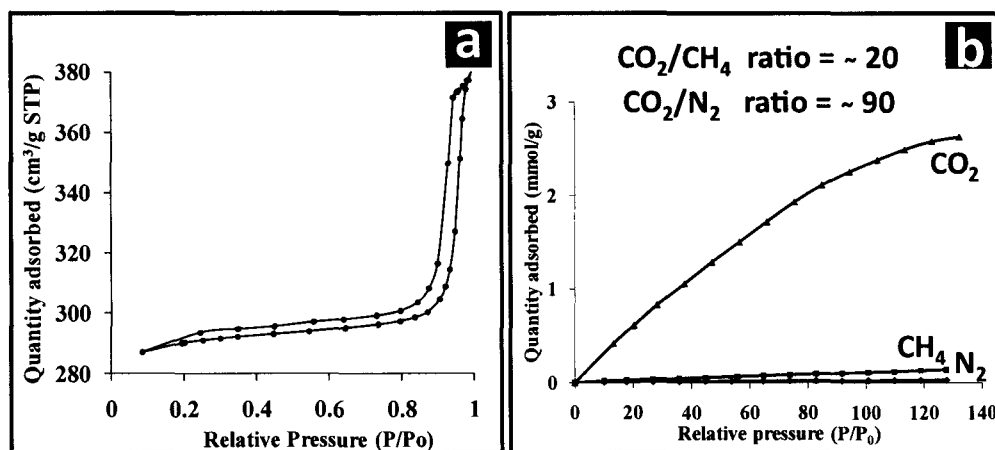
Figure 7.4. ZIF-8 seeds employed for membrane synthesis; a) Nitrogen adsorption-desorption isotherm; and b) CO_2 and CH_4 adsorption isotherms.

7.2. CO₂/ CH₄ separation performance of ZIF-8 membranes

ZIF-8 membranes were synthesized by in-situ crystallization on tubular porous α-alumina supports. The hydrothermal synthesized seeds provided nucleation sites for membrane growth. CO_2/CH_4 separation performance of the alumina supported ZIF-8 membranes is shown in Table 7.2. All membranes were coated with two layers except Z4, which was coated with eight layers. The thickness of the two layer membrane was ~5 μm as shown in Figure 7.5a, whereas the eight layer membrane was ~9 μm thick (Figure 7.5b). The small thickness difference between the two layered and eight layered membranes suggests partial dissolution of the first layers. ZIF-8 crystals of ~110 ± 15 nm allowed the formation of continuous thin membranes as shown in Figure 7.5c. The size of the well-defined spherical-like crystals on the membrane increased considerably as compared to the size of the seed crystals (Figure 7.3a). This increase in crystal size may be related to the recrystallization and sintering of the crystals with the incorporation of the ZIF-8 layers. It is important to mention that although TEM images show the presence of well-defined hexagonal crystals for ZIF-8 seeds (Figure 7.3a), SEM images (Figure 7.3b) revealed spherical-like particles of similar size. The prolonged exposure time of the SEM electron beam promoted the amorphization of the hexagonal like crystals to spherical like morphology. In fact, a detailed inspection of figure 7.3a reveals that even with minimum TEM exposure time, some hexagonal crystals transformed to spherical shapes as a result of surface energy minimization. This phenomenon has been referred in the literature as roughening transition.[225,226]

116
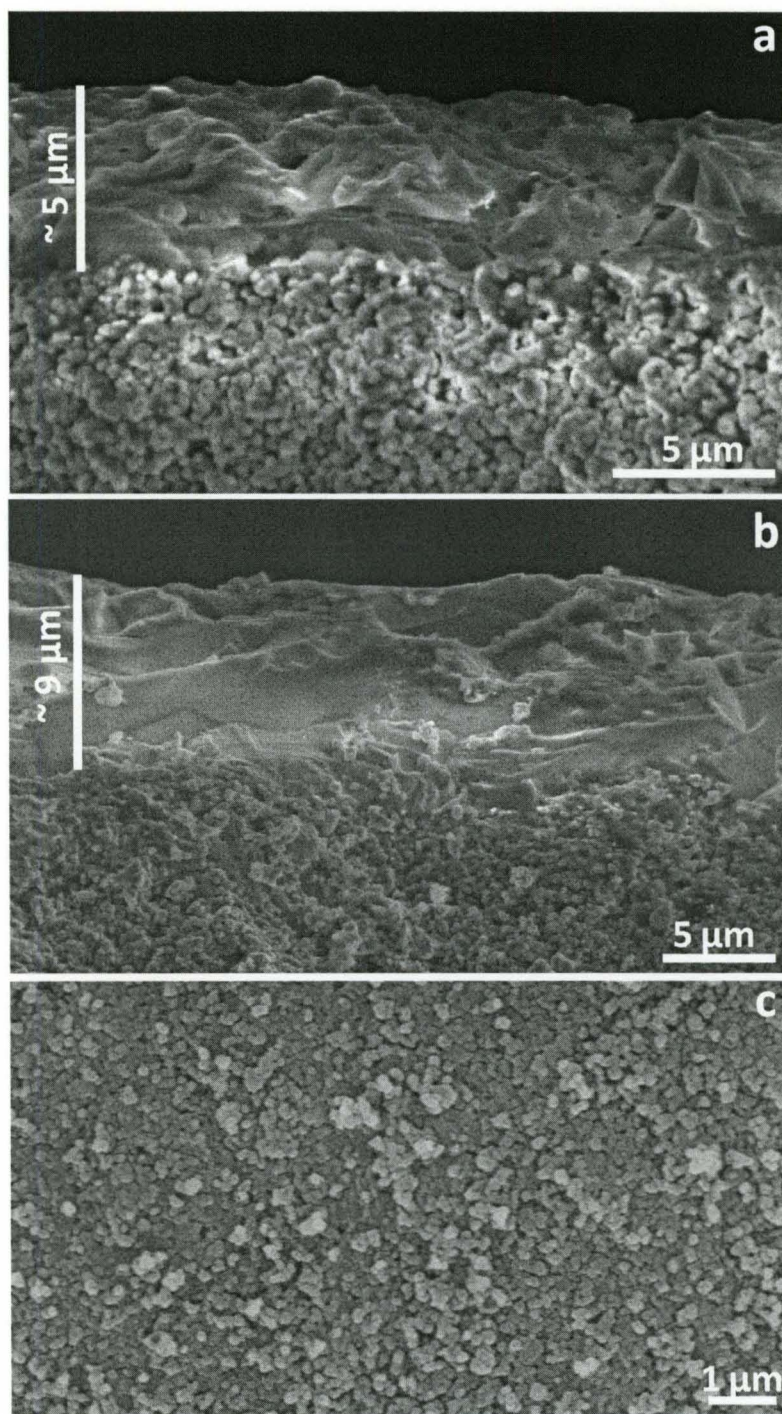
Figure 7.5. ZIF-8 membranes: cross sectional view of a) two layer; and b) eight layer membranes and c) top view of the two layer membrane

Table 7.2. $CO_2/$ CH_4 separation properties of ZIF-8 membranes at a permeate pressure of 99.5 KPa and pressure drop of 139.5 KPa.

Membrane ID[a]	P_{CO2} (x10^{5})	P_{CH4} (x10^{6})	CO_2/CH_4 selectivity	Separation index (π)[b]
Z1	2.43	4.72	5.1	9.9
Z2	2.19	4.63	4.7	8.0
Z3	2.11	5.17	4.1	6.5
Z4	1.69	2.42	7.0	10.0

[a] Z1-Z3 are 2 layered membranes; Z4 is 8 layered membrane

[b] $\pi = (P_{CO2}$ x (selectivity-1)) x Permeate pressure[23]

ZIF-8 membranes displayed unprecedented high CO_2 permeances up to ~ 2.4 x 10^{-5} mol/ $m^2 \cdot s \cdot Pa$ and CO_2/CH_4 selectivities from ~ 4 to 7 at 295 K and a feed pressure of 139.5 KPa, the maximum pressure that the membranes could hold. The separation index of the membranes ranged from ~ 6.5 to 10, which is comparable with that of some alumina supported SAPO-34 membranes.[21] The addition of multiple layers in sample Z4 increased the CO_2/CH_4 selectivity and decreased the CO_2 permeance, most likely due to the reduction of nonzeolite pores and increase in membrane thickness respectively (Table 7.2).

The high CO_2 permeances are not only due to the presence of small crystals with narrow size distribution, which led to thin membranes, but also due to the textural properties of the alumina porous support which is composed of an outer layer of 0.2 μm average pore size and a porous area of 0.8 μm average pore size. The outer layer provided a smoother surface for uniform intergrowth of the ZIF-8 crystals with the

support surface, while porous are of 0.8 μm average pore size translated into higher fluxes. The CO_2/CH_4 selectivity of the membranes was low, most likely due to a high concentration of nonzeolite pores. Improving the interaction between the alumina support and the ZIF-8 will increase the selectivity at the expense of the CO_2 permeance. Despite the low CO_2/CH_4 selectivity, the high CO_2 permeances contributed to the relatively high separation indexes. Although ZIF-8 is composed of large 11.6 Å pores and small pore apertures of 3.4 Å, density functional theory simulation data suggests that the smaller pores are the preferential adsorption sites for CO_2 molecules.[227] Therefore, the pore aperture of ZIF-8 is 0.34 nm, favors the diffusion of CO_2 (kinetic diameter ~ 0.33 nm) over CH_4 (kinetic diameter of ~ 0.38 nm). This molecular sieving property along with preferential adsorption of CO_2 over CH_4 of ZIF-8 membrane resulted in high separation performance.

7.3. Conclusions

In summary, reproducible thin ZIF-8 membranes with ~ 5 - 9 μm thickness were synthesized by secondary seeded growth on tubular α-Al_2O_3 porous supports. The separation performance of these membranes for equimolar CO_2/CH_4 gas mixtures is presented. The membranes displayed unprecedented CO_2 permeances as high as ~2.4 x 10^{-5} mol/m^2·s·Pa with CO_2/CH_4 separation selectivities of ~ 4 to 7 and separation indexes in the ~ 6.5 to 10 range at 295 K and a feed pressure of 139.5 KPa. Future experiments will focus on exploring diverse chemical (compositions, reagents nature) and processing (number of layers, hydrothermal synthesis time and temperature) parameters to prepare more robust and more selective membranes able to hold high pressures for CO_2/CH_4 separation.

CHAPTER 8

CONCLUDING REMARKS

We have demonstrated the development of continuous zeolite (SAPO-34) and metal organic framework (ZIF-8) membranes able to separate CO_2 /CH_4 and CO_2/N_2 gas mixtures. The resultant SAPO-34 membranes displayed CO_2/CH_4 selectivities as high as 245 with CO_2 permeances of ~5 x10^{-7} mol/m^2 s Pa at 295 K and 138 KPa. To our best knowledge, our SAPO-34 membranes display one of the best (if not the best) overall separation performance for the separation of CO_2/CH_4 gas mixtures. Moreover, we demonstrate the successful synthesis of novel ZIF-8 membranes for CO_2/CH_4 gas separation. This work represents one of the first examples (and the only example on CO_2/CH_4 separation) of the successful preparation of continuous, thin, and reproducible zeolitic imidazolate framework membranes for a functional *gas mixture* separation. Our ZIF-8 membranes displayed unprecedented high CO_2 permeances up to ~ 2.4 x 10^{-5} mol/ m^2·s·Pa and CO_2/CH_4 selectivities from ~ 4 to 7 at 295 K at a feed pressure of 139.5 KPa. The specific deliverables from this work are:

1.   SAPO-34 was synthesized employing the growth inhibitors such as polyethylene glycol, brij-35 and methylene blue, to decrease the crystal size. The SAPO-34 crystals displayed higher BET surface areas up to 700m^2/g compared to the sample synthesized

without crystal growth inhibitors. The crystal size is decreased to ~0.6-0.9 μm range with narrow particle size distribution from ~1.5 μm. The relatively high N/H molar ratios observed in the SAPO-34 crystals prepared with crystal growth inhibitors, led to high CO_2/CH_4 adsorption capacities. Due to its small crystal size, narrow particle size distribution, higher surface area and preferential CO_2 adsorption capacities over CH_4, these crystals represent ideal phases to prepare thin supported membranes for CO_2/CH_4 separations.

2.   SAPO-34 was successfully synthesized in less time with small crystal size using microwave reactor compared to the conventional oven. Pure SAPO-5 was formed after the gel was treated for 30 min under MW heating. As the synthesis time increased to 500 min, SAPO-34 has been formed by the transformation of SAPO-5. The synthesized SAPO-5 and SAPO-34 phases displayed small and narrow particle size distribution with crystallites of ~ 2.5 and ~ 0.5 μm respectively. The synthesized SAPO-34 displayed high CO_2/CH_4 adsorption ratio (~ 29), making it highly attractive for CO_2/CH_4 gas separations. The short synthesis time, smaller crystal size and narrow particle size distribution of the synthesized SAPO phases, make the MW heating an attractive and useful approach for the potential preparation of the thinner membranes for practical gas separation applications.

3.   SAPO-34 seeds and membranes were functionalized with several organic amino cations to increase the CO_2 adsorption capacity of SAPO-34 seeds by increasing the basicity of the surface. The amino cations were successfully incorporated in the SAPO-34 framework, preserving its chabazite structure, which is confirmed by FTIR. The functionalized SAPO-34 membranes effectively separated CO_2/CH_4 and CO_2/N_2 gas

mixtures. An optimum concentration of ethylenediamine led to highly CO_2 selective membranes with CO_2/CH_4 selectivities of 245 with CO_2 permeances of ~ 5 x10^{-7}mol/m^2 s Pa at 295 K and 138 KPa, Similarly, CO_2/N_2 separation performance was highly improved with the incorporation of ethylenediamine. CO_2/N_2 selectivities as high as 39 with CO_2 permeances of ~ 2.1 x10^{-7}mol/m^2 s Pa at 295 K and 138 KPa, were observed for an optimum ethylenediamine functionalized membrane. The presence of amino groups in the SAPO-34 structure led to higher CO_2/CH_4 and CO_2/N_2 selectivities mainly due to preferential adsorption of CO_2 on a basic SAPO-34 surface.

4.   We studied the ZIF-8 structural evolution as a function of time at room temperature. We have identified the different stages of ZIF-8 formation: nucleation, crystallization, growth, and stationary periods; and elucidated its kinetics of transformation. We hypothesize that the observed semicrystalline to crystalline transformation may take place via solution and solid mediated mechanisms as suggested by the observed phase transformation evolution and Avrami's kinetics respectively. We found that the reduction in solution pH played an important role as the driving force for the crystallization process. A fundamental understanding of ZIF-8 structural evolution demonstrated in this study would facilitate the preparation of novel functional materials. This study will allow us to effectively control ZIF-8 crystal size and membrane thickness, which in principle, are critical parameters in the preparation of efficient membranes.

5.   Reproducible thin ZIF-8 membranes with ~ 5 - 9 μm thickness were synthesized by secondary seeded growth on tubular α-Al_2O_3 porous supports. Initially, ZIF-8 seeds were prepared with the size of ~ 55 nm and surface area of 1072 m^2/g. They also showed high CO_2 adsorption capacity (~14 times) than CH_4. These ZIF-8 crystals were as

secondary seeds to prepare the membrane using hydrothermal treatment. The separation

performance of these membranes for equimolar CO_2/CH_4 gas mixtures is presented. The

membranes displayed unprecedented CO_2 permeances as high as ~2.4 x 10^{-5} mol/m^2·s·Pa

with CO_2/CH_4 separation selectivities of ~ 4 to 7 and separation indexes in the ~ 6.5 to 10

range at 295 K and a feed pressure of 139.5 KPa. This is one of the first examples of the

preparation of ZIF-8 membranes for a functional gas separation application.

CHAPTER 9

FUTURE DIRECTIONS

Our results demonstrated that SAPO-34 membranes performed much better than any existing polymeric membranes and other zeolite membranes for CO_2/CH_4 and CO_2/N_2 gas mixture separation. The separation performance of these membranes can be further improved by exploring different chemical parameters during membrane preparation such as nature of the inorganic precursors, gel composition, pH of the solution, as well as processing parameters such as hydrothermal treatment temperature and time, calcination environment, and mode of layer deposition. Furthermore, future works needs to be focused on the long term stability of the membranes as well as on the performance of the membranes in the presence of typical natural gas and flue gas impurities (H_2O, H_2S and lower alkanes) to meet the industry requirements.

Although zeolite membranes can effectively separate CO_2 from light gases, the development of superior performance membranes for gas mixture separations requires novel materials with fundamentally different structural, compositional, adsorption and transport properties than those of zeolites. In this respect, zeolitic imidazolate frameworks (ZIFs) a subclass of metal organic frameworks, have emerged as a novel type of crystalline porous materials which combine highly desirable properties, such as

uniform micropores, high surface areas, and exceptional thermal and chemical stability, making them ideal candidates for molecular separations. We have demonstrated that ZIF-8 membranes can separate CO_2 from CH_4 at high CO_2 permeances. But the CO2 selectivities were too low. Therefore, future experiments should focus on employing different seeding techniques, and membrane preparation methods to prepare more robust and continuous ZIF-8 membranes able to selectively separate CO_2. Alternatively, different ZIF compositions need to be explored and be prepared as seeds and membranes. These particular compositions need to be chosen based on two important criteria: a) limiting pore aperture and b) CO_2 preferential adsorption capacity. ZIF-65, 67, 78, 90, 91 and 100 are in particular attractive systems to synthesize as membranes. In the future, a gradual shift will take place from the exploration of new membrane materials and concepts towards a better control of membrane preparation and an understanding of performance, long-term stability and process integration in various applications.

REFERENCES

1. International Energy Outlook 2010 – Highlights, Energy Information Administration, Report #: DOE/EIA-0484(2010), **2010.**

2. Emissions of Greenhouse Gases in the United States, Energy Information Administration, *Report # DOE/EIA-0573(2007),* **2007.**

3. Draper, E.L.; Becker, R.A. "Research and Development Needs for Sequestration of Carbon Dioxide As part of a Carbon Management Strategy", *The national Coal Council,* Washington, D.C., **2000.**

4. Emissions of Greenhouse Gases Report, Energy Information Administration, *Report #: DOE/EIA-0573(2008),* **2008.**

5. Energy Information Administration, Annual Energy Outlook 2004, *Report #: DOE/EIA-0383(2004)***2004.**

6. Hoang, D.L.; Chan, S.H. "Experimental investigation on the effect of natural gas composition on performance of auto-thermal reforming" *International Journal of Hydrogen Energy,* **2007,** *32,* 548 – 556.

7. Red Mountain Energy, gas separation process unit

8. Bottoms, R. R. "Separating acid gases," *U.S. Patent 1783901,* **1930.**

9. Ho, M.T.; Allinson, G.W.; Wiley, D.E. "Reducing the Cost of CO_2 Capture from Flue Gases using Pressure Swing Adsorption" *Ind. Eng. Chem. Res.***2008,***47,*4883–4890.

10. Financial and operating review-25, Exxon Mobil Corporation, **2007.**

11. Strathmann, H. "Membrane Separation Processes: Current Relevance and Future Opportunities" *AIChE Journal*, **2001,** *47*, 1077-1087

12. Barrer, R. M. J. Chem. Soc. 1948, 2158

13. Barrer, R. M.; Denny, P. J. J. Chem. Soc. 1961, 971-982.

14. Beck, L.W. *Zeolite synthesis*, University of Michigan.

15. R.J. Francis, D. O'Hare, J. Chem. Soc., Dalton Trans. (1998) 3133.

16. D. Uzca'tegui, G. Gonza'lez, Catal. Today 107–108 (2005) 901.

17. C.S. Cundy, P.A. Cox, Micropor. Mesopor. Mater. 82 (2005) 1.

18. Li, S.; Falconer, J.L.; Noble, R.D. "SAPO-34 membranes for CO_2/CH_4 separation" *J. Membr. Sci.* **2004,** *241*, 121-135.

19. Poshusta, J.C.; Tuan, V.A.; Pape, E.A.; Noble, R.D.; Falconer, J.L. "Separation of Light Gas Mixtures Using SAPO-34 Membranes" *AIChE J.* **2000,** *46*, 779-789.

20. Li, S.; Falconer, J.L.;Noble, R.D. "Improved SAPO-34 membranes for CO_2/CH_4 separations"*Adv. Mater.* **2006,** *18*, 2601-2603.

21. Carreon, M.A.; Li, S.; Falconer, J.L.; Noble, R.D, "Alumina-Supported SAPO-34 Membranes for CO_2/CH_4 Separation" *J. Am. Chem. Soc.* **2008,** *130*, 5412-5413.

22. Li, S.; Falconer,J.L.; Noble, R.D."SAPO-34 membranes for CO_2/CH_4 separations: Effect of Si/Al ratio" *Micro. Meso. Mater.* **2008,** *110*, 310-317.

23. Carreon, M.A.; Li, S.; Falconer, J.L.; Noble, R.D. "SAPO-34 Seeds and Membranes Prepared Using Multiple Structure Directing Agents" *Adv.Mater.* **2008,** *20*, 729-732.

24. Ashtekar, S.; Chilukuri, S.V.V.; Prakash, A. M.; Chakrabarty, D.K. "Small-Pore Molecular Sieves SAPO-34 and SAPO-44 with Chabazite Structure: A Study of Silicon Incorporation" *J. Phys. Chem.* **1994,** 98, 4878-4883.

25. Park, J. W.; Lee, J. Y.; Kim, K. S.; Hong, S. B.; Seo, G. "Effects of cage shape and size of 8-membered ring molecular sieves on their deactivation in methanol-to-olefin (MTO) reactions" *Appl. Catal. A: General.* **2008,** *339,* 36-44.

26. Wilson, S.; Barger, P. "The characteristics of SAPO-34 which influence the conversion of methanol to light olefins" *Microporous Mesoporous Mater.* **1999,** *29,* 117-126.

27. Oikawa, H.; Shibata, Y.; Inazu, K.; Iwase, Y.; Murai, K.; Hyodo, S.; Kobayashi, G.; Baba, T. "Highly selective conversion of ethene to propene over SAPO-34 as a solid acid catalyst" *Appl. Catal. A: General.* **2006,** *312,* 181-185.

28. Elangovan, S.P.; Ogura, M.; Zhang, Y.; Chino, N.; Okubo, T. "Silicoaluminophosphate molecular sieves as a hydrocarbon trap" *Appl. Catal. B: Environ.* **2005,** *57,* 31-36.

29. Jaenchen, J.; Ackermann, D.; Weiler, E.; Stach, H.; Broesicke, W. "Calorimetric investigation on zeolites, AlPO$_4$'s and CaCl$_2$ impregnated attapulgite for thermochemical storage of heat" *Thermochim. Acta.* **2005,** *434,* 37-41.

30. Lok, B. M.; Messina, C. A.; Patton, R. L.; Gajek, R. T.; Cannan, T. R.; Flanigen, E. M. "Silicoaluminophosphate Molecular Sieves: Another New Class of Microporous Crystalline Inorganic Solids" *J. Am. Chem. Soc.* **1984,** *106,* 6092-6093.

31. Ito, M.; Shimoyama, Y.; Saito, Y.; Tsurita, Y.; Otake, M. *Acta Crystallogr., Sect. C: Cryst. Struct. Commun.* **1985,** *C41,* 1698.

32. Vistad, Ø. B.; Akporiaye, D. E.; Taulelle, F.; Lillerud, K. P. "Morpholine, an in Situ ^{3}C NMR pH Meter for Hydrothermal Crystallogenesis of SAPO-34" *Chem. Mater.* **2003,** *15,* 1650-1654.

33. Dumitriua, E.; Azzouza, A.; Huleaa, V.; Lutica, D.; Kesslerb, H. "Synthesis, characterization and catalytic activity of SAPO-34 obtained with piperidine as templating agent" *Microporous Mater.* **1997,** *10,* 1-12.

34. Liu, G.; Tian, P.; Zhang, Y.; Li, J.; Xu, L.; Meng, S.; Liu, Z. "Synthesis, characterization and catalytic properties of SAPO-34 synthesized using diethylamine as a template" *Microporous Mesoporous Mater.* **2008,** *111,* 143-149.

35. Liu, G.; Tian, P.; Zhang, Y.; Li, J.; Xu, L.; Meng, S.; Liu, Z. "Synthesis of SAPO-34 templated by diethylamine: Crystallization process and Si distribution in the crystals" *Microporous Mesoporous Mater.* **2008,** *114,* 416-423.

36. Wei, Y.; He, Y.; Zhang, D.; Xu, L.; Meng, S.;Liu, Z.; Su, B.L. "Study of Mn incorporation into SAPO framework: Synthesis, characterization and catalysis in chloromethane conversion to light olefins" *Microporous Mesoporous Mater.* **2006,** 90, 188-197.

37. Zhou, H.; Wang, Y.; Wei, F.; Wang, D.; Wang, Z. "In situ synthesis of SAPO-34 crystals grown onto α-Al$_2$O$_3$ sphere supports as the catalyst for the fluidized bed conversion of dimethyl ether to olefins" *Appl. Catal. A: General.* **2008,** *341,* 112-118.

38. Nevenka, R.; Djordje, S.; Stanko, H.; Venceslav, K. "On the possibility of incorporating Mn(II) and Cr(III) in SAPO-34 in the presence of isopropylamine as a template" *Zeolites,* **1993,** *13,* 384-387.

39. Heyden, H. V.; Mintova, S.; Bein, T. Nanosized SAPO-34 Synthesized from Colloidal Solutions" *Chem. Mater.* **2008,** *20,* 2956-2963.

129

40. Yao, J.; Wang, H.; Ringer, S.P.; Chan, K.Y.; Zhang, L.; Xu, N. "Growth of SAPO-34 in polymer hydrogels through vapor-phase transport" *Micro. Meso. Mater.* **2005**, *85*, 26-2727.

41. Zhang, L.; Yao, J.; Zeng, C.; Xu, N. "Combinatorial synthesis of SAPO-34 via vapor-phase transport" *Chem. Commun.* **2003**, 2232-2233.

42. Li-ming, K.; Xiao-qin, L.; Ding-hua, L. "Effects of Ultrasound on SAPO-34 Molecular Sieve Synthesis" *J. Nanjing Univ. Sci. Tech,* **2007**, 31, 528-532.

43. Mertens, M.; Strohmaier, K.G. *U.S. Patent 6696032 B2,* **2004**.

44. Rivera-Ramos, M. E.; Ruiz-Mercado, G. J.; Hernandez-Maldonado, A. J. "Separation of CO2 from Light Gas Mixtures using Ion-Exchanged Silicoaluminophosphate Nanoporous Sorbents" *Ind. Eng. Chem. Res.* **2008**, *47,* 5602-5610.

45. Uzunova, E. L.; Mikosch, H.; Hafner, J. "Adsorption of NO on Cu-SAPO-34 and Co-SAPO-34: A Periodic DFT Study" *J. Phys. Chem. C* **2008**, *112*, 2632-2639.

46. Wei, Y.; Zhang, D.; Xu, L.; Chang, F.; He, Y.; Meng, S.; Su, B.L.; Liu, Z. "Synthesis, characterization and catalytic performance of metal-incorporated SAPO-34 for chloromethane transformation to light olefins" *Catal. Today.* **2008**, *131,* 262-269.

47. Tosheva, L.; Valtchev, V. P. Chem. Mater. 2005, 17, 2494.

48. Botella, P.; Corma, A.; Iborra, S.; Monton, R.; Rodriguez, I.; Costa, V. J. Catal. 2007, 250, 161.

49. Waller, P.; Shan, Z.; Marchese, L.; Tartaglione, G.; Zhou, W.; Jansen, J. C.; Maschmeyer, T. Chem.sEur. J. 2004, 10, 4970.

50. Chu, P.; Dwyer, F. G.; Vartuli, J. C. *US Patent 4,778,666,* **1988**.

51. A. Arafat, J.C. Jansen, A.R. Ebaid, H. Vanbekkum, Microwave preparation of zeolite-Y and ZSM-5, Zeolites 13 (1993) 162–165.

52. X.C. Xu, W.S. Yang, J. Liu, L.W. Lin, Fast formation of NaA zeolite membrane in the microwave field, Chin. Sci. Bull. 45 (2000) 1179–1181.

53. Li, Y.; Yang, W. "Microwave synthesis of zeolite membranes: A review" *J. Membr. Sci.* **2008**, *316*, 3-17.

54. Heyden, H. V.; Mintova, S.; Bein, T. "Nanosized SAPO-34 Synthesized from Colloidal Solutions" *Chem. Mater.,***2008**, *20*, 2956-2963.

55. Yang, W.; Zhang. B.; Liu, X. "Synthesis and characterization of SAPO-5 membranes on porous α-Al$_2$O$_3$ substrates" *Micro. Meso. Mater.* 2009, *117*, 391-394.

56. N. Kumar, J.I. Villegas, T. Salmi, Y.D. Murzin, T. Heikkilä, "Isomerization of n-butane to isobutane over Pt-SAPO-5, SAPO-5, Pt-H-mordenite and H-mordenite catalysts" *Catal. Today.* **2005**, *100*, 355-361.

57. Tosheva, L.; Ng, E.P.; Mintova, S.; Holzl, M.; Metzger, T.H.; Doyle, A.M. "AlPO$_4$-18 Seed Layers and Films by Secondary Growth" *chem. mater.* 2008, **20**, 5721-5726.

58. Cundy, C. S. "Microwave Techniques in the Synthesis and Modification of Zeolite Catalysts: A Review." *Collection of Czechoslovak Chem. Comm.* **1998**, *63*, 1699-1723.

59. Tompsett, G. A.; Conner, W. C. "Microwave Synthesis of Nanoporous Materials" *Chem. Phys. chem.,* **2006**, *7*, 296-319.

60. Burmaster, B.M.; Carter, D.C. "Proceedings American Chemical Society Symposium", Houston, USA, **1983**.

61. Shekhawat, D.; Luebke, D.R.; Pennline, H.W. *A Review of Carbon Dioxide Selective Membranes: A Topical Report*", DOE/NETL-2003/1200, **2003.**

62. Ma,Y.; Kanezashi, M.; Tsuru, T. "Preparation of organic/inorganic hybrid silica using methyltriethoxysilane and tetraethoxysilane as co-precursors" *J Sol-Gel Sci. Technol.***2010**,*53*,93–99.

63. McLeary, E.E.; Jansen,J.C.; Kapteijn,F. "Zeolite based films, membranes and membrane reactors:Progress and prospects"*Micro. Meso. Mater.***2006,** *90*, 198–220

64. Budda, P.M.; Msayib, K.J.; Tattershall, C.E.; Ghanema, B.S.; Reynolds, K.J.; McKeown, N.B.; Fritsch, D. "Gas separation membranes from polymers of intrinsic microporosity" *J. Membr. Sci.***2005,** *251*, 263–269.

65. Powell, C.E.; Qiao, G.G. "Polymeric CO_2/N_2 gas separation membranes for the capture of carbon dioxide from power plant flue gases" *J. Membr. Sci.***2006,** *279*, 1–49.

66. Watson, E.R.; Rowley, G.V.; Wunderlich, C.R. *US3432585,* **1969.**

67. Scholes, C.A.; Kentish, S.E.; Stevens, G.W. "Carbon Dioxide Separation through Polymeric Membrane Systems for Flue Gas Applications" *Recent Patents on Chem. Engg.* **2008,** *1,* 52-66.

68. Robeson, L.M. "Polymer membranes for gas separation" *Current Opinion in Solid State and Materials Science,* **1999,** *4,* 549–552.

69. Tremblay, P.; Savard, M.M.; Vermette, J.; Paquin, R. "Gas permeability, diffusivity and solubility of nitrogen, helium, methane, carbon dioxide and formaldehyde in dense polymeric membranes using a new on-line permeation apparatus" *J. Membr. Sci.* **2006,** *282,* 245–256.

70. Costello, L.M.; Walker, D.R.B.; Koros, W.J. "Analysis of a Thermally Stable Polypyrrolone for High Temperature Membrane-Based Gas Separations." *J. Membrane Sci.*, **1994,** *90,* 117-130.

71. Merkel, T.C.; Gupta, R.P.; Turk, B.S.; Freeman, B.S. "Mixed-Gas Permeation of Syngas Components in Poly(Dimethylsiloxane) and Poly(1-Trimethylsilyl-1-Propyne) at Elevated Temperatures." *J. Membrane Sci.*, **2001,** *191,* 85-94.

72. Feng, H.; Zhang, H.; Xu, L. "Polymeric Membranes for Natural Gas Conditioning" *Energy Sources, Part A* **2007,** *29,* 1269–1278.

73. Robeson, L. M. "The upper bound revisited" *J. Membr. Sci.* **2008,** *320,* 390-400.

74. Jia, W.; Murada, S. "Separation of gas mixtures using a range of zeolite membranes: A molecular-dynamics study"*J. Chem. Phys.* **2005,** *122,* 234708.

75. Rao, M.B.; Sircar, S. "Performance and Pore Characterization of Nanoporous Carbon Membranes for Gas Separation." *J. Membrane Sci.*, **1996,** *110,* 109-118.

76. Keizer, K.; Uhlhorn, R.J.R.; Van Vuren, R.J.; Burggaaf, A.J. "Gas Separation Mechanism in Microporous Modified Al_2O_3 Membranes"*J. Membrane Sci.*, **1988,** *39,* 285-300.

77. Uhlhorn, R.J.R.; Keizer, K.; Burggraaf, A.J. "Gas transport and separation with ceramic membranes. Part I: Multilayer diffusion and capillary condensation" *J. Membrane Sci.*, **1992,** *66,* 259-269.

78. Choi, J.G.; Do, D.D.; Do, H.D."Surface Diffusion of Adsorbed Molecules in Porous Media:Monolayer, Multilayer, and Capillary Condensation Regimes"*Ind. Eng. Chem. Res.* **2001,** *40,* 4005-4031.

79.   Xing, W.; Costa, J.C.D.; Lu, G.Q.; Yan, Z.F. "Environmental Separation and Reactions: Zeolite Membranes" *Dekker Encyclopedia of Nanosci. Nanotech.* DOI: 10.1081/E-ENN-120009406, **2004,** 1157-1166.

80.   Freemantle, M. "Membranes for Gas Separation" *Chemical and Engineering News,* **2005,** *83,* 49-57.

81.   Gavalas, G.R. "Diffusion in Microporous Membranes: Measurements and Modeling" *Ind. Eng. Chem. Res.* **2008,** *47,* 5797–5811.

82.   Morigami, Y.; Kondo, M.; Abe, J.; Kita, H.; Okamoto, K. "The first large-scale pervaporation plant using tubular-type module with zeolite NaA membrane" *Sep. Purif. Technol.* **2001,***25,* 251-260.

83.   Tavolaro, A.;Drioli, E. "Zeolite Membranes" *Adv. Mater.* **1999,** *11,* 975-996.

84.   Bein, T. "Synthesis and Applications of Molecular Sieve Layers and Membranes" *Chem. Mater.* **1996,** *8,* 1636-1653.

85.   Caro, J.; Noack, M.; Kolsch, P.; Schafer, R. "Zeolite membranes – state of their development and perspective" *Micro.Meso. Mater.* **2000,** *38,* 3-24.

86.   McLeary, E.E.; Jansen, J.C.; Kapteijn,F. "Zeolite based films, membranes and membrane reactors: Progress and prospects" *Micro. Meso. Mater.* **2006,** *90,* 198-220.

87.   Noack, M.; Caro, J.; in: Schuth, F.; Sing, K.S.W.; Weitkamp, J. (eds). *Handbook of Porous Solids,* Wiley-VCH, Weinheim, **2002,** 2478.

88.   J. Caro, M. Noack, P. Kolsch, "Zeolite Membranes: From the Laboratory Scale to Technical Applications" *Adsorption* **2005,** *11,* 215-227.

89. Ramsay, J.D.F.; Kallus, S.; Kanellopoulos, N.K. "Recent Advances in Gas Separation by Microporous Ceramic Membranes" *Membr. Sci. and Tech.* Elsevier, Amsterdam, **2000,** 373.

90. Julbe, A. "Zeolite Membranes – A Short Overview", in: Cejka, J; van Bekkum, H. (eds.), "Zeolites and Ordered Mesoporous Materials: Progress and Prospects", *Stud.Surf. Sci. Catal.* **2005,** *157,* 135.

91. Lewis, J. E.; Gavalas, G. R.;Davis, M.E. "Permeation Studies on Oriented Single-Crystal Ferrierite Membranes" *AIChE J.,* **1997,** *43,* 83-90.

92. Wang, Y.; Tang, Y.; Dong, A.; Wang, X.; Ren, N.; Shan, W.; Gao, Z. "Self-Supporting Porous Zeolite Membranes with Sponge-like Architecture and Zeolitic Microtubes" *Adv. Mater.* **2002,** *14,* 994–997.

93. Choi, J.; Jeong, H.K.; Snyder, M.A.; Stoeger, J.A.; Masel, R.I.; Tsapatsis, M. "Grain Boundary Defect Elimination in a Zeolite Membrane by Rapid Thermal Processing" *Science* **2009,** *325,* 590-593.

94. Zhu, G.; Wang, J.; Zhang, Y.; Lu, J.; Xiu, J. "Preparation and permeability of ZSM-35 zeolite membranes on porous stainless steel tubes" *Frontiers of Chemical Engineering in China,* **2007,** *1,* 217-220.

95. Bernal, M.P.; Xomeritakis, G.; Tsapatsis, M. "Tubular MFI zeolite membranes made by secondary (seeded) growth" *Catalysis Today* **2001,** *67,* 101–107.

96. Takata, Y.; Tsuru, T.; Yoshioka, T.; Asaeda, M. "Gas permeation properties of MFI zeolite membranes prepared by the secondary growth of colloidal silicalite and application to the methylation of toluene" *Micro. Meso. Mater.***2002,** *54,* 257–268.

97. Tang, Z.; Kim, S.J.; Gu, X.; Dong, J. "Microwave synthesis of MFI-type zeolite membranes by seeded secondary growth without the use of organic structure directing agents"*Micro. Meso. Mater.* **2009**, *118*, 224–231.

98. Li, Y.; Pera-Titusa, M.; Xiongb, G.;Yangb, W.; Landrivona, E.; Miachona, S.; Dalmona, J-A. "Nanocomposite MFI-alumina membranes via pore-plugging synthesis: Genesis of the zeolite material" *J. Membr. Sci.* **2008**, *325*, 973–981.

99. Hedlund, J.; Jareman, F.; Bons, A.-J.; Anthonis, M. "A masking technique for high quality MFI membranes" *J. Membr. Sci.* **2003**, *222*, 163-179.

100. Wong, W.C.; Au,L.T.Y.; Ariso, C.T.; Yeung, K.L. "Effects of synthesis parameters on the zeolite membrane growth" *J. Mem. Sci.* **2001**, *191*, 143–163.

101. L.T.Y. Au, J.L.H. Chau, C. Tellez, K.L. Yeung, Aluminum,titanium and vanadium silicalite-1 membranes: preparation, characterization and permeation measurements, J. Membr. Sci. 183 (2001) 269.

102. Chiang, A. S. T.; Chao, K-J. "Membranes and films of zeolite and zeolite-like materials", *J. Phys. Chem. of Solids,* **2001**, *62*, 1899-1910.

103. Kim, D.S.; Chang, J-S.; Hwang, J-S.; Park, S-E.; Kim, J.M. "Synthesis of zeolite beta in fluoride media under microwave irradiation", *Micro. Meso. Mater.***2004**,*68*, 77–82.

104. Tang, Z.; Kim, S-J.; Gu, X.; Dong, J. "Microwave synthesis of MFI-type zeolite membranes by seeded secondary growth without the use of organic structure directing agents", *Micro. Meso. Mater.***2009**, *118*, 224–231.

105. Conner, W.C.; Tompsett, G.; Lee, K-H.; Yngvesson, K.S. "Microwave Synthesis of Zeolites: 1. Reactor Engineering" *J. Phys. Chem. B* **2004**, *108,* 13913-13920.

106. Tompsett, G.A.; Conner, W.C.; Yngvesson, K.S. "Microwave synthesis of nanoporous materials" *Chem. Phys. Chem.* **2006**, *7*, 296–319.

107. O'Brien-Abraham, J.; Lin, Y.S. "Effect of Isomorphous Metal Substitution in Zeolite Framework on Pervaporation Xylene-Separation Performance of MFI-Type Zeolite Membranes" *Ind. Eng. Chem. Res.* **2010**, *49*, 809–816.

108. Dyer, A.; Emms, T.I. "Cation exchange in high silica zeolites" *J. Mater. Chem.* **2005**, *15*, 5012–5021.

109. Hernandez-Huesca, R.; Diaz, L.; Aguilar-Armenta, G. "Adsorption equilibria and kinetics of CO_2, CH_4 and N_2 in natural zeolites" *Separation and Purification Tech.* **1999**, *15*, 163–173.

110. Vansant, E.F. "Pore Size Engineering in Zeolites", *Wiley,* **1990**

111. Hong, M.; Falconer, J.L.; Noble, R.D. "Modification of Zeolite Membranes for H_2 Separation by Catalytic Cracking of Methyldiethoxysilane" *Ind. Eng. Chem. Res.* **2005**, *44*, 4035-4041.

112. Kusakabe, K.; Kuroda, T.; Morooka, S. "Separation of carbon dioxide from nitrogen using ion-exchanged faujasite-type zeolite membranes formed on porous support tubes", *J.Membr. Sci.* **1998**, *148*, 13-23.

113. Tomita, T.; Nakayama, K.; Sakai, H. "Gas separation characteristics of DDR type zeolite membrane" *Micro. Meso. Mater.* **2004**, *68*, 71-75.

114. Yang, M.; Crittenden, B. D.; Perera, S. P.; Moueddeb, H.; Dalmon, J. A. "The hindering effect of adsorbed components on the permeation of a non-adsorbing component through a microporous silicalite membrane: the potential barrier theory" *J. Membr. Sci.* **1999**, *156*, 1-9.

115. Xu, X.; Zhao, X.; Sun, L.; Liu, X.; "Adsorption separation of carbon dioxide, methane, and nitrogen on Hβ and Na-exchanged β-zeolite" *J. Natural Gas Chem.* **2008,** 17, 391–396.

116. Jee, S.E.; Sholl, D.S. "Carbon Dioxide and Methane Transport in DDR Zeolite: Insights from Molecular Simulations into Carbon Dioxide Separations in Small Pore Zeolites" *J. Am. Chem. Soc.* **2009,** *131,* 7896–7904.

117. Cui, Y.; Kita, H.; Okamoto, K. I. "Preparation and gas separation performance of zeolite T membrane" *J. Mat. Chem.* **2004,** *14,* 924-932.

118. Guo, H.; Zhu, G.; Li, H.; Zou, X.; Yin, X.; Yang, W.; Qiu, S.; Xu, R. "Hierarchical Growth of Large-Scale Ordered Zeolite Silicalite-1 Membranes with High Permeability and Selectivity for Recycling CO_2" *Angew. Chem. Int. Ed.* **2006,** *45,* 7053-7056.

119. Van den Bergh, J.; Zhu, W.; Gascon, J.; Moulijn, J.A.; Kapteijn, F. "Separation and permeation characteristics of a DD3R zeolite membrane" *J. Membr. Sci.* **2008,** *316,* 35-45.

120. Kusakabe, K.; Kuroda, T.; Murate, A.; Morooka, S. *Ind. Eng. Chem. Res.* **1997,** *36,* 649-655.

121. Hasegawa, Y.; Tanaka, T.; Watanabe, K.; Jeong, B-H.; Kusakabe, K.; Morooka, S. "Separation of CO_2-CH_4 and CO_2-N_2 systems using ion-exchanged FAU-type zeolite membranes with different Si/Al ratios" *Kor. J. Chem. Eng.* **2002,** *19,* 309-313.

122. Poshusta, J.C.; Tuan, V.A.; Noble, R.D.; Falconer, J.L. "Synthesis and permeation properties of SAPO-34 tubular membranes" *Ind. Eng. Chem. Res.* **1998**, *37*, 3924-3929.

123. Lixiong, Z.; Mengdong, J.; Enze, M. "Synthesis of SAPO-34/ceramic composite membranes" *Stud. Surf. Sci. Catal.* **1997**, *105*, 2211-2216.

124. Li, S.; Alvarado, G.; Noble, R.D.; Falconer, J.L. "Effects of impurities on CO_2/CH_4 separations through SAPO-34 membranes" *J. Membr. Sci.* **2005**, *251*, 59–66.

125. Poshusta, J.C.; Noble, R.D.; Falconer, J.L. "Characterization of SAPO-34 membranes by water adsorption" *J. Membr. Sci.* **2001**, *186*, 25–40.

126. Li, S.G.; Martinek, J.G.; Falconer, J.L.; Noble, R.D.; Gardner, T.Q. "High-pressure CO_2/CH_4 separation using SAPO-34 membranes" *Ind. Eng. Chem. Res.* **2005**, *44*, 3220-3228.

127. Hong, M.; Li, S.G.; Funke, H.H.; Falconer, J.L.; Noble, R.D. "High-pressure CO_2/CH_4 separation using SAPO-34 membranes" *Micro. Meso. Mater.* **2007**, *106*, 140-146.

128. Li, S.; Carreon, M.A.; Zhang, Y.; Funke, H.H.; Noble, R.D.; Falconer, J.L. "Scale-up of SAPO-34 membranes for CO_2/CH_4 separation" *J. Mem. Sci.* **2010**, *352*, 7-13.

129. Zhang, Y.; Avila, A.M.; Tokay, B.; Funke, H.H.; Falconer, J.L.; Noble, R.D. "Blocking defects in SAPO-34 membranes with cyclodextrin" *J. Mem. Sci.* **2010**, *358*, 7-12.

130. Zhang, Y.; Tokay, B.; Funke, H.H.; Falconer, J.L.; Noble, R.D. "Template removal from SAPO-34 crystals and membranes" *J. Mem. Sci.* **2010**, *363*, 29-35.

131. Hong, M.; Li, S.; Falconer, J.L.; Noble, R.D. "Hydrogen purification using a SAPO-34 membrane, Journal of Membrane Science" *J. Mem. Sci.* **2008**, *307*, 277-283.

132. Chew, T.L.; Ahmad, A.L.; Bhatia, S. "Rapid synthesis of thin SAPO-34 membranes using microwave heating" *J. Porous. Mat.* **2010**, *doi: 10.1007/s10934-010-9385-1.*

133. Tian, Y; Fan, L.; Wang, Z.; Qiu, S.; Zhu, G. "Synthesis of a SAPO-34 membrane on macroporous supports for high permeance separation of a CO_2/CH_4 mixture" *J. Mater. Chem.* **2009**, *19*, 7698-7703.

134. Karatay, E.; Kalipcilar‚H.; Yilmaz, L. "Preparation and Performance Assessment of Binary and Ternary PES-SAPO 34-HMA Based Gas Separation Membranes" *J. Mem. Sci.* **2010**, *doi:10.1016/j.memsci.2010.08.004.*

135. Li, S.; Fan, C.Q. "High-Flux SAPO-34 Membrane for CO_2/N_2 Separation" *Ind. Eng. Chem. Res.* **2010**, *49*, 4399-4404.

136. Anderson, M.A.; Qunyin, X. "Metal oxide porous ceramic membranes with small pore sizes" *US Patent 5104539,* **1992.**

137. Barrer, R. M.; Strachan, E. "Sorption and surface diffusion in microporous carbon cylinders"*Proc. R. Soc. A* **1955**, *231*, 52-74.

138. Hinds, B. J.; Chopra, N.; Rantell, T.; Andrews, R.; Gavalas, V.; Bachas, L. G. "Aligned multiwalled carbon nanotube membranes"*Science,***2003**,*303*, 62-65.

139. Lee, H-J.;S uda, H.; Haraya, K. "Gas permeation properties in a composite mesoporous alumina ceramic membrane"*Kor. J. Chem. Engg.* **2005**, *22*, 721-728.

140. Renate, M.; de Vos,Verweij, H. "High-Selectivity, High-Flux Silica Membranes for Gas Separation" *Science,* **1998**, *279*, 1710-1711.

141. Kim, Y-S.; Kusakabe, K.; Morooka, S.; Yang, S-M. "Preparation of microporous silica membranes for gas separation"*Kor. J. Chem. Engg.* **2001,** *18,* 106-112.

142. Gopalakrishnan, S.; Diniz da Costa, J.C. "Hydrogen gas mixture separation by CVD silica membrane"*J. Membr. Sci.* **2008,** *323,* 144-147.

143. Wang, H.; Gavalas, G.R. "Mesoporous Glass Films Supported on α-Al$_2$O$_3$." *J. Membrane Sci.* **2000,** *176,* 75-85.

144. Ma, Y.H.; Akis, B.C.; Ayturk, M.E.; Guazzone, F.; Engwall, E.E.; Mardilovich, I.P. "Characterization of Intermetallic Diffusion Barrier and Alloy Formation for Pd/Cu and Pd/Ag Porous Stainless Steel Composite Membranes" *Ind. Eng. Chem. Res.* **2004,** *43,* 2936-2945.

145. Zornoza, B.; Irusta, S.;Tellez, C.; Coronas, J. "Mesoporous Silica Sphere-Polysulfone Mixed Matrix Membranes for Gas Separation" *Langmuir* **2009,** *25,* 5903-5909.

146. Jia, M.; Peinemann, K.V.; Behling, R.D. "Molecular sieving effect of the zeolite-filled silicone rubber membranes in gas separation" *J. Membr. Sci.* **1991,** *133,* 231-243.

147. Kulprathipanja, S., R.W. Neuzil, and N.N. Li. "Separation of Fluids by Means of Mixed Matrix Membranes." *U.S. Patent No. 4,740,219,* **1988.**

148. Okui, T.; Saito, Y.; Okubo, T.; Sadakata, M. "Gas Permeation of Porous Organic/Inorganic Hybrid Membranes." *J. Sol-Gel Sci. Tech.,* **1995,** *5,* 127-134.

149. Mueller, U.; Schubert, M.; Teich, F.; Puetter, H.; Schierle-Arndt, K.; Pastre, J. "Metal - organic frameworks - prospective industrial applications" *J. Mater. Chem.* **2006,** 16, 626-636.

150. Kupplera, R.J.; Timmons, D.J.; Fanga, Q-R.; Li, J-R.; Makala, T.A.; Younga, M.D.; Yuana, D.; Zhaoa, D.; Zhuanga, W.; Zhoua, H-C. "Potential applications of metal-organic frameworks" *Coordination Chemistry Reviews* **2009**, *253*, 3042–3066.

151. Li, Y.; Yang, R.T. "Gas Adsorption and Storage in Metal-Organic Framework MOF-177" *Langmuir*, **2007**, *23*, 12937–12944.

152. Rosi, N.L.; Eckert, J.; Eddaoudi, M.; Vodak, D.T.; Kim, J.; O'Keeffe, M.; Yaghi, O.M. "Hydrogen Storage in Microporous Metal-Organic Frameworks" *Science*, **2003**, *300*, 1127-1129.

153. Gascon, J.; Kapteijn, F. "Metal-Organic Framework Membranes—High Potential, Bright Future?" *Angew. Chem. Int. Ed.* **2010**, *49*, 1530 –1532.

154. Bux, H.; Liang, F.; Li, Y.; Cravillon, J.; Wiebcke, M.; Caro, J."Zeolitic Imidazolate Framework Membrane with Molecular Sieving Properties by Microwave-Assisted Solvothermal Synthesis" *J. Am. Chem. Soc.* **2009**, *131*, 16000-16001.

155. Biemmi, E.; Darga, A.; Stock, N.; Bein, T. "Direct growth of $Cu_3(BTC)_2$ $(H_2O)_3 \cdot xH_2O$ thin films on modified QCM-gold electrodes–Water sorption isotherms" *Micro. Meso. Mater.* **2008**, *114*, 380–386.

156. Banerjee, R.; Phan, A.; Wang, B.; Knobler, C.; Furukawa, H.; O'Keeffe, M. "High-Throughput Synthesis of Zeolitic Imidazolate Frameworks and Application to CO_2 Capture" *Science* **2008**, *319*, 939-943.

157. Wang, B.; Cote, A. P.; Furukawa, H.; O'Keeffe, M.; Yaghi, O. M. "Colossal Cages in Zeolitic Imidazolate Frameworks as Selective Carbon Dioxide Reserviors" *Nature* **2008**, *453*, 207-211.

158. Morris, W.; Doonan, C.J;. Furukawa, H.; Banerjee, R.; Yaghi, O.M. "Crystals as Molecules: Postsynthesis Covalent Functionalization of Zeolitic Imidazolate Frameworks" *J. Am. Chem. Soc.* **2008**, *130*, 12626-12627.

159. Banerjee, R.; Furukawa, H.; Britt, D.; Knobler, C.; O'Keeffe, M.; Yaghi, O.M. "Control of Pore Size and Functionality in Isoreticular Zeolitic Imidazolate Frameworks and their Carbon Dioxide Selective Capture Properties" *J. Am. Chem. Soc.* **2009**, *131*, 3875-3877.

160. Phan, A.; Doonan, C.J.; Uribe-Romo, F.J.; Knobler, C.B.; O'Keeffe, M.; Yaghi, O.M. "Synthesis, Structure, and Carbon Dioxide Capture Properties of Zeolitic Imidazolate Frameworks" *Acc. Chem. Res.* **2010**, *43*, 58-67.

161. Park, K.S.; Ni, Z.; Cote, A.P.; Choi, J.Y.; Huang, R.; Uribe-Romo, F.J.; Chae, H.K.; O'Keeffe, M.; Yaghi, O.M. "Exceptional chemical and thermal stability of zeolitic imidazolate frameworks" *PNAS*, **2006**, *103*, 10186–10191.

162. Hayashi, H.; Cote, A.P.; Furukawa, H.; O'Keeffe, M.; Yaghi, O.M. "Zeolite A imidazolate frameworks" *Nat. Mater.* **2007**, *6*, 501-506.

163. Huang, X-C.; Lin, Y-Y.; Zhang, J-P.; Chen, X-M. "Ligand-Directed Strategy for Zeolite-Type Metal–Organic Frameworks: Zinc(II) Imidazolates with Unusual Zeolitic Topologies" *Angew. Chem. Int. Ed.* **2006**, *45*, 1557-1559.

164. Cravillon, J.; Muzer, S.; Lohmeier, S.J.; Feldhoff, A.; Huber, K.; Wiebcke, M. "Rapid Room-Temperature Synthesis and Characterization of Nanocrystals of a Prototypical Zeolitic Imidazolate Framework" *Chem. Mater.* **2009**, *21*, 1410-1412.

165. Moggach, S.A.; Bennett, T.D.; Cheetham, A.K. "The Effect of Pressure on ZIF-8: Increasing Pore Size with Pressure and the Formation of a High-Pressure Phase at 1.47 GPa" *Angew. Chem. int. ed.* **2009**, 121, 7221 –7223.

166. Ordonez, M.J.C.; Balkus, K.J.; Ferraris, J.P.; Musselman, I.H. "Molecular sieving realized with ZIF-8/Matrimid mixed-matrix membranes" *J. Membr. Sci.* **2010**, *361*, 28–37.

167. Li, Y.; Liang, F.; Bux, H.; Yang, W.; Caro, J. "Zeolitic imidazolate framework ZIF-7 based molecular sieve membrane for hydrogen separation" *J. Membr. Sci.* **2010**, *354*, 48-54.

168. Li, Y.; Bux, H.; Feldhoff, A.; Li, G.; Yang, W.; Caro, J. "Controllable Synthesis of Metal–Organic Frameworks: From MOF Nanorods to Oriented MOF Membranes" *Adv. Mater.* **2010**, *22*, 3322-3326.

169. Jiang, H.L.; Liu, B.; Akita, T.; Haruta, M.; Sakurai, H.; Xu, Q. "Au@ZIF-8: CO Oxidation over Gold Nanoparticles Deposited to Metal–Organic Framework" *J. Am. Chem. Soc.* **2009**, *131*, 11302-11303.

170. Chizallet, C.; Lazare, S.; Bazer-Bachi, D.; Bonnier, F.; Lecocq, V.; Soyer, M.; Quoineaud, A.; Bats, N. "Catalysis of Transesterification by a Nonfunctionalized Metal-Organic Framework: Acido-Basicity at the External Surface of ZIF-8 Probed by FTIR and *ab Initio* Calculations" *J. Am. Chem. Soc.* **2010**, *132*, 12365–12377.

171. Lu, G.; Hupp, J.T. "Metal–Organic Frameworks as Sensors: A ZIF-8 Based Fabry–Perot Device as a Selective Sensor for Chemical Vapors and Gases" *J. Am. Chem. Soc.* **2010**, *132*, 7832-7833.

172. Li, Q.; Mihailova, B.; Creaser, D.; Sterte, J. "Aging effects on the nucleation and crystallization kinetics of colloidal TPA-silicalite-1" *Microporous Mesoporous Mater.* **2001**, *43*, 51-59.

173. Szostak, R. *Handbook of molecular sieves*, Van Nostrand Reinhold, Newyork, **1992**, p. 416

174. Akolekar, D.B.; Bhargava, S.; Bronswijk, W.V. "Fourier Transform Raman Spectroscopy of Novel Aluminophosphate Molecular Seives" *Appl. Spectroscopy*, **1999**, *53*, 931-937.

175. Hosokowa, H.; Oki, K. "Synthesis of Nanosized A-type Zeolites from Sodium Silicates and Sodium Aluminates in the Presence of a Crystallization Inhibitor" *Chem. Letters*, **2003**, *32*, 586-587.

176. Lew, C. M.; Li, Z.; Zones, S.I.; Sun, M.; Yan, Y. "Control of size and yield of pure-silica-zeolite MFI nanocrystals by addition of methylene blue to the synthesis solution" *Microporous Mesoporous Mater.* **2007**, *105*, 10-14.

177. Hoppe, R.; Schulz-Ekloff, G.; Rathousky, J.; Starek, J.; Zukal, A. "Effect of the addition of methylene blue to the reaction mixture for the hydrothermal synthesis of aluminophosphate molecular sieves on their morphology" *Zeolites.* **1994**, *14*, 126-129.

178. Garcia, J.M.; Wick, L.Y.; Harms, H. "Influence of the Nonionic Surfactant Brij 35 on the Bioavailability of Solid and Sorbed Dibenzofuran" *Environ. Sci. Technol.* **2001**, *35*, 2033-2039.

179. Wang, S.C.; Wang, C.K.; Chang, F.M.; Tsao, H.K. "Second Viral Coefficients of Poly(ethylene glycol) in Aqueous Solutions" *Macromolecules*, **2002**, *35*, 9551-9555.

180. Zhu, Z.; Hartmann, M.; Kevan, L. "Catalytic Conversion of Methanol to Olefins on SAPO-n (n) 11, 34, and 35), CrAPSO-n, and Cr-SAPO-n Molecular Sieves" *Chem. Mater.*, 2000, **12,** 2781-2787.

181. Xu, L.; Du, A.; Wei, Y.; Wang, Y.; Yu, Z.; He, Y.; Zhang, X.; Liu, Z. "Synthesis of SAPO-34 with only Si(4Al) species: Effect of Si contents on Si incorporation mechanism and Si coordination environment of SAPO-34" *Micro. Meso. Mater.* **2008**, *115*, 332-337.

182. Roldan, R.; Sanchez-Sanchez, M.; Sankar, G.; Romero-Salguero F.J.; Jimenez-Sanchidrian, C. "Influence of pH and Si content on Si incorporation in SAPO-5 and their catalytic activity for isomerisation of n-heptane over Pt loaded catalysts" *Micro. Meso. Mater.* **2007,** *99,* 288-298.

183. Jhung, S.H.; Chang, J.S.; Hwang, J.S.; Park, S.E. "Selective formation of SAPO-5 and SAPO-34 molecular sieves with microwave irradiation and hydrothermal heating" *Micro. Meso. Mater.* **2003,** *64,* 33-39.

184. Ciobanu, G.; Carja, G.; Ciobanu, O. "Structure of mixed matrix membranes made with SAPO-5 zeolite in polyurethane matrix" *Micro. Meso. Mater.* **2008,** *115,* 61-66.

185. Briend, M.; Peltre, M.J.; Massaiani, P.; Man, P.P.; Vomscheid, M.; Derewinski, Barthomeuf, D. "Modifications of structure and Si environment upon heating of SAPO-5, SAPO-34 and SAPO-37" *Stud. Surf. Sci. Catal.* **1994,** *84,* 613-620.

186. Liu, G.; Tian, P.; Zhang, Y.; Li, J.; Xu, L.; Meng, S.; Liu, Z. "Synthesis of SAPO-34 templated by diethylamine: Crystallization process and Si distribution in the crystals" *Micro. Meso. Mater.* **2008,** *114,* 416-423.

187. Tan, J.; Liu, Z.; Bao, X.; Liu, X.; Han, X.; He, C.; Zhai, R. "Crystallization and Si incorporation mechanisms of SAPO-34" *Micro. Meso. Mater.* **2002**, *53*, 97-108.

188. Tsai, T.G.; Shih, H.C.; Liao, S.J.; Chao, K.J. "Well-aligned SAPO-5 membrane: preparation and characterization" *Micro. Meso. Mater.* **1998**, *22*, 333-341.

189. Yang, W.; Zhang, B.; Liu, X. "Synthesis and characterization of SAPO-5 membranes on porous α-Al$_2$O$_3$ substrates" *Micro. Meso.Mater.* **2009**, *117*, 391-394.

190. Kuanchertchoo, N.; Kulprathipanja, S.; Aungkavattana, P.; Atong, D.; Hemra, K.; Rirksomboon, T.; Wongkasemjit, S.; "Preparation of uniform and nano-sized NaA zeolite using silatrane and alumatrane precursors" *Applied Organometallic Chemistry*, **2006**, *20*, 775-783.

191. Vengrenovich, R.D.; Gudyma, Y.V.; Yarema, S.V. "Ostwald ripening of quantum-dot nanostructures" *Semiconductors*, **2001**, *35*,1378-1382.

192. Concepción, P.; López Nieto, J.M.; Mifsud, A.; Pérez-Pariente, J. "Preparation and characterization of Mg-containing AFI and chabazite-type materials" *Zeolites*, **1996**, *16*, 56-64.

193. Inoue, M.; Dhupatemiya, P.; Phatanasri, S.; Inui, T. "Synthesis course of the Ni-SAPO-34 catalyst for methanol-to-olefin conversion" *Micro. Meso. Mater.* **1999**, *28*, 19-24

194. T. Brar, P. France, P. G. Smirniotis, Ind. Eng. Chem. Res. 2001, 40, 1133 –1139.

195. D. Baek, U. Y. Hwang, K. S. Lee, Y. Shul, K. K. Koo, J. Ind. Eng. Chem. 2001, 7, 241– 249.

196. J. Cai, J. Liu, Z. Gao, A. Navrotsky, S. L. Suib, Chem. Mater. 2001, 13, 4595 – 4602.

197. J. Chen, D. K. Sun, S. C. Dong, M. Huang, Q. H. Xu, Chin. J. Inorg. Chem. 2000, 16, 769 –774.

198. X. H. Xu, W. H. Yang, J. Liu, L. W. Lin, Sep. Purif. Technol. 2001, 25, 241 –249.

199. T. G. Tsai, H. C. Shih, S. J. Liao, K. J. Chao, Microporous Mesoporous Mater. 1998, 22, 333– 341.

200. H. Wang, H. R. Zhang, J. J. Zhu, J. Cryst. Growth, 2001, 233, 829 –836.

201. D. S. Kim, J.-S. Chang, W. Y. Kim, H. Y. Kim, S. E. Park, Bull. Chem. Soc. Jpn. 1999, 20, 408 –410.

202. Callister, W.D.; Rethwisch, D.G. "Fundamentals of Material Science and Engineering" *wiley publishing*, 3rd Editon, 401-411.

203. P. M. Slangen, J. C. Jansen, H. Van Bekkum, G. W. Hofland, F. Van der -Ham, G. J. Witkamp in Proceedings of the International Zeolite Conference,Vol. 3, Materials Research Society, Baltimore, 1999, pp. 1553–1560.

204. M. D. Romero, J. M. Gomez, G. Ovejero, A. Rodriguez, Mater. Res. Bull. 2004, 39, 389 –400.

205. Chang, F.Y.; Chao, K.J.; Cheng, H.H.; Tan, C.S. "Adsorption of CO_2 onto amine-grafted mesoporous silicas" *Separation and Purification Tech.* **2009**, *70*, 87-95.

206. Jiang, H.; Chen, F.; Lagally, M.G.; Denes, F.S. "New Strategy for Synthesis and Functionalization of Carbon Nanoparticles" *Langmuir*, **2010**, *26*, 1991-1995.

207. Pelegrini, M.V.; Pereyra, I. *Phys. Status Solidi C*, □Characterization of AlN films deposited by r.f. reactive sputtering aiming MEMS applications" **2010**, *7*, 840-843.

208. Zubkov, S.A.; Kustov, S.A.; Kazansky, V.B; Girnus, I; Fricke, R. "Investigation of hydroxyl groups in crystalline silicoaluminophosphate SAPO-34 by diffuse reflectance infrared spectroscopy" *J. Chem. Soc., Faraday Trans.* **1991,** *87,* 897-900.

209. Jeanvoine, Y.; Angyan, J.G. "Brønsted Acid Sites in HSAPO-34 and Chabazite: An Ab Initio Structural Study" *J. Phys. Chem. B,* **1998,** *102,* 5573-5580.

210. Huang, J.; Zou, J.; Ho, W.S.W. "Carbon Dioxide Capture Using a CO_2-Selective Facilitated Transport Membrane" *Ind. Eng. Chem. Res.* **2008,** *47,* 1261-1267.

211. Zou, J.; Ho, W.S.W. "CO_2-selective polymeric membranes containing amines in crosslinked poly(vinyl alcohol)" *J. Memb. Sci.* **2006,** *286,* 310-321.

212. Tee, Y.H.; Zou, J.; Ho, W.S.W. "CO_2-Selective Membranes Containing Dimethylglycine Mobile Carriers and Polyethylenimine Fixed Carrier" *J. Chin. Inst. Chem. Engg.* **2006,** *37,* 37-47.

213. Choi, S.Y.; Mamak, M.; Speakman, S.; Chopra, N.; Ozin, G.A. "Evolution of Nanocrystallinity in Periodic Mesoporous Anatase Thin Films" *Small,* **2005,** *1,* 226-232.

214. Choi, S.Y.; Lee, B.; Carew, D.B.; Mamak, M.; Peiris, F.C.; Speakman, S.; Chopra, N.; Ozin, G.A. "3D Hexagonal (*R*-3*m*) Mesostructured Nanocrystalline Titania Thin Films: Synthesis and Characterization" *Adv. Funct. Mater.* **2006,** *16,* 1731-1738.

215. Avrami, M. "Kinetics of Phase Change. I General Theory" *J. Chem. Phys.* **1939,** *7,* 1103-1112.

216. Avrami, M. "Granulation, Phase Change, and Microstructure Kinetics of Phase Change. III" *J. Chem. Phys.* **1941,** *9,* 177-184.

217. Hillier, I.H. "Modified avrami equation for the bulk crystallization kinetics of spherulitic polymers" *Journal of Polymer Science Part A: Polymer chemistry*, **1965**, *3*, 3067-3078.

218. Hay, J.N. "Determination of the avrami exponent" *Journal of Polymer Science Part C: Polymer Letters* **1976**, *14*, 543-548.

219. Mintova, S.; Olson, N.H.; Valtchev, V.; Bein, T. "Mechanism of Zeolite A Nanocrystal Growth from Colloids at Room Temperature" *Science,* **1999**, *283,* 958-960.

220. Mintova, S.; Olson, N.H.; Bein, T. "Electron Microscopy Reveals the Nucleation Mechanism of Zeolite Y from Precursor Colloids" *Angew. Chem. Int. Ed.* **1999**, *38,* 3201-3204.

221. Mintova, S.; Olson, N.H.; Senker, J.; Bein, T. "Mechanism of the Transformation of Silica Precursor Solutions into Si-MFI Zeolite" *Angew. Chem. Int. Ed.* **2002**, *41,* 2558-2561.

222. Burkett, S.L.; Davis, M.E. "Mechanism of Structure Direction in the Synthesis of Si-ZSM-5 - An Investigation by Intermolecular H-1-Si-29 CP MAS NMR" *J. Phys. Chem.* **1994**, *98,* 4647-4653.

223. Lorenz, R.; Voorhess, P.W. "Growth and Coarsening: Ostwald Ripening in Material Processing" *Springer* **2002**, 117.

224. Davis, M.E.; Lobo, R.F. "Zeolite and molecular sieve synthesis" *Chem. Mater.* **1992**, **4**, 756-768.

225. Vogels, L.J.P.; van Hoof, P.J.C.M.; Grimbergen, R.F.P. "On the roughening transition of anisotropic and (pseudo) hexagonal lattices" *J. Crystal Growth* **1998,** *191,* 563-572.

226. Cundy, C.S.; Henty, M.S.; Plaisted, R.J. "Zeolite synthesis using a semicontinuous reactor, Part 1: Controlled nucleation and growth of ZSM-5 crystals having well-defined morphologies" *Zeolites* **1995,** *15,* 353-372.

227. Liu, D.; Zheng, C.; Yang, Q.; Zhong, C. "Enhanced Performance of ZnO Nanocomposite Transistor by Simple Mechanical Compression" *J. Phys. Chem C.* **2009,** *113,* 5004-5009.

CIRRICULUM VITAE

Surendar R. Venna

PhD Candidate, Chemical Engineering

782 Raymond Kent Ct, Apt # 1, Louisville, KY 40217 (USA)

surendarrvenna@gmail.com, (502) 599-8254

Professional summary

Chemical engineer with strong academic and research experience in material science, gas separation, membrane science reaction engineering and catalysis. Recognized by several awards, fellowships and publications. Possess good communication skills and involved in various professional and social organizations. Seeking a demanding position where I can apply my experience and learn continuously.

Professional preparation

University of Louisville	Chemical Engineering	GPA: 3.76/4	PhD	Oct' 2010
OUCT, India	Chemical Engineering	GPA: 3.95/4	M.Tech	Feb' 2007
OUCT, India	Chemical Engineering	GPA: 3.80/4	B.Tech	Apr' 2004

Experience

August 2007 –Present **Graduate Research Assistant**, University of Louisville, USA.

- Surface modified SAPO-34 zeolite molecular sieve membranes, with high CO_2 adsorption capacity and capability for selective separation of CO_2 from mixtures of CO_2/CH_4 have been synthesized using conventional and microwave heating methods. These highly stable membranes with superior separation performance were synthesized inside alumina and stainless steel tubular supports. These membranes can also be used for the separation of CO_2 from gas mixtures like nitrogen, hydrogen and oxygen. A lab-scale testing facility for evaluating the

- separation performance of these membranes was designed, fabricated and installed.

- Various zeolites were prepared with controlled crystal sizes and properties using different techniques hydrothermal and microwave heating.

- Zeolitic Imidazolate Framework membranes, a novel metal organic framework, have been prepared for the separation of CO_2 from CH_4 using secondary seeded growth. These membranes showed high carbon dioxide permeances with good selectivities. This is one of the first examples of using ZIFs for these separations. Explored diverse chemical and processing parameters to prepare robust and selective membranes.

- Worked on the synthesis of biofuels using Metal organic frameworks as catalysts.

- Functional mesoporous metal oxide catalysts have been synthesized for photo catalysis of dyes.

- Extensive experience in characterization of materials using porosimeter, transmission and scanning electron microscopy, X-ray diffraction spectroscopy, Infrared spectroscopy and gas chromatography, Ultraviolet-Visible spectroscopy.

- Mentored Master's, undergraduates and high school assistants in research projects.

August 2004 – February' 07   **Graduate Research Assistant**, Osmania University, India

- Designed a fluidized bed reactor for fluidization of cohesive powders. Successfully performed the solid-solid reaction for phathalic anhydride and p-nitroaniline system. Higher rate of heat transfer and diffusion obtained for the reaction. Effect of reaction temperature, stirrer speed, flow rate of fluidizing medium and static bed height on conversion and rate of reaction. Achieved higher conversions than conventional reactor in less time. Experiments are performed using statistically designed factorial experiments and modeled the reaction.

May 2006– June 2006   **Summer Internship**, Nuclear Fuel Complex (NFC), India

- Study to improve the efficiency of the extraction, stripping and vacuum distillation operations.

July 2003 – April 2004   **Undergraduate Research,** Osmania University, India.

- Energy and product optimization of process conditions for phthalic anhydride synthesis.

153

Awards

- 2010: **Doctoral dissertation completion award** from University of Louisville, USA

- 2009: Elias Klein Founder's travel Award from North American Membrane Society, USA.

- 2007-2009: **J.B. Speed Graduate Fellowship** from University of Louisville, USA.

- 2006: **Young Research Scholar Award** for outstanding graduate research work by Indian Institute of Chemical Engineers (IIChE), India.

- 2004-2006: All Indian Council for Technical Education Scholarship, India.

- 2006: **Best Student Award** for highest GPA in Graduate Chemical Engineering from OUCT, India.

- 2004: Scored 93 percentile in Graduate Aptitude Test in Engineering-India.

Professional Affliations

- American Institute of Chemical Engineers, Material Research Society, North American Membrane Society, North American Catalysis Society, International Zeolite Association.

Publications

- **Venna, S.R.**, Carreon, M.A., "Novel ZIF-8 membranes for CO_2 separation from CH_4", *Journal of American Chemical Society*, **2010**, 132, 76-78.

- **Venna, S.R.**, Murthy, J.S.N., Sankarshana, T., "Solid-solid reactions in fluidized bed", *Asia-Pacific Journal of Chemical Engineering*, , **2010**, DOI: 10.1002/apj.429

- **Venna, S.R.**, Carreon, M.A., "Microwave assisted phase transformation of silicoaluminophosphate zeolite crystals", *Journal of Materials Chemistry*, **2009**, 19, 3138-3140.

- Katti, A., **Venna, S.R.**, Carreon, M.A., "Self assembly hydrothermal assisted synthesis of mesoporous anatase titania employing ethylene glycol", *Catalysis Communications*, **2009**, 10, 2036-2040.

- **Venna, S.R.,** Carreon, M.A., "Synthesis of SAPO-34 Crystals in the Presence of Crystal Growth Inhibitors", *Journal of Physical Chemistry B*, **2008**, 112, 16261-16265.

- **Venna, S.R.,** Jasinski J.B., Carreon, M.A., "Structural Evolution of Zeolitic Imidazolate Framework-8", *Angew. Chem. Int. Ed.,* **Under Review.**

- **Venna, S.R.,** Carreon, M.A., "Surface modified SAPO-34 membranes for CO_2 separation from CH_4", *Ready to submit.*

- **Venna, S.R.,** Carreon, M.A., Zeolitic Imidazolate frameworks (ZIF-8) membranes for CO_2 capture, Office of Technology transfer, Uinversity of Louisville, *ULRF research disclosure number: 10092*, May **2010**.

Presentations

- "Surface modified SAPO-34 membranes for CO_2/CH_4 separation" Annual Meeting of the North American Membrane Society, Washington DC, July 2010.

- "Zeolitic Imidazolate Framework-8 membranes for CO_2/CH_4 separation" Annual Meeting of the North American Membrane Society, Washington DC, July 2010.

- "SAPO-34 seeds and membranes for CO_2/CH_4 separation" MRS meeting, Boston, December 2009.

- "Microwave assisted preparation of SAPO-34 crystals and membranes" AICHE annual meeting, Nashville, November 2009.

- "SAPO-34 membranes synthesis, characterization and CO_2/CH_4 separation" AICHE annual meeting, Nashville, November 2009.

- "SAPO-34 membranes prepared employing crystal growth inhibitors for CO_2/CH_4 separation" Annual Meeting of the North American Membrane Society, Charleston, June 2009.

- "Microwave assisted synthesis of SAPO-34 molecular sieves by phase transformation of SAPO-5" Annual Meeting of the North American Membrane Society, Charleston, June 2009.

- "Synthesis of SAPO-34 catalysts via controlled crystal growth" annual meeting of the North American Catalysis Society, San Francisco, June 2009.

- "Zeolite Membrane Synthesized Employing Crystal Growth Inhibitors for Carbon Dioxide Separation" AIChE annual meeting, Philadelphia, November 2008.

- "Effect of Crystallization Growth Inhibitors in the Synthesis of SAPO-34" AIChE annual meeting, Philadelphia, November 2008.

- "Synthesis and Characterization of SAPO-34 Zeolite Crystals and Membranes Employing Crystal Growth Inhibitors" International Conference on Membranes, Hawaii, July 2008.

- "Synthesis of SAPO-34 employing growth inhibitors", KYnanomat-2008, Louisville, March 2008.

- "Solid-Solid Reactions in Fluidized Bed" European Congress of Chemical Engineering, Copenhagen, September 2007.

- "Plastic waste management" Emerging Technology for Sustainable Environment in Chemical Allied Industries, National Institute of Technology, India, October 2005.

Referee

- Peer reviewer for the journals; *Microporous & Mesoporous Materials* and *Journal of Porous Materials.*

Other skills

- Judged poster presentations in Engineering Expo-2008 and 2010 at University of Louisville, USA.

- Well trained in LABVIEW, POLYMATH, MATLAB, MINITAB and MS office software.

- Trained in Six Sigma application and design of experiments.

- President of Chemical Engineering Graduate Student Association, University of Louisville and Public Relations Officer for Indian Student Association of University of Louisville.

- Organizing team member of Chemcon-2002 and Ichescon-2004 (technical symposia), Osmania University, India.

- Spearheaded planning efforts to hold first annual Holiday Bash for college students.

- Participated in Football Intramural sports at University of Louisville